Isolation and characterization of the functional breadth of neutralizing antibodies that cross-react with diverse sarbecovirus strains

Felicitas Ruiz

A dissertation

submitted in the partial fulfillment of the

requirements for the degree of

Doctor of Philosophy

University of Washington

2024

Reading Committee:

Michael Emerman, Chair

Julie Overbaugh

Dara A Lehman

Program Authorized to Offer Degree:

Molecular and Cellular Biology

University of Washington

Abstract

Isolation and characterization of the functional breadth of neutralizing antibodies that cross-react with diverse sarbecovirus strains

Felicitas Ruiz

Chair of the Supervisory Committee:

Michael Emerman

Department of Microbiology and Department of Global Health

Coronaviruses, specifically viruses in the *Betacoronavirus* genus, recurrently spillover into humans from other animal reservoirs and are a cause of substantial morbidity and mortality globally. Severe acute respiratory syndrome coronavirus (SARS-CoV-1) and severe acute respiratory syndrome coronavirus-2 (SARS-CoV-2) have caused significant outbreaks, and there are numerous diverse SARS-like coronavirus strains (sarbecoviruses) circulating in animal reservoirs with human spillover potential. In the context of SARS-CoV-2, the viral entry protein, spike (which is the major target of neutralizing antibodies), continues to accumulate mutations leading to reduced efficacy of therapeutic monoclonal antibodies (mAbs) and the elicited plasma response against variants of concern. Cross-reactive mAbs, defined here as antibodies capable of recognizing SARS-CoV-2 as well as diverse sarbecovirus strains, have been isolated from SARS-CoV-2 convalescent and vaccinated individuals. This indicates there are conserved sarbecovirus spike epitopes recognized by cross-reactive mAbs, though many are not durable

against SARS-CoV-2 evolution. Harnessing what has been learned from studying the immune response to SARS-CoV-2, could inform what a protective immune response may look like and minimize the impact of future outbreaks. To improve our understanding of the development of broad mAbs that can neutralize across sarbecoviruses and gauge their durability against evolving SARS-CoV-2, here we conducted two studies to comprehensively characterize a collection of cross-neutralizing antibodies elicited in different SARS-CoV-2 contexts.

We previously identified a cross-reactive mAb in one individual, C68, that experienced a vaccine breakthrough infection with the Delta SARS-CoV-2 variant, which led us to hypothesize the existence of additional broad neutralizing antibodies in this individual. In chapter II, I explore the functional activities of multiple cross-reactive mAbs isolated from this individual that target epitopes within the receptor binding domain (RBD) of the spike protein. Not all cross-reactive mAbs are equal and I describe some mAbs displaying broad and potent binding and neutralizing activity against recently circulating SARS-CoV-2 variants and animal sarbecoviruses with spillover potential. Given this finding, I collaborated on studies to identify the escape pathways of these antibodies in a SARS-CoV-2 deep mutational scanning assay. In most instances, these identified sites of escape would negatively impact viral functions (like proper RBD folding), and thus SARS-CoV-2 spike would be less tolerant to variation at these sites. For cross-reactive mAbs with limited breadth, these escape maps largely predicted loss of neutralization activity against SARS-CoV-2 variants or explained loss of activity against sarbecovirus strains (due to variation at these sites). Since the identified broadly neutralizing antibodies have complementary neutralization profiles and minimal to no overlapping escape maps, they could form the basis for a pan-sarbecovirus antibody cocktail.

In the studies of chapter III, we sought to determine whether mAbs with even greater breadth or potency might be present in C68 after subsequent exposures to SARS-CoV-2 based on studies showing that multiple antigen exposures and antigenic diversity may drive the development of enhanced neutralizing antibody responses. To address this, we examined the

affinity maturation of clonal lineage members using a longitudinal sample from C68 after additional vaccination and breakthrough infection (Omicron strain). We applied an antibody isolation approach using both SARS-CoV-1 and SARS-CoV-2 spike protein to select for broadly active memory B cells and did identify a collection of cross-reactive mAbs from multiple expanded clonal lineages, some of which exhibited enhanced neutralizing activity relative to clonal lineage members from the earlier time point. We also identified a broadly reactive mAb that exhibited pan-sarbecovirus binding and robust neutralization activity against every single sarbecovirus tested in a multi-clade virus panel.

Overall, the major targets for mAbs with broad sarbecovirus activity were epitopes within conserved regions of the RBD. This includes RBD class 5 (explored in chapter II) that rarely mutates in nature for SARS-CoV-2 variants and may be functionally constrained from evolving. In addition, it includes the RBD class 4 epitope (explored in chapter III) that is highly conserved across all sarbecoviruses assessed though targeting an interface that is susceptible to evolving SARS-CoV-2. Thus, these studies describe a diversity of broad-spectrum, and in some cases potent, mAbs targeting different epitopes that could be valuable medical countermeasures against sarbecoviruses with spillover potential. Additionally, these studies demonstrate that exposure to SARS-CoV-2 can lead to cross-reactive mAbs that target conserved epitopes and additional exposure to diverse SARS-CoV-2 spike can lead to enhancement of neutralizing activity for clonal lineage members. Future studies should focus on characterizing cross-reactive mAbs from individuals with multiple diverse exposures to SARS-CoV-2 antigen to inform how to elicit broadly neutralizing antibodies by vaccination.

Table of Contents

List of Figures

Acknowledgements

In every stage of my career, I have been fortunate to work with intelligent and incredibly supportive group of people. Graduate school is not easy but the people I have met along the way have impacted my personal and professional growth. Research blooms through collective effort, so I share this moment with you.

My very first research experience was the Undergraduate Research Center's (URC) Biomedical Sciences Enrichment Program (BISEP) at UCLA. It was a summer research intensive program meant to introduce basic cloning techniques and reading scientific literature but most importantly I learned that being a scientist could be a profession. I met Mai, Jennifer, and Carmine at BISEP, and they became long-term friends. I also met the director of the URC, Dr. Tama Hasson, who is a strong proponent of diversity, equity, and inclusion in undergraduate research. Over the years, Dr. Hasson was my academic and research career advisor that would give much needed direct and honest feedback. Her and Dr. Elissa Hallem are two academic advisors that impacted my undergraduate research experience and helped shaped me into the scientist I am today.

Shortly after BISEP, I joined Dr. Elissa Hallem's lab at UCLA. Although I did not have a strong neurobiology background, her enthusiasm for nematodes are why I wanted join her lab. I also heard from another student that she fostered a rich learning environment for developing scientists, especially underrepresented minorities. Elissa's enthusiasm was infectious, creating a work environment that didn't feel like work. Over the years, I had the opportunity to work with and learn from intelligent and kind individuals: Michelle Castelletto, Joon Ha Lee, Taylor Brown, Astra Bryant, Mayra Carrillo, Tiffany Mao, Spencer Gang, Navonil Banerjee, Sophie Rengarajan, Manon Guillermin, Leopoldo Bello-Luna, Wendy Fung, Ivan Chavez, Emily Yang, Elisa Rojas Palato, Ryo Okubo, Jackie Lopez, and Kristen Yankura. Their approach to science, communication, and mentorship is what I strive to apply in my current and in future endeavors. Thank you, Elissa, for helping cultivate my curiosity and excitement for science.

Transitioning from a neurobiology and parasitology lab to an immunology lab for graduate school was an adjustment, but I am very thankful to Dr. Julie Overbaugh for her guidance. Under Julie's guidance, I have had the opportunity to learn about the adaptive immune response and the different ways that one could elicit broad antibodies. I have been able to work on collaborative projects with interesting findings that have furthered our research on SARS-CoV-2 antibodies. I

am especially grateful for her patience and guidance throughout the manuscript writing process, I have seen improvements in my writing and reading of literature! Julie has also fostered a work environment where coworkers are generously available to brainstorm ideas and troubleshoot experimental approaches. Thank you to the entire Overbaugh and Dara Lehman Labs (past and present): Dara, Caitlin Stoddard, Alex Willcox, Jamie Guenthoer, Caroline Phan, Delphine Depierreux, Michelle Lilly, Morgan Litchford, Vrasha Chohan, Sahil Bhatti, Zak Yaffe, Hannah Itell, Ryan Yucha, Haidyn Weight, Mackenzie Shipley, Carolyn Fish, Elise Kang, Laura Doepker, Daryl Humes, and Meghan Garrett. Thank you to Zak, Michelle, Mackenzie, Ryan, and Delphine (team antibody) for troubleshooting the antibody cloning pipeline and performing B cells sorts with me. I am also grateful to have worked with Jamie, Michelle, Vrasha and Delphine on the different SARS-CoV-2 antibody projects. I also want to thank Caitlin, Alex and Morgan for being generous with their time and knowledge as I dived into innate immune projects. Thank you, Julie, for being an incredible mentor.

I also want to thank the Molecular and Cellular PhD program administrators, both on the UW and Fred Hutch side, for their support during my graduate career. Thank you Maia Low, Denise Barnes, Amber Ismael, Andrea Brocato and many more for coordinating graduate events and being so approachable with any questions we may have.

To the Estrada family, thank you for welcoming me into your lives. Brittany and Junior, I love exploring the world with you guys. Mari y Joel, estoy muy orgullosa de tener su apoyo. To my family: thank you to my brother, my sister-in-law and my niece and nephew. Whenever I call, you guys know how to place a smile on my face. Thank you, Joao, for helping create my passion for film and its potential for storytelling. To you and Lili, thank you for being my role models. I would not be the person I am today, and in a position to conduct research, without the love and support of my wife, Liz. I am so happy our family has grown with the addition of our boy, Quinn. Can’t wait to try new coffee and explore the world with you. You are my rock and my guiding light, te amo LLBFF.

Thesis Dedication

This thesis is dedicated to Dr. Taylor M. Brown (1993-2019). Thank you for always fighting for what is right, leading diversity efforts in science, and being a friend.

Chapter 1:

Introduction

Coronaviruses pose a serious health threat to humans as three major human coronaviruses have spilled over from animal reservoirs to cause severe disease in the twenty-first century: severe acute respiratory syndrome coronavirus (SARS-CoV-1) (1, 2), severe acute respiratory syndrome coronavirus-2 (SARS-CoV-2) (3, 4), and Middle East respiratory syndrome coronavirus (MERS-CoV) (5). The catastrophic global disease burden of human coronaviruses is highlighted with the recent pandemic caused by SARS-CoV-2, resulting in more than 7 million deaths and 775 million cases of COVID-19 worldwide as of 2024 (6). SARS-CoV-2 continues to accumulate adaptive mutations and circulate in the human population, entering an endemic phase. Other known human endemic coronaviruses that generally cause mild respiratory symptoms, such as OC43 and 229E, have circulated in the human population for some time (7).

With the emergence of SARS-CoV-2 in late 2019, the scientific community investigated SARS-CoV-2 biology (including structural and functional characterization of the surface protein, spike, involved in viral attachment and entry), immune response in convalescent serum and antigenicity of the spike glycoprotein (3, 8). These efforts were aided by previous research on the closely-related SARS-CoV-1 (3, 8), including studies in animal models that support a protective role of spike targeting antibodies in SARS-CoV-1 infection (9–11). These collective efforts led to several nucleic acid and protein-based vaccines that were developed and deployed to elicit antibodies targeting the spike protein (12).

Despite widespread SARS-CoV-2 exposure by vaccination or prior SARS-CoV-2 infection, reinfection and vaccine breakthrough cases can occur, in large part due to immune evasion from emerging variants (13, 14). Given that SARS-CoV-2 continues to acquire mutations, and several

SARS-like coronaviruses have been identified in animal reservoirs with emergent potential, it is critical to understand what a protective and robust immune response looks like. Isolation and characterization of monoclonal antibodies (mAbs) can inform a protective pan-coronavirus vaccine against SARS-CoV-2 and related coronaviruses and serve as both pre- and post-exposure prophylactics that are important medical countermeasures to contain future infectious diseases before evolving into pandemics (15). Thus, the need for broad-spectrum and durable mAbs has become increasingly apparent for pandemic preparedness.

Below, I will provide an introduction on SARS-CoV-2 and related coronaviruses genetic diversity, biology and the antibody response following antigen exposure.

1.1 Overview into taxonomy and recent outbreaks of pathogenic human coronaviruses

Coronaviruses are within the order *Nidovirales*, the family *Coronaviridae* and the subfamily of *Coronavirineae* (**Figure 1-1**) (16). The *Coronavirineae* subfamily can be further divided into four genera: *Alphacoronavirus, Betacoronavirus, Gammacoronavirus,* and *Deltacoronavirus* based on rooted phylogenetic clustering and pairwise evolutionary distances in the replicase-transcriptase polyprotein (16). Gamma- and deltacoronaviruses primarily infect avian species, whereas alpha- and aetacoronaviruses infect mammalian hosts and will be the focus of this chapter because viruses in these genera have caused human disease (16). In particular, the *Betacoronavirus* genus includes five out of the seven coronaviruses known to infect humans. Viruses within each genus are sorted by amino acid sequence identity based on the more sequence conserved replicase domains, specifically the RNA-dependent RNA polymerase (RdRp) of the replicase-transcriptase polyprotein (16, 17). Within the *Alphacoronavirus* genus, the two known human coronaviruses include 229E and NL63 (7).

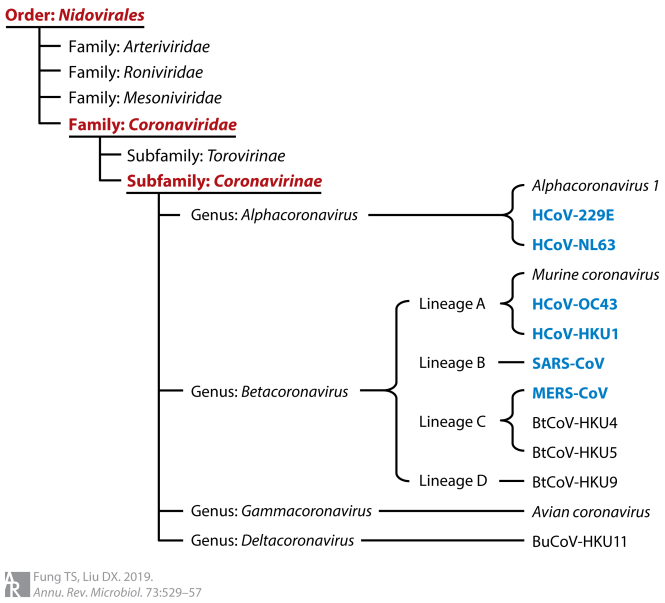

Figure 1.1. Classification of human and other coronaviruses according to the International Committee on Taxonomy of Viruses.
Taxonomy, from order to lineage, of human and other coronaviruses with classification based on the replication-transcriptase polyprotein sequence. Order, family and subfamily of betacoronaviruses depicted in red. In blue are coronaviruses known to infect humans (H-CoVs), with the exception of SARS-CoV-2, which spilled over at a later time. Lineage (A-D) is an outdated term and has been replaced by the following subgenera: embecoviruses replacing lineage A, sarbecoviruses representing lineage B (SARS-like betacoronavirus), merbecovirus (MERS-like betacoronavirus) representing lineage C, nobecovirus replacing lineage D and hibecovirus. Other abbreviations include BtCoV for bat coronavirus and BuCoV for bulbul coronavirus. The old classification shown here is adapted from Fung and Liu et al 2019 with permission from Copyright Clearance Center license # 1553852-1 (CCC Online Granting service) (12).

International Committee on Taxonomy of Viruses (ICTV) further divides the betacoronavirus genus into 5 subgenera: *Embecovirus, Sarbecovirus* (SARS-like betacoronavirus), *Merbecovirus* (MERS-like betacoronavirus), *Nobecovirus* and *Nibecovirus* (the first 4 subgenera were formerly known as lineages A, B, C, and D, respectively) (18). The subgenera *Nobecovirus* and *Hibecovirus* consists only of mammalian coronaviruses that infect *Rousettus* and *Hipposideros* bats, respectively (18). The two alphacoronaviruses, 229E and NL63, along with the betacoronaviruses, OC43 and HKU1 (which are in the subgenus *Embecovirus*) typically cause mild upper respiratory tract infections and “common cold” like symptoms, though severe infection can occur in elderly and immunocompromised individuals (19, 20). In stark contrast, MERS-CoV

(in the subgenus *Merbecovirus*), SARS-CoV-1 and SARS-CoV-2 (both in the subgenus *Sarbecovirus*) are more pathogenic and cause severe lower respiratory tract infections, that have caused two epidemics and one pandemic.

Emergence of SARS-CoV-1:

In the fall of 2002, a mysterious respiratory illness emerged in China and resulted in 8096 cases with 774 deaths over the course of nine months (21, 22). A novel coronavirus was identified as the etiological agent of severe acute respiratory syndrome (SARS) and named severe acute respiratory syndrome related coronavirus, or SARS-CoV (herein referred to as SARS-CoV-1) (1, 2). It is widely accepted that SARS-CoV-1 had a zoonotic origin (23) as viral RNA recovered from convalescent individuals were subjected to PCR, sequenced and found to closely align with viral sequences isolated from masked palm civets and raccoon dogs in a nearby live animal market (consistent with zoonosis transmission) (21). Analysis of mutations and deletions in recovered human and animal viral sequences suggested that these sequences may be phylogenetically distinct with palm civets representing an intermediate host (24). Since then, horseshoe bats have been identified as the likely natural reservoir for SARS-CoV-1 (and related coronaviruses) (23), as a plethora of viral genome sequences have been isolated that closely matched that of SARS-CoV-1 (25–27).

When that initial outbreak occurred, it was unknown if SARS-related coronavirus outbreaks would strike again. In just a year after the 2002-03 outbreak, 5 additional SARS-CoV-1 cases were reported that were likely due to zoonosis (28), but additional SARS-CoV-1 cases have not been identified since then.

Repeated outbreaks of MERS-CoV:

Like SARS-CoV-1, MERS-CoV is a respiratory virus that can result in acute respiratory distress syndrome with a high case fatality rate (29, 30). MERS-CoV has repeatedly spilled over into the human population with cases in 2012, 2015 and 2024 due to zoonotic transmission from

dromedary camels in Saudi Arabia (31). Similar to SARS-CoV-1, while dromedary camels are thought to be intermediate hosts, the natural reservoir is believed to be bats (32). Both SARS-CoV-1 and MERS-CoV share less than 50% sequence identify in the spike protein, and as stated above both are classified in the *Betacoronavirus* genus though cluster in different subgenera (30). While this thesis will focus on the immune response to SARS-related coronaviruses in the sarbecovirus subgenera, MERS-CoV represents a noteworthy example of a more divergent coronavirus that threatens human populations (5, 28, 31).

SARS-CoV-2 Pandemic:

In December 2019, cases of a pneumonia-like respiratory illness emerged, and by January 2020, the causative agent was identified as a pathogenic coronavirus named severe acute respiratory syndrome related-coronavirus-2 (SARS-CoV-2) (3, 33). The scientific community, including scientists at the Chinese CDC, deposited viral genome sequences within a few weeks of initial cases (34, 35), which led to the identification of the viral entry receptor and structural characterization of the viral entry protein (further discussed below). By February 2020, over 83,000 global cases had been reported, which was over 10 times the number of the entire SARS-CoV-1 outbreak (33).

Relative to SARS-CoV-1, SARS-CoV-2 appeared to have increased person-to-person transmission, and infected individuals transmitted the virus before symptom onset (36). Also, relative to SARS-CoV-1, SARS-CoV-2 had a shorter incubation window for shedding of infectious viral particles and delayed symptom onset or more presymptomatic transmission (36) contributing to increased transmissibility of SARS-CoV-2. This increased person-to-person transmission may in part be because SARS-CoV-2 spike has increased affinity to the host receptor, angiotensin-converting enzyme 2 (ACE2; discussed later) compared to SARS-CoV-1 (37). SARS-CoV-2 shares approximately 80% genomic identity to SARS-CoV-1, 74% in the RBD of spike, and only shares approximately 50% identity in the receptor-binding motif (RBM; contains residues critical for ACE2 recognition within the RBD) (37). These alterations in the RBM:ACE2 interaction site

can enhance binding of RBD to the human receptor, which may contribute to increased transmissibility of SARS-CoV-2 (38, 39).

1.2 Genome replication and basic biology of human coronaviruses

Coronaviruses are enveloped, positive-sense, single-stranded RNA viruses with large genomes approximately 30 kb and a largely similar genomic replication and organization across members of the *Coronaviridae* family (16, 40) (**Figure 1-2**). The coronavirus genome is flanked by 5' and 3' untranslated regions (UTRs) that are required for RNA synthesis (41). The 5' end contains two overlapping large open reading frames (ORF1a and ORF1b) that consists of three-fourths of the RNA genome that mediates the synthesis of two polyproteins. These polyproteins are proteolytically processed into 15–16 non-structural proteins (nsp; number of nsps vary among coronaviruses) by the viral protease nsp3 and nsp5 which contain papain-like (PL) and 3C-like (3L) protease domains (**Figure 1-2**) (42, 43). These nsps are broadly involved in shutting down host RNA replication, subgenomic RNA transcription and driving full-length viral plus-strand genome RNA replication (**Figure 1-2**) (44). In particular, nsp7, nsp8 and nsp12 together encode the RdRp and cofactors involved in the replication-transcription complex (RTC) that mediates genome replication (44). Complete genome sequencing and analysis of animal and human SARS-CoV-1 isolates suggests that regions encoding the RdRp are under much less selective pressure than other regions, such as the spike coding region (45, 46), which is why the RdRp coding region has been used for coronavirus taxonomy. Other nsps also play vital roles in viral replication, such as nsp14, including encoding proteins involved in proofreading, exonuclease activity and viral mRNA capping activities.

In subgenomic RNA (sgRNA) transcription, a set of negative-strand sgRNAs are produced that are used to synthesize a nested set of positive-sense sgRNAs that encode structural and accessory proteins (**Figure 1-2**) (42). This viral RNA synthesis step involves discontinuous RNA transcription, template switching, in which the viral RdRp will recognize virus-specific

transcriptional regulatory sequences (TRSs) that are found upstream of each subgenomic ORF (42). The RdRp will either read through to the next TRS or pauses RNA synthesis at the 3' end, dissociates from the template strand and relocates to 5' end of the template, generating overlapping subgenomic templates for RNA synthesis (42). These negative-strand sgRNAs will serve as templates for plus strand transcription of structural proteins, such as the spike protein, and accessory proteins, such as 3a, from the 3' end of the virus genome (**Figure 1-2**). This template switching during RNA replication and discontinuous transcription, along with the presence of full-length and sgRNA templates may be one avenue by which genetic diversity and recombination occurs in coronaviruses (42, 47).

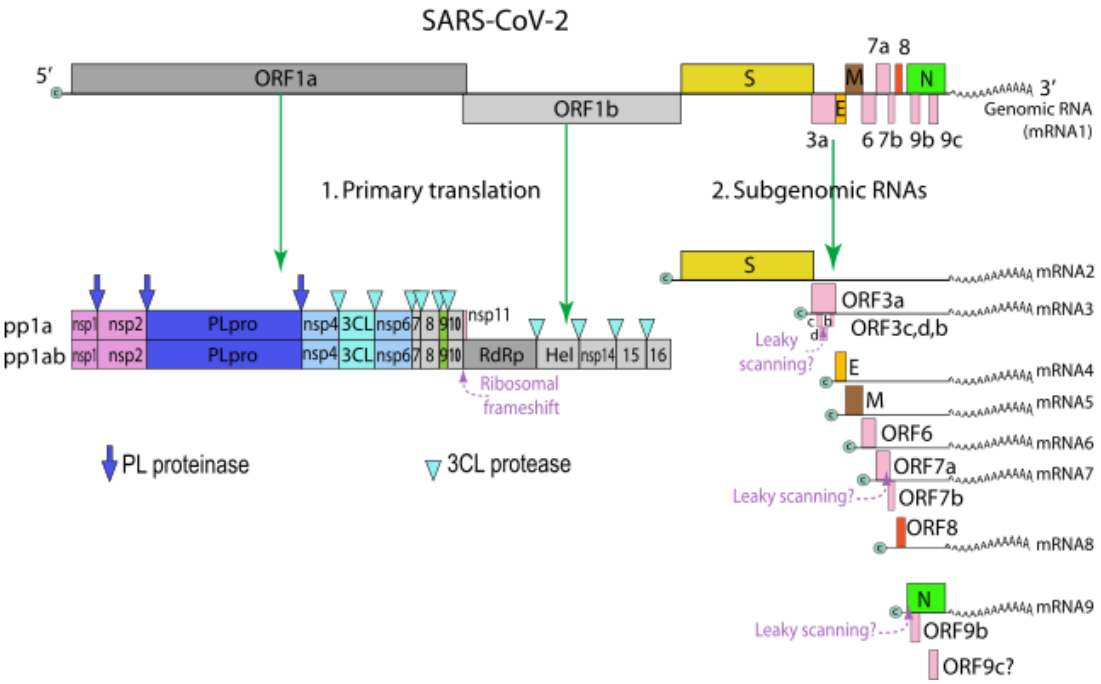

Figure 1.2. Overview of the coronavirus genome replication and organization. Basic gene organization and replication is similar for all coronaviruses. Depicted is primary translation of the viral genome along with the nonstructural proteins that are generated after two polyproteins are processed (purple arrows and blue triangles denote cleavage sites). Also depicted are the subgenomic RNAs that encode the viral structural and accessory proteins. Relevant abbreviations include nsp corresponding to the nonstructural proteins, UTR = untranslated region, RNA-dependent RNA polymerase= RdRp, S= spike, ORF= open-reading frame. Credit to SwissBioPics and adapted from Viralzone (48) with permission under Creative Commons Attribution 4.0 International License (CC BY 4.0).

The remaining portion of the genome encodes the structural proteins, which vary in number among the different coronaviruses. There are four 'universal' coronavirus structural proteins: the surface protein spike (further discussed later), a transmembrane protein (M), an envelope (E) protein and a nucleocapsid (N) protein (49). Though, members of the subgenus *Embecovirus* employ a second type of surface protein comprised of the hemagglutinin-esterase glycoprotein (49). For sarbecoviruses, the spike protein mediates attachment and entry (8). The M protein is an integral membrane protein that interacts with all structural proteins and plays a role in virion assembly (49). The E protein is responsible for wrapping viral genomic RNA into helical structures in the cytoplasm, plays a role in virion assembly, and identified as a virulence factor for SARS-CoV-1 and SARS-CoV-2 (50). The N protein is an RNA-binding phosphoprotein involved in forming the helical capsid and, in the context of SARS-CoV-2, antagonizes the interferon response (49, 51). While the antibody response is largely focused on the structural protein spike (because of its involvement in attachment and entry), the N protein is also highly immunogenic and relatively more sequence conserved than spike (52–54). High titers of N targeting antibodies have been identified in convalescent serum and thus used in diagnostics of SARS-CoV-2 infection (52–54).

1.3 Coronavirus spike protein

Spike is the viral entry protein expressed on the surface of sarbecovirus viral particles and is the main target of neutralizing antibodies due to its role essential role in infection. Spike is synthesized as a polypeptide chain of 1100-1600 amino acid residues (depending on the virus) and is a class 1 fusion protein, meaning it is a homotrimeric glycoprotein that exhibits both pre- and post-fusion conformations for attachment and entry (**Figure 1-3**) (55–57). During maturation of the virus, spike is cleaved by cellular proteases into two functional subunits, S1 and S2, (at the S1/S2 site) that form a homotrimer of heterodimers (**Figure 1-3**) (55, 56). This cleavage can occur

in the host cell by cellular proteases and the two subunits remain non-covalently linked until host receptor engagement (19).

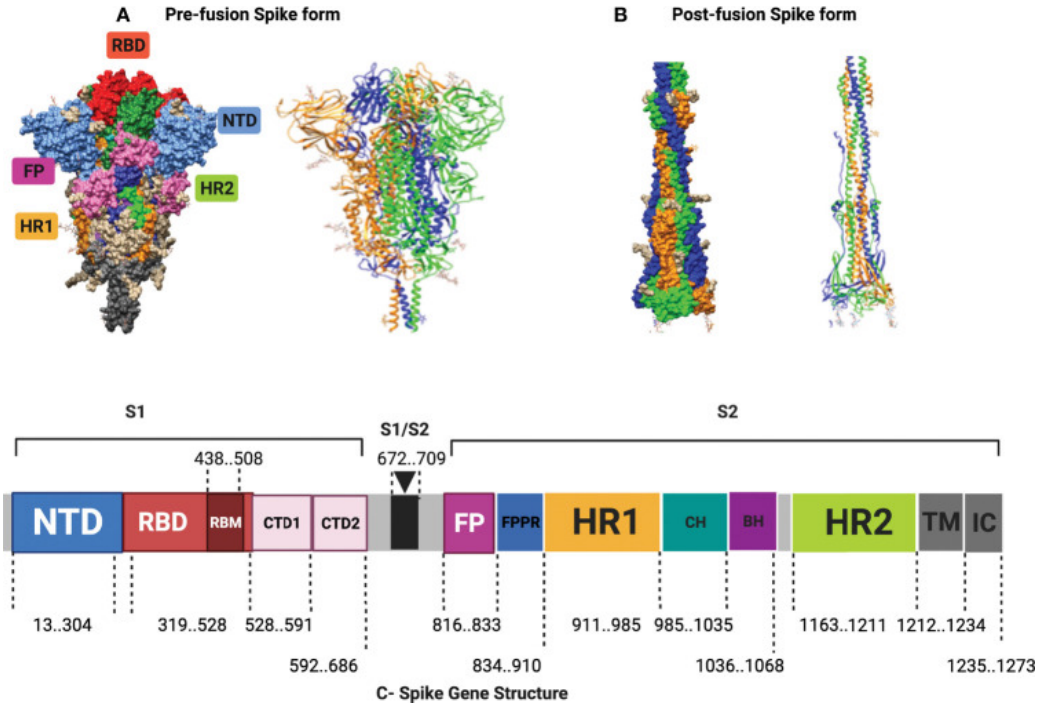

Figure 1.3. Pre-fusion and post-fusion confirmations of the coronavirus spike glycoprotein and the different domains and motifs of spike (SARS-CoV-2 represented here).
Panel A depicts a space-filled structure of spike in a pre-fusion conformation (a ribbon structure rendering to the right) with each domain color coded as the coding region in the bottom panel. **Panel B** depicts spike in a post-fusion conformation. The sequences of the domains and motifs of spike are marked by the locations of the different regions shown according to the Wuhan-Hu-1 strain with residue numbers indicated in the bottom panel. S1/S2 cleavage site denoted with a black triangle in the bottom panel. Figure adapted from (58), used under Creative Commons Attribution License (CC BY 4.0).

In the prefusion conformation (**Figure 1-3**), the S1 subunit is found at the apex of the spike trimer and mediates recognition of host receptors by adopting open or closed conformations. In the prefusion open state, at least one RBD swings up (open) to facilitate host receptor attachment, while all RBDs are down in the closed state (8, 55). These conformational dynamics of the RBD in the open and closed state can expose or occlude RBD antibody epitopes and may thus contribute to immune evasion (59, 60) (RBD epitopes further discussed later). In the case of SARS-CoV-2, multiple variants have emerged that alter RBD conformational dynamics and thus

contribute to altered transmissibility and resistance to neutralizing antibodies by conformational masking of epitopes (61–63).

Following binding to its receptor, host proteases (such as the cell surface serine protease TMPRSS2) will trigger fusion of the viral envelope with the host membrane (8, 57). The S2 subunit is the functional subunit that mediates fusion and connects to the viral membrane. The S2 gene sequence is highly conserved among betacoronaviruses, presumably due to its integral function in mediating fusion of the viral envelope with the host cellular membrane (56). The S2 subunit contains the fusion peptide (FP: a hydrophobic domain that is inserted into the cell membrane during fusion) along with two heptad repeat regions (HR1 and HR2) and stem helix (SH: involved in fusion). Engagement of the RBD to the host receptor induces conformational changes inducing S1 shedding and subsequent membrane fusion that also exposes or occludes S2 antibody epitopes (**Figure 1-3**) (19, 55, 56) (S2 epitopes further discussed later).

Host receptor usage and avenue for viral tropism expansion:

Betacoronaviruses demonstrate complexity across subgenera in the primary host receptor or attachment factor they use to gain entry. For instance, the embecoviruses, OC43 and HKU1, use 9-O-acetylated sialic acids (64), whereas the merbecoviruses, MERS-CoV and bat coronavirus NeoCoV, use human dipeptidyl peptidase 4 (hDPP4) (65) and ACE2 (66). Sarbecovirus receptor dependency has generally been assessed using cell lines expressing different known human endemic coronavirus receptors (human aminopeptidase N, hDPP4, human ACE2), attachment factors and cells expressing different ACE2 bat orthologs (67–69). The majority of SARS-related coronaviruses in the *Sarbecovirus* subgenus utilize the host receptor ACE2 to gain entry (67, 68, 70–72), but for some sarbecoviruses entry receptor usage has not been determined.

Some studies have found that certain sarbecovirus spike proteins mediate ACE2-independent, trypsin-dependent host cell entry (73). The ACE2-independent bat sarbecoviruses, Rs4237 and Rs4081, were unable to mediate entry into the human cell lines 293T-ACE2 (kidney

cell line overexpressing ACE2), Calu-3 (lung cell line overexpressing ACE2 and TMPRSS2), and Huh-7 (liver cell line) the African green monkey Vero cells (kidney cell line overexpressing TMPRSS2 along with ACE2) (72, 74). Yet, pre-treatment of viral particles with trypsin promoted viral entry into some cell lines and different ACE2 expression levels did not promote entry suggesting these Spike proteins might mediate entry in an ACE2-independent manner (72, 74). These alternative ACE2-independent, trypsin-dependent, pathways to entry are worth noting because these pathways are associated with reduced susceptibility to antibody-mediation neutralization (74).

Some sarbecoviruses remain largely uncharacterized because the entry receptor is unknown. As of result of this, characterizing the antibody response against these sarbecoviruses has been limited to binding assays (68, 75) but capacity to bind viral antigen does not necessarily indicate capacity to neutralize virus. While pseudotyping platforms, such as lentiviral viral particles expressing full-length sarbecovirus spike with human ACE2-expressing target cells, have been helpful in assessing efficacy of neutralizing antibodies against ACE2-dependent sarbecoviruses, this platform would not be applicable to ACE2-independent viruses for which receptor engagement is unknown (75, 76).

Recombination may drive the evolution of sarbecoviruses and contribute to cross-species transmission of viruses. As mentioned earlier, coronavirus genome replication involves template switching resulting in full-length and subgenomic RNA, which is an avenue by which shuffling portions of the viral genome may occur. In line with this, full-genome analysis of multiple sarbecoviruses has found several recombination events upstream, downstream and within the spike-coding sequence, which suggests that portions of the surface entry protein may be transferred between coronaviruses upon coinfection of the same host (45, 46, 77). Reconstruction of bat SARS-like coronaviruses spikes by replacing the bat-SARS-CoV RBD with RBDs from human SARS-CoV isolates led to infectious progeny with enhanced receptor engagement in cell culture meaning the recombinants exhibited enhanced infectivity (78). So while some

sarbecoviruses lack the ability to bind human ACE2 (the host receptor shared by both SARS-CoV-2 and SARS-CoV-1), or utilize an unknown entry receptor, capacity for recombination during viral replication may lower the barrier to cross-species transmission (18). Additionally, recombination may contribute to genetic diversity and immune evasion, as has been observed with SARS-CoV-2 variants that have emerged from recombination events with portions of the receptor-binding domain (which is the major antigenic target of neutralizing antibodies) from different SARS-CoV-2 strains (79, 80).

1.4 Diversity and classification of viruses within the *Sarbecovirus* subgenus based on spike genome sequence

When the epidemic of SARS-CoV-1 occurred, extensive efforts were made to identify the animal origins of SARS-CoV-1, as well as other mammalian coronaviruses that could spill over, leading to the identification of additional SARS-like coronaviruses in animal reservoirs (81, 82). Multiple genera of bat species have been assessed for the presence of coronaviruses and it is believed that the genus, *Rhinolophus,* is the primary natural reservoir of sarbecoviruses. Within the *Rhinolophus* genus*,* there are 69 species that are geographically distributed from Australia to Europe (83, 84). Isolated sarbecovirus genome sequences usually phylogenetically cluster according to the geographic region and host species, meaning viral sequences isolated in Europe are most related to other isolates from Europe (83, 84). Most epidemiological surveillance has been focused on China but only recently have sampling efforts extended into Africa and Europe. This has yielded the isolation of highly divergent sarbecovirus sequences relative to SARS-CoV-1, SARS-CoV-2 and other sarbecoviruses sampled in Asia thus far (84–86). As *Rhinolophus* bats geographic distribution range from Australia and Japan to Europe and Africa, there could be even greater genetic diversity in animal reservoirs than is currently appreciated.

One early classification of sarbecoviruses was based on partial RdRp sequences with the premise that the RdRp would be functionally constrained from evolving due to its role in replication

(83, 84). However, this classification proved difficult because full-length viral sequences from bat-derived isolates were limited and arduous to obtain due to shallow or lack of sequencing data. In order to explore the phylogenetic relationship of closely related sarbecovirus strains, recent studies have examined other regions with enough variability to separate viruses into different taxa (3, 84). Specifically, phylogenetic analysis of SARS-related coronaviruses has applied the spike gene sequence (3) or the RBD of spike (67, 87), for generating phylogenetic trees. One study found that phylogenetic analysis of a large panel of RBD sequences clustered all ACE2-dependent viruses separately from the ACE2-independent viruses (**Figure 1-4,** phylogenetic tree that clusters sarbecoviruses based on RBD). ACE2-independent sarbecoviruses clustering separately from ACE2-dependent viruses based on the RBD sequence makes sense given that ACE2-independent viruses are much more closely related in the RBD than the RdRp. And the RBM, which contacts the host receptor and thus determines viral tropism, is found in the RBD. Thus, while clustering based on the RdRp has historically been used for coronavirus taxonomy, classifying sarbecoviruses into clades based on the RBD sequence identity (as in **Figure 1-4** from Starr et al (44)) could cluster viruses based on sequence in a more informative approach (**Figure 1-4**) (18, 68, 75).

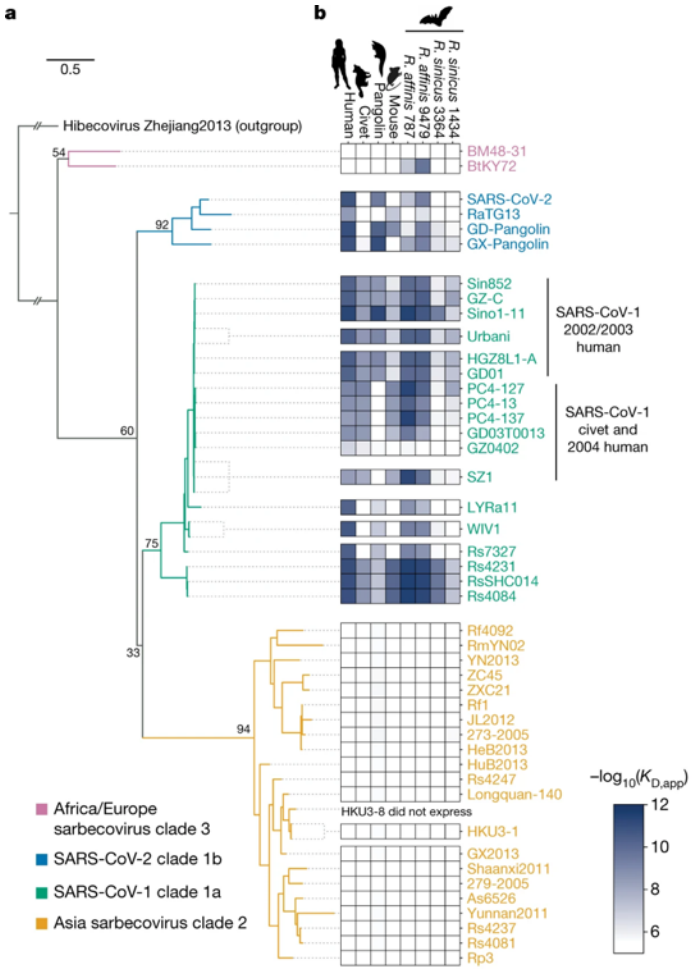

Figure 1.4. Maximum likelihood phylogeny tree based on RBDs sequences across sarbecoviruses.
In panel A, sarbecovirus RBD sequences phylogenetically cluster into four clades, with the hibecovirus sequence Hp-BetaCoV/Zhejiang2013 was used as an outgroup to root the sarbecovirus phylogeny tree. These RBD sequences tend to cluster by the countries of origin of the virus and known host receptors usage (ACE2-dependency). As such, clade 3 represents closely related sarbecoviruses found in Africa and Europe depicted in purple. Clade 1a depicts SARS-CoV-1 and closely related sarbecoviruses in green. Clade 1b depicts SARS-CoV-2 and closely related sarbecoviruses in blue. Clade 2 are closely related sarbecoviruses that are ACE2-indpendent cluster in yellow. **Panel B** depicts a heatmap representing ability for yeast-displaying RBDs from multiple sarbecoviruses to bind ACE2 orthologues (including ACE2 orthologues of human, bat, civet, pangolin and mouse) with darker blue indicating higher affinity and white depicting lack of binding. The Adapted from (68) with Creative Commons CC BY license.

Using RBD phylogenetic analysis, there is additional clustering within the ACE2-dependent viruses. The clade 1 sarbecoviruses include SARS-CoV-1 (clade 1a), SARS-CoV-2 (clade 1b) and closely related viruses that are more generalists in their ACE2 binding. These sarbecoviruses have been shown to bind human ACE2 (hACE2) and certain bat strain ACE2 orthologues (**Figure**

1-4). For example in 2013, WIV1 and RsSHC014 clade 1a sarbecoviruses were isolated from Chinese horseshoe bats and at that time were the closest related virus to SARS-CoV-1 (26). WIV1 was shown to share 11 out of 14 ACE2 contact residues that are targeted by SARS-CoV-1. Ge et al (26) showed that WIV1 can infect HeLa cells expressing human, civet or Chinese horseshoe bats ACE2, as well infect primary human airway epithelial (HAE) cells, indicating they have the potential to infect diverse species including humans. This *in vitro* broad species tropism has been observed by other clade 1a and 1b sarbecoviruses (68). While these clade 1 viruses collectively can bind different ACE2 orthologs, affinities differ between host ACE2s *in vitro* (shown in **Figure 1-4**) and this may be due to substitutions found in the RBM of these different sarbecoviruses (as is the case for SARS-CoV-1 and SARS-CoV-2 which exhibit different ACE2 affinities) (67, 68).

Isolates from Africa and Europe cluster separately than isolates from Asia. These isolates from Africa and Europe form the clade 3 sarbecoviruses (**Figure 1-4**) which exhibit host-specific ACE2 binding (68, 83, 88). The key differences found among clade 3 viruses relative to clade 1 sarbecoviruses is that they have one deletion in the RBM and have different key residues responsible for ACE2 binding (83, 89, 90). These amino acid differences at the ACE2 interface in the RBM may explain their narrow host species ACE2 usage relative to SARS-CoV-1 and SARS-CoV-2 (67, 68) (**Figure 1-4**). For example, the clade 3 sarbecovirus BTKy72 exhibits limited species tropism: does not bind human and civet ACE2 and only binds to some *Rhinolophus* species ACE2 (68). The clade 3 sarbecovirus Khosta-2 exhibits broader species tropism: can bind hACE2 and infect human cell lines (68, 69, 75). Mutations in the RBM has been shown to confer hACE2 binding in a number of clade 3 sarbecoviruses, suggesting that single mutations can expand species tropism and poise some sarbecoviruses to spillover (68, 88).

The ACE2-independent viruses, which form sarbecovirus clade 2, have two large deletions in the RBM, which is critical for ACE2 binding, and may explain their lack of binding to human and host ACE2 (67, 75). Though as noted earlier, sarbecoviruses have the potential for recombination,

SARS-CoV-2 has shown the potential for these viruses to tolerate mutations (particularly in the RBM), and single mutations have been shown to expand receptor tropism (in vitro) meaning there is a plethora of viruses with spillover potential.

1.5 Vaccines and sarbecovirus spike antibodies

Through tremendous effort from the scientific community, it is quite extraordinary how far antibody-based therapeutics have come in the management and treatment of SARS-CoV-2 infections due to the extensive characterization of the antibody response to SARS-CoV-1 and SARS-CoV-2. These efforts began during the SARS-CoV-1 outbreak and accelerated considerably with the recent SARS-CoV-2 pandemic. This led to the identification of therapeutic monoclonal antibodies and has informed the development of vaccines.

Vaccine efforts and therapeutic antibodies in the setting of SARS-CoV-1:

During the SARS-CoV-1 outbreak, initial treatment was supportive care to minimize acute respiratory distress syndrome and hypoxemia (7). ACE2 analogues, protease inhibitors, and interferons showed promise *in vitro* and in animal studies but few antiviral compounds were clinically evaluated (91). The potential to use mAbs as therapeutics was evaluated extensively in animal models where the passive transfer of spike-targeting mAbs reduced viral load and helped clear infection after viral challenge in animals (92). However, these therapeutic antibodies, which have been shown to be efficacious in animal models, were never used in humans as that outbreak resolved quickly. Though, in some cases, the passive transfer of convalescent serum did lead to management of viral load in humans.

mAbs also have a role in prevention. The passive transfer of spike-targeting mAbs prior to exposure reduced viral load upon virus challenge (10). *In vitro*, neutralizing antibodies can mediate protection by preventing viral replication (93). Interestingly, a two antibody cocktail targeting different regions of SARS-CoV-1 spike prevented viral replication in macrophages *in*

vitro (92), meaning antibodies targeting different regions can synergize to provide optimal neutralizing titers.

The efficacy in controlling SARS-CoV-1 infection in animal models upon the passive transfer of spike targeting antibodies and the management of viral load upon passive transfer of convalescent serum lead to numerous spike targeting vaccines (91, 94). Animals immunized with a range of vaccines (inactivated whole virus, Adenovirus-vector based) did elicit spike-specific neutralizing antibodies that conferred protection against viral challenge in animal models (95). Vaccines that lacked spike protein expression did not induce a detectable SARS-CoV-1 neutralizing antibody response and did not protect against virus challenge (96), reinforcing the idea that a vaccine conferring protective immunity would need to induce spike targeting antibodies.

Antibody development in response to SARS-CoV-1:

Serum IgG and neutralizing antibodies against SARS-CoV-1 peaked at 4 months following infection but dramatically decreased overtime, with undetectable neutralizing antibody titers at 36 months in 16% of patients (94, 97). China and US initiated early stage clinical trials to assess toxicity and immunogenicity in response to immunogens, though similar to infection-elicited antibodies, vaccine-elicited antibodies rapidly declined just weeks after exposure (94, 97, 98). It was then not known if these vaccine candidates would have been protective against emerging SARS-related coronaviruses.

Overview into the antibody response in the context of SARS-CoV-2:

Knowing the importance of spike-targeting antibodies in neutralizing SARS-CoV-1, spike-specific antibodies against SARS-CoV-2 were a major focus of research to inform vaccine and therapeutic development (and a major focus of my thesis). Within the first few months of the SARS-CoV-2 outbreak, the antibody response was evaluated. In SARS-CoV-2, high levels of neutralizing antibodies targeting the spike protein correlated with positive disease outcomes (99, 100). The efficacy of passively transferred mAbs targeting the spike protein has also been

evaluated and shown to reduce viral load in animal studies of SARS-CoV-2 (87, 101, 102). Passively transferred plasma from SARS-CoV-2 recovered individuals was correlated with improved patient outcomes (103).

Screening of large cohorts has revealed that SARS-CoV-2-infected individuals develop neutralizing antibodies targeting the RBD, NTD and C-terminal subdomain (also known as sub-domain-1 and sub-domain-2) of the S1 domain (59, 104–109) and epitopes in the S2 domain. It has been shown that most (approximately 90%) of the plasma neutralizing response is mediated by antibodies directed at the RBD, as depletion of RBD-targeting antibodies greatly reduces the plasma neutralizing response (104, 105). Potent neutralizing antibodies have also been described against the NTD (110, 111), C-terminal subdomain (107, 111, 112), and less potent antibodies directed at the S2 domain (107, 111, 113–116). Within the S2 domain, neutralizing antibodies targeting the fusion peptide or the stem helix (SH) linker region have been discovered (107, 111, 113–116). Though, most potent neutralizing antibodies target the RBD (59, 104–106) and will be a focus of this introduction and the topic of my thesis.

S2-targeting neutralizing antibodies:

Relative to the S1 domain, the S2 domain exhibits a high degree of sequence conservation not only among sarbecoviruses but also among other betacoronaviruses. Broad-spectrum SH mAbs exhibit cross-reactive binding across sarbecoviruses and human endemic coronaviruses, like the embecovirus OC43 (114–116). Other SH targeting mAbs (**Figure 1-5**) have been identified that broadly neutralize against clade 1a/b (SARS-CoV-1, WIV1, SHC014, SARS-CoV-2) sarbecoviruses and the merbecovirus MERS-CoV but are generally weakling neutralizing (114). SH mAbs can bind both prefusion and postfusion SARS-CoV-2 spike (**Figure 1-3**) indicating the epitope is accessible in both conformations (116). Pinto et al (116) also showed that the mAb S2P6 blocked cell fusion of Vero-E6 cells expressing full-length SARS-CoV-2 spike suggesting that the mechanism of action for this antibody is inhibiting membrane fusion by blocking S2 fusion machinery rearrangement. Likewise, FP antibodies (**Figure 1-5**) target a

conserved region of the viral spike protein, exhibit broad betacoronavirus activity and act by preventing cell fusion (111).

While antibodies directed at the S2 domain have been presented as viable broadly neutralizing antibodies due to the high-sequence conservation among sarbecoviruses and other betacoronaviruses (116, 117), these antibodies tend to be less potent than RBD-directed antibodies (113, 114, 118). As noted above, the mechanism of action for S2 directed antibodies includes inhibition of viral fusion, which would contribute to low neutralization potencies for these S2 antibodies, whereas most potent neutralizing antibodies inhibit viral attachment to the host receptor (i.e. RBD-directed antibodies) (114, 118). Additionally, S2-directed neutralizing antibodies are subdominant in the plasma neutralizing response and S2 epitopes may be partially occluded by the S1 domain in the prefusion conformation (116, 119). Aside from neutralization, the effector functions of S2-directed antibodies may be important for protection (116) (further described in the next section). Thus, S2 targeting antibodies may contribute to protection from SARS-CoV-2 infection due to their Fc-mediated effector functions rather than neutralization, though the Fc effector function of antibodies is still a field being investigated.

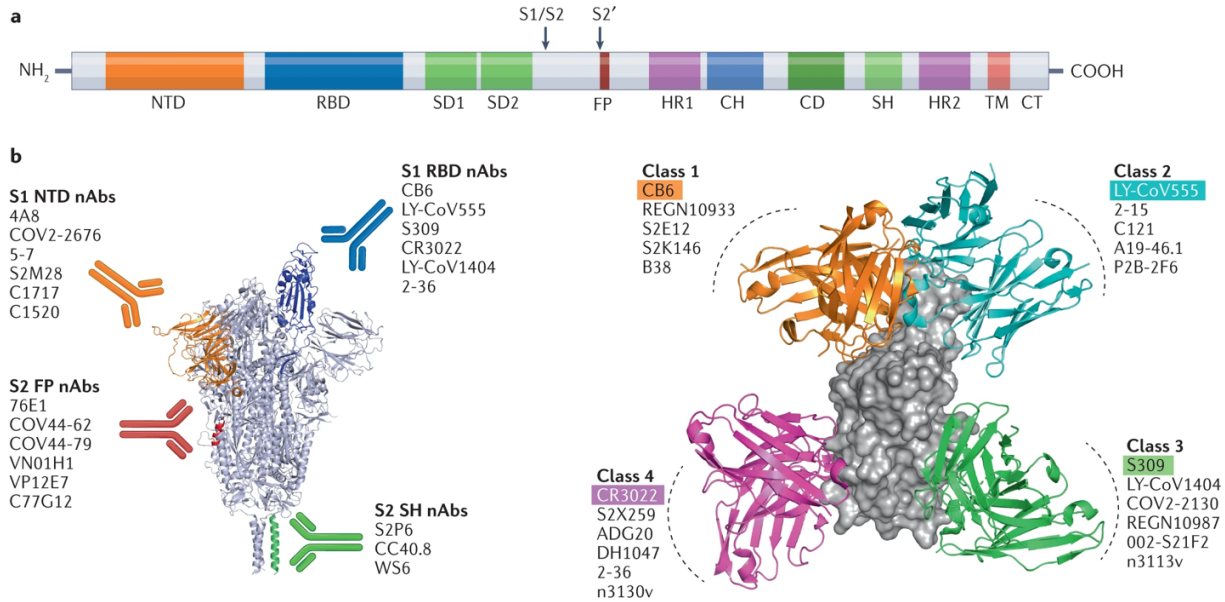

Figure 1.5. Schematic representing some epitope targets of neutralizing antibodies on the SARS-CoV-2 spike trimer.

Panel A: Different domains of the spike protein are denoted and color coded. **Panel B, left**: The ribbon structure of SARS-CoV-2 spike is depicted in the pre-fusion open conformation state (with one RBD up). NTD targeting mAbs shown in orange, in blue are RBD targeting mAbs, in red are fusion peptide targeting mAbs and in green are stem-helix targeting mAbs. This is not an exhaustive figure as it does not represent the entire antigenic landscape of spike (SD-1 targeting mAbs additionally contribute to the antibody response).
Panel B, right: Classification of neutralizing antibodies targeting the RBD and representative mAbs. Epitope targets and the Barnes et al (59, 120) RBD classification. Representative mAbs directed at each epitope denoted. For instance, the class 3 mAb, S309, ribbon structure is shown in green bound to a space-filled RBD structure in grey. Adapted from Chen et al. (111) with permission provided by Springer Nature and Copyright Clearance Center under license number: 5926600752165.

NTD targeting mAbs:

Within the NTD, there are five structural loops (N1–N5) that are targeted by neutralizing antibodies (121). In terms of neutralization, NTD targeting antibodies, in some cases, have similar neutralization potency as RBD-directed antibodies (121, 122). Structural studies of NTD Fab-bound spike particles showed structures where all RBD protomers were in a down confirmation, suggesting that NTDs act by locking RBD down in the closed conformation preventing viral attachment (109). Like the RBD, the NTD accumulates mutations across SARS-CoV-2 variants and is highly divergent across sarbecoviruses. In summary, while in some cases NTDs may match RBD neutralizing antibodies as far as potency, these epitopes are sites of immense variation and these mAbs marginally contribute to the plasma neutralizing response (104, 105).

RBD targeting mAbs:

Antibodies to different epitopes within the RBD arise after infection or vaccination (59, 104, 106, 120) (**Figure 1-5**). One of the earliest comprehensive RBD epitope classification came from structural studies of eight monoclonals antibodies isolated from SARS-CoV-2 convalescent individuals (59). Utilizing cryo-electron microscopy to resolve the Fab–RBD crystal structure, 4 RBD-classes were created to minimally overlapping epitopes. RBD class 1, which include the mAb REGN10933, recognize residues at the apex of the RBD when spike is in the prefusion “RBD-up” open conformation (123). LYCoV-555 is one example of a RBD class 2 mAb that can bind RBD in an “RBD -up or -down” confirmation (124). Both classes heavily overlap with the

ACE2 binding motif and thus can directly block RBD-ACE2 interaction. These mAbs also tend to be more potently neutralizing relative to other classes and other domain targeting antibodies due to their mechanism of neutralization, by directly blocking ACE2 engagement. A number of these class 1/2 (RBD-class 1 and 2 mAbs) potent neutralizing antibodies have advanced to clinical application, though they have lost activity against SARS-CoV-2 variants that have emerged (125). mAbs targeting these class 1/2 epitopes tend to be SARS-CoV-2 variant specific, as this interface is highly variable not only between SARS-CoV-2 variants but also across sarbecoviruses (87).

RBD class 3 and 4 mAbs target residues distal from the RBM in the RBD core, which are residues that are highly sequence conserved across sarbecovirus strains (60, 87, 126). As such, cross reactive class 3 and 4-directed mAbs have been isolated from both SARS-CoV-1 and SARS-CoV-2 convalescent individuals (112, 127–130). A notable example of a class 3 mAb is S309 (131), which was isolated from a SARS-CoV-1 individual but approved for treatment against SARS-CoV-2 due to its cross-neutralizing activity. Class 3 mAbs can bind the RBD in and up and down confirmation, whereas class 4 mAbs can only bind in the RBD down confirmation (59, 120). Meaning, class 4 mAbs may be subject to greater neutralization escape by conformational masking of epitopes exhibited by some SARS-CoV-2 variants (wherein some SARS-CoV-2 variants alter RBD up/down conformational dynamics and thus epitope accessibility) (60). Though, class 4 mAbs target cryptic sites in RBD that contacts other spike trimer regions in the closed RBD down conformation, suggesting they may be functionally constrained from evolving as substitutions may affect these interactions (132). As SARS-CoV-2 continued to evolve, most of these mAbs exhibited dramatic losses in neutralization activity meaning their epitopes are subject to antigenic drift (126, 133). Thus, while antibodies targeting class 3/4 epitopes may represent plausible broadly neutralizing antibodies across sarbecovirus clades, they display reduced neutralizing activity against SARS-CoV-2 variants.

Since the initial Barnes et al (59, 120) classification, RBD class 5 mAbs have been described that are incredibly resistant to SARS-CoV-2 antigenic drift and display broad

sarbecovirus cross-reactivity (87, 134, 135). These mAbs are targeting a cryptic region in the RBD core between class 3 and 4 mAbs that is accessible in the RBD up conformation. In the closed conformation, this region of the RBD would contact NTDs from a neighboring protomer in both SARS-CoV-2 and SARS-CoV-1 (134), meaning mutations in this region would be functionally constrained among sarbecovirus strains. RBD class 5 mAbs are a plausible component of a as therapeutic cocktail for pandemic preparedness because they are target functionally constrained regions on the RBD surface and have exhibited minimal reduction in neutralization activity across SARS-CoV-2 variants and sarbecoviruses.

Antibody epitope profiling:

Investigating the epitope specificity of antibodies is important for understanding the interactions occurring at the antibody-antigen interface and so I will briefly describe epitope profiling antibodies in the context of SARS-CoV-2. Structural characterization of antibody antigen binding domain (Fab) bound to SARS-CoV-2 spike trimer has allowed a greater appreciation of the structural correlates of SARS-CoV-2 neutralization and these structural epitopes led to the classification of four distinct RBD-directed antibody classes in the Barnes et al (59) classification. Piccoli et al (104) is another commonly cited classification based on structural characterization that proposed 6 epitope classes that largely overlap with the Barnes classification (136). In this thesis, we have used the Barnes et al (59) antibody epitope classification because multiple comparisons have been made between this classification schema and epitope profiling by deep mutational scanning (DMS) and generally there is strong agreement between sites of escape and contact sites identified by structural determination (87, 129, 137–139).

Epitope profiling using DMS of the RBD is one approach to define the epitopes involved in the functional properties of antibodies. In this approach, every possible single mutation in the SARS-CoV-2 RBD is displayed on yeast and antibody-protein interaction is assessed to identify the sites and specific amino acids that facilitate viral escape from antibody binding. Epitope profiling using DMS of the RBD has generally aligned well with contact residues identified by

structural studies (137, 139), though there is some overlap in escape profiles among the different RBD classes (87, 137). Yunlong Cao, in the labs of Youchun Wang and Xiaoliang Sunney Xie, performed DMS of thousands of mAbs isolated from SARS-CoV-2 and SARS-CoV-1 convalescent individuals providing insights into the contribution of antibodies directed at different RBD epitopes in different exposure histories (a feat that would be difficult to achieve with other techniques) (140–142). These antibody escape profiles have been useful for predictions of neutralization escape against emerging strains of SARS-CoV-2.

Selection experiments have also been conducted to identify escape mutations in the presence of mAbs and replication competent pseudotyped virus (143, 144). These escape mutations largely align with residues identified by structural studies and DMS (137, 145). However, selection experiments may not identify all the mutations revealed by DMS and can include stochastic mutations that only arise due to cell culture (146).

Collectively, these profiling techniques can offer amino acid level insights into the escape profiles and help predict the durability and failure of neutralizing antibodies.

1.6 Non-neutralizing Fc effector function of antibodies

In addition to neutralization, antibodies can also mediate non-neutralizing Fc-effector functions. The Fc-mediated effector function of spike-targeting antibodies has also been associated with protection against SARS-CoV-2 infection both after vaccination and infection in animal and human cohort studies (147, 148). Cohort studies have found that compromised Fc-effector responses to SARS-CoV-2 were significantly associated with increased mortality rates, with higher Fc effector functions observed in survivors (149). Fc effector function also correlated with improved disease outcomes in hospitalized individuals (147). In an 8-month study of convalescent individuals, spike targeting antibodies exhibited decreased neutralization titers while the Fc effector response antibody-dependent cellular cytotoxicity (ADCC) activity remained

relatively stable (150). Vaccination can also induced spike-binding antibodies that mediate robust ADCC (151).

In some cases, intact Fc effector function contributes to optimal protection afforded by neutralizing antibodies. This has been shown in animal models where intact Fc effector function of passively administered mAbs was required for optimal protection from lethal SARS-CoV-2 challenges (152–155).

Overall, the presence of binding antibodies and Fc-effector responses seems to be more stable to antigenic drift than neutralization activity against evolving SARS-CoV-2 overtime (156). Thus, eliciting antibodies that target more conserved regions in RBD for optimal neutralization activity and that exhibit Fc-effector functions might offer insights into achieving durable immunity.

1.7 Affinity maturation of the antibody response and vaccine boosters

Since its emergence in 2019, SARS-CoV-2 has rapidly evolved throughout the course of the pandemic, accumulating mutations throughout the spike glycoprotein. This has been described as waves of variants, with the Delta variant emerging in India and becoming dominant in late 2020, followed by Omicron in South Africa, which emerged in late 2021 (157). These SARS-CoV-2 variants harbor numerous mutations throughout the spike protein, some of which have been linked to increased replication efficiency, altered viral transmissibility (due in part to altered ACE2 affinity), and immune evasion from elicited and therapeutic antibodies (13, 125, 133, 158, 159). For instance, compared to the ancestral strain (Wuhan-Hu-1) and early lineages (Kappa variant) of SARS-CoV-2, the Delta variant exhibited increased replication rate and reduced susceptibility *in vitro* to neutralizing antibodies in sera from infection and vaccinated individuals (157). This may have contributed to altered transmissibility of the Delta variant as it outcompeted pre-existing lineages, like the Kappa variant, in India despite high a prevalence of prior infection and vaccination (157).

Among Omicron variants, a number of mutations have been identified that increase ACE2 affinity, such as mutations at site 493, and have been linked to reduction in neutralization activity by infection and vaccine elicited sera (160). Likewise, mutations that negatively impact the ability of RBD to bind human ACE2 (161–164), such as mutations at site 505 and 417, have also been found to contribute to immune evasion (125, 160). Variants with these mutations may be predicted to have lower infectivity yet, other Omicron mutations have been found that promote ACE2 binding and compensate for these negative effects (125, 160, 165). Thus, numerous mutations have been identified that collectively contribute to increased immune evasion of Omicron variants and subvariants while also increasing viral fitness (125, 140, 166).

A major concern against SARS-CoV-2 continuing to acquire mutations is that pre-Omicron vaccination and infection elicited sera have greatly reduced neutralization titers against emerging highly mutated variants like Omicron, which may lead to SARS-CoV-2 reinfections (141, 142). However, repeated exposure by vaccination or infection (in particular exposure to Omicron) is able to increase neutralization activity against Omicron variants (140, 167–169). The strong immune evasion displayed by recent Omicron Variants (subvariants of XBB, JN.1 and KP.3 variants) highlights the need for updated vaccine boosters and isolation of neutralizing antibodies that could serve as therapeutics (170).

One important aspect of vaccine boosting and selecting the optimal vaccine antigen is antigenic distance and immune imprinting (171). Antigenic distance is a measure of antigen recognition (can be determined by neutralization titer), and is a useful metric for interpreting immune imprinting, which is when prior antigen exposure negatively affects responses to a second exposure (172). This antigenic distance metric has been used to interpret the variable efficacies of influenza vaccine formulations (172). One strategy to overcome immune imprinting is to vaccinate with an antigenically distant strain (173) as this more likely to re-activate memory B cells against conserved epitopes. In the context of animal models, animals that are vaccinated with ancestral spike and then boosted with a SARS-CoV-2 Omicron variant (XBB) spike have

enhanced neutralization titers against Omicron variants compared to animals vaccinated with ancestral spike and then boosted with Omicron BA5 (167). This difference in elicited neutralization titers between Omicron BA5 and XBB boosting could be because there is greater antigenic divergence from the ancestral spike to Omicron XBB than to Omicron BA5 that may aid in overcoming immune imprinting (171). Enhancement of neutralizing titers have also been observed in cohort studies after vaccination with updated vaccines (167, 174).

Omicron antigen exposure by infection elicited higher levels of broadly-reactive (defined here as reactive against multiple SARS-CoV-2 variants) memory B cells in Omicron breakthrough infections compared to multiple exposures of early strains of SARS-CoV-2 (non-Omicron) (140, 175). Additionally, multiple Omicron breakthrough infections elicited higher neutralization titers than a single Omicron breakthrough infection (140, 167). In these contexts, broadly-reactive mAbs elicited in repeat Omicron breakthrough infections elicited higher levels of somatic hypermutation (SHM) compared to a single Omicron BTI (167). Thus, in the context of repeat and diverse antigen exposure, affinity maturation of the B cell repertoire can contribute to enhanced neutralization activity. However, few studies have looked at the affinity maturation of B cell lineages after repeated antigen exposure to SARS-CoV-2 (176) to understand how antibodies evolve overtime and what affect this has on functional properties. Understanding the affinity maturation of monoclonal antibodies in the face of repeated exposure could inform the development of next-generation vaccines and the isolation of broad mAbs.

1.8 Thesis Overview

The continued emergence of SARS-CoV-2 variants and the possibility of future SARS-like sarbecoviruses spill over events underscores the need to understand how antibodies maintain breadth and cross react with these viruses and identify broad-spectrum therapeutics. Capacity to tolerate mutations displayed by coronaviruses like SARS-CoV-2 demonstrates the adaptability and large mutational space of the spike protein while maintaining critical viral functions like ability

to properly fold and bind the host receptor. This capacity to tolerate mutations presents significant hurdles in developing a broadly protective vaccine and identification of durable neutralizing antibodies. We sought to identify antibodies targeting conserved sarbecovirus spike epitopes with the hypothesis that cross-reactive mAbs may inform functionally constrained epitopes.

In chapter 2, we demonstrate that neutralizing antibodies can provide valuable insight into the epitopes of cross-reactive antibodies and potential sites of vulnerability of the sarbecovirus spike protein. We provide a comprehensive functional characterization of cross-reactive antibodies against a panel of sarbecovirus antigens and pseudoviruses. To understand the evolution of the antibody response after additional exposure to SARS-CoV-2, we isolated and characterized mAbs from longitudinal samples (chapter 3), some of which are clonal to neutralizing antibodies isolated at an earlier time point (chapter 2). We identified clonal mAbs that exhibited increased levels of SHM and enhanced neutralization activity. We also modified our antibody isolation approach to select for cross-reactive antibodies using diverse spike antigens and successfully identified a broadly-reactive neutralizing antibody that is highly potent against all sarbecoviruses tested. Meaning this strategy could be applied in other exposure contexts, such as more recently circulating Omicron variants, to discover additional cross-reactive antibodies against evolving viruses. Among them, we identified mAbs targeting conserved regions across sarbecovirus clades that can neutralize human and animal sarbecoviruses.

In summary, the following chapters describe the characterization of antibodies elicited in different antigen exposure contexts targeting conserved RBD regions across SARS-CoV-2 variants and sarbecoviruses that can serve as therapeutics for pandemic preparedness as well as blueprints for the design of immunogens capable of eliciting cross-neutralizing responses.

Chapter 2:

Delineating the functional activity of antibodies with cross-reactivity to SARS-CoV-2, SARS-CoV-1 and related sarbecoviruses

The text in this chapter was adapted from (135). Sections of text in this chapter have been modified from the following manuscript:
Felicitas Ruiz^, Will Foreman^, Michelle Lilly, Viren A. Baharani, Delphine M. Depierreux, Vrasha Chohan, Ashley L. Taylor, Jamie Guenthoer, Duncan Ralph, Frederick A. Matsen IV, Helen Y. Chu, Paul D. Bieniasz, Marceline Côté, Tyler N. Starr, Julie Overbaugh. Delineating the functional activity of antibodies with cross-reactivity to SARS-CoV-2, SARS-CoV-1 and related sarbecoviruses. PLoS Pathog. 2024 Oct 28;20(10):e1012650. doi:10.1371/journal.ppat.1012650. eCollection 2024 Oct.

^Co-contributors.

I lead antibody isolation, the functional studies, including binding and neutralization assays, data interpretation and wrote the manuscript. Will Foreman performed the RBD DMS profiling, yeast-display pan-sarbecovirus binding assay and Alphafold predictions.

ABSTRACT

The recurring spillover of pathogenic coronaviruses and demonstrated capacity of sarbecoviruses, such SARS-CoV-2, to rapidly evolve in humans underscores the need to better understand immune responses to this virus family. For this purpose, we characterized the functional breadth and potency of antibodies targeting the receptor binding domain (RBD) of the spike glycoprotein that exhibited cross-reactivity against SARS-CoV-2 variants, SARS-CoV-1 and sarbecoviruses from diverse clades and animal origins with spillover potential. One neutralizing antibody, C68.61, showed remarkable neutralization breadth against both SARS-CoV-2 variants

and viruses from different sarbecovirus clades. C68.61, which targets a conserved RBD class 5 epitope, did not select for escape variants of SARS-CoV-2 or SARS-CoV-1 in culture nor have predicted escape variants among circulating SARS-CoV-2 strains, suggesting this epitope is functionally constrained. We identified 11 additional SARS-CoV-2/SARS-CoV-1 cross-reactive antibodies that target the more sequence conserved class 4 and class 5 epitopes within RBD that show activity against a subset of diverse sarbecoviruses with one antibody binding every single sarbecovirus RBD tested. A subset of these antibodies exhibited Fc-mediated effector functions as potent as antibodies that impact infection outcome in animal models. Thus, our study identified antibodies targeting conserved regions across SARS-CoV-2 variants and sarbecoviruses that may serve as therapeutics for pandemic preparedness as well as blueprints for the design of immunogens capable of eliciting cross-neutralizing responses.

AUTHOR SUMMARY

There is a large collection of sarbecoviruses related to SARS-CoV-2 circulating in animal reservoirs with the potential to spillover into humans. Neutralizing antibodies have the potential to protect against infection, although viral escape is common. In this study, we isolated several monoclonal antibodies that show broad activity against different sarbecoviruses. The antibodies target epitopes in the core of the receptor binding domain that are highly conserved in sequence across sarbecoviruses and emerging SARS-CoV-2 variants. One antibody showed remarkable breadth against both SARS-CoV-1 variants as well as diverse sarbecoviruses. The results of deep mutational scanning suggest that mutations at these predicted sites of escape may functionally constrain viral fitness. Our functional profiling of cross-reactive antibodies highlights vulnerable sites of sarbecoviruses, with some antibodies poised as broadly neutralizing candidates for therapeutic use against future sarbecovirus emergence.

INTRODUCTION

In the past two decades, zoonotic betacoronaviruses, most notably SARS-CoV-1 and SARS-CoV-2 (sarbecoviruses), have infected humans and caused large-scale outbreaks with

significant associated morbidity and mortality (1–3, 5). Humans are permissive to many members of the sarbecovirus family because they encode a functional cellular receptor that permits viral entry. Both SARS-CoV-1 and SARS-CoV-2 initiate entry by binding to the angiotensin-converting enzyme 2 (ACE2) receptor via the receptor-binding domain (RBD) in the spike glycoprotein (8, 71). Many bat sarbecoviruses that utilize human ACE2 for entry *in vitro* have been identified through epidemiological surveillance of animal reservoirs in East and Southeast Asia, suggesting the potential for more introduction of sarbecoviruses into humans (25, 67–69, 177). Most bat isolates from Africa and Europe cannot infect human cells and exhibit more narrow host species ACE2 usage (68, 75). Recently, one of these clade 3 sarbecovirus has been found to utilize human ACE2 to infect cells, and human ACE2-independent clade 3 sarbecoviruses can acquire mutations that permit binding to human ACE2 with just two substitutions thus potentially broadening their host cell range to include humans as well (68, 88). The COVID-19 pandemic has demonstrated the ability of the SARS-CoV-2 RBD to tolerate mutations (161, 163), and evidence of recombinants (79) highlights the diversity of RBD that can be generated within a single sarbecovirus lineage that has circulated in the human population in just a few years. The large number of sarbecoviruses in animal reservoirs that can use the human ACE2 receptor for entry, coupled with the pathways for diversity and mutational tolerance among these viruses, underscores the urgent need to understand the immune responses that may be useful for eliciting in future spillover events.

Because of its role in viral entry, the RBD is a major target of neutralizing antibodies and many RBD-specific monoclonal antibodies (mAbs) have been characterized, providing insights into the major antigenic sites in the SARS-CoV-2 RBD (59, 104, 106, 178). Several of the potent neutralizing mAbs identified to date target residues overlapping the ACE2 footprint (receptor binding motif; RBD class 1/2 mAbs based on Barnes et al (59) classification) and directly interfere with RBD-ACE2 binding (133, 179). However, this binding interface is highly variable not only within the SARS-CoV-2 lineage but also across more diverse sarbecoviruses; thus class 1/2

mAbs typically show limited breadth against SARS-CoV-2 variants and limited cross-reactivity against other sarbecoviruses (87, 180, 181). In contrast, neutralizing antibodies that target the RBD core (class 4-5) target regions with high sequence conservation, which is thought to be driven by functional constraints in this region (134, 182). These antibodies have been found to exhibit breadth in binding and neutralization across SARS-CoV-2 variants as well as some cross-reactive activity against animal sarbecoviruses indicating that broadly active RBD-targeting mAbs can be elicited by SARS-CoV-2 infections (87, 129, 131, 133, 183). However, few mAbs with cross-reactivity across the diverse classes of sarbecoviruses have been comprehensively characterized despite the potential utility of these for future spillover events (87, 112, 129–131, 183, 184).

mAbs that cross-react with diverse sarbecoviruses have been isolated from both SARS-CoV-1 and SARS-CoV-2 infected individuals (87, 112, 129–131, 183–185). S309, which is a class 3 neutralizing mAb isolated from a SARS-CoV-1 infected individual (131), previously received emergency authorization for the treatment of SARS-CoV-2 infection (186). S309 not only showed neutralizing activity, but also the ability to kill infected cells via antibody-dependent cellular cytotoxicity (ADCC), and both neutralization and ADCC have been implicated in protection from infection and disease progression (154, 187). Several class 4 cross-reactive mAbs have demonstrated protection against SARS-CoV-2 in animal models (129, 184, 188) although they have more limited clinical value because they show reduced breadth across SARS-CoV-2 variants (127, 189). One class 5 mAb, S2H97, which has broad neutralization activity against SARS-CoV-2 Omicron variants and some animal sarbecoviruses, showed protection against SARS-CoV-2 challenge in animal models (87). Studies have suggested that S2H97 class 5-like mAbs contribute to less than ~17% of infection- and vaccine-elicited antibody responses and are thus understudied (140, 142).

We previously described a class 5-like neutralizing antibody C68.61, isolated from an individual with a Delta breakthrough infection, that binds a conserved epitope in the core of RBD

and demonstrates neutralization breadth across SARS-CoV-2 variants as well as cross reactivity with SARS-CoV-1 (112). In this study, we demonstrate cross-reactivity of the C68.61 mAb across sarbecovirus clades and show that it is refractory to viral escape both in cell culture and in nature. We further isolate additional mAbs from this individual, including several class-4 and class-5 RBD-specific mAbs that display neutralization activity across multiple sarbecoviruses in an *in vitro* pseudovirus neutralization assay. One such mAb, C68.185, displayed extensive binding and retained potent neutralization across tested bat-derived sarbecoviruses. Some mAbs also displayed potent ADCC activity in-line with the activity of therapeutic antibodies shown to reduce SARS-CoV-2 viral load in animal models (154). Taken together, these cross-reactive mAbs with differential functional activity and distinct epitope footprints in the RBD may contribute to pan-coronavirus pandemic preparedness and inform vaccine efforts.

RESULTS

Isolation of C68 cross-reactive antibodies targeting the RBD

We previously reported the identification of four potent neutralizing mAbs from an individual (C68) at 30 days after a SARS-CoV-2 Delta breakthrough infection, three were directed to epitopes in the RBD and the fourth to an epitope in SD1 (112). These mAbs were reconstructed from memory B cells that bound the SARS-CoV-2 Delta prefusion-stabilized spike trimer and/or the Wuhan-Hu-1 S2 spike subunit. To explore the range of RBD cross-reactive neutralizing antibodies elicited in this Delta breakthrough infection case, in this study we recovered additional antibodies from this 30-day post-infection time point. We identified 42 antibodies that bound the SARS-CoV-2 spike trimer and RBD protein in an enzyme-linked immunosorbent assay (ELISA). All C68 antibodies bound the SARS-CoV-2 Wuhan-Hu-1 (WH-1) vaccine strain trimer and RBD subunit to comparable levels (**Figure 2.1A, C**) when tested at a fixed concentration (500 ng/ml) and to higher levels than the negative control Fl6v3 (190), an influenza-specific mAb. Of the newly isolated C68 antibodies, we identified 11 additional antibodies that exhibited cross-reactive binding between SARS-CoV-2 and SARS-CoV-1 (**Figure 2.1A, C**). Ten of the 11 (91%) cross-

reactive mAbs exhibited binding activity against the SARS-CoV-2 Omicron XBB trimer; in contrast, a much smaller fraction (3 of 31; 10%) of the SARS-CoV-2 specific mAbs retained binding activity against the Omicron XBB trimer.

A

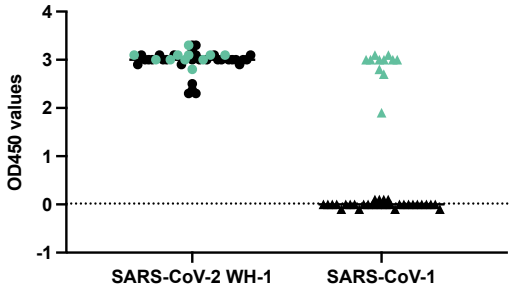

B

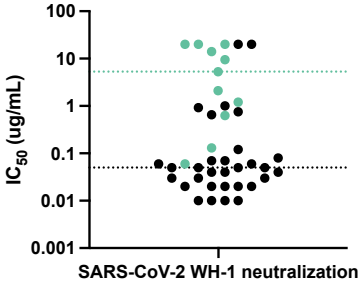

C

		Binding activity (OD450 nm)				Neutralization (IC50 ug/ml)	Gene family characteristics							
	mAb	SARS-CoV-2 WH-1 RBD	SARS-CoV-2 WH-1 trimer	SARS-CoV-2 XBB trimer	SARS-CoV-1 trimer	SARS-CoV-2 WH-1	% SHM VH	VH gene	D gene	J gene	% SHM VL	VL gene	J gene	Clonal family
SARS-CoV-2 specific mAbs	C68.10	3.2	3.0	3.1	0.0	0.92	3.4	V5-51	D3-10	J4	2.3	LV3-19	J2	1
	C68.15	3.2	3.2	0.0	0.0	0.05	4.3	V3-66	D3-10	J4	1.5	KV1-9	J5	2
	C68.17	3.2	3.3	0.0	0.0	0.02	2.6	V4-34	D1-7	J4	2.2	KV1-NL1	J1	3
	C68.34	3.1	3.0	0.0	0.0	0.04	1.2	V4-34	D3-16	J5	3.7	KV1-NL1	J4	4
	C68.62	3.2	3.0	0.0	0.1	0.05	3.4	V3-53	D5-18	J4	0.6	KV1-9	J2	5
	C68.69	3.2	3.0	0.0	0.1	0.02	2.1	V5-10	D5-24	J6	2.2	KV3-15	J4	6
	C68.78	2.2	3.0	0.0	0.0	>20	3.3	V1-2	D6-19	J4	2.6	KV2-40	J5	7
	C68.79	3.2	3.1	0.0	0.0	0.01	3.2	V1-58	D2-2	J3	2.5	KV3-20	J1	8
	C68.233	3.2	2.9	0.0	0.0	0.01	3.5				2.2			
	C68.86	3.2	3.3	0.0	0.0	0.02	2.8	V2-70	D6-19	J4	1.2	KV1D-39	J1	9
	C68.98	3.2	3.1	0.0	0.1	0.04	3.7	V3-66	D1-26	J3	1.5	KV1-9	J1	10
	C68.99	3.2	3.0	2.9	0.0	0.06	2.9	V3-23	D3-22	J1	1.9	KV1-12	J1	11
	C68.100	2.8	2.3	0.0	0.0	>20	3.5	V5-10-1	D3-10	J4	1.6	KV1D-39	J2	12
	C68.102	3.1	3.0	0.0	0.0	0.02	4.0	V4-39	D2-2	J4	1.3	KV1-NL1	J1	13
	C68.123	3.1	3.0	0.0	0.0	0.03	2.7	V3-64	D3-3	J4	1.3	KV1-5	J1	14
	C68.136	3.1	3.0	0.0	0.0	0.05	2.5	V3-23	D2-21	J6	2.5	KV1-33	J4	15
	C68.138	3.1	2.9	0.0	0.0	1.0	2.2	V5-10-1	D4-17	J5	4.0	KV1D-39	J2	16
	C68.170	3.2	3.0	0.0	0.0	0.07	3.2	V4-31	D6-13	J4	4.1	KV1-33	J4	17
	C68.180	3.1	3.0	0.0	0.0	0.03	3.6	V3-11	D5-18	J4	2.2	KV1-33	J4	18
	C68.194	3.1	3.0	0.0	0.0	0.02	4.1	V1-3	D1-26	J4	0.6	KV1-5	J1	19
	C68.220	3.1	3.0	0.0	-0.1	0.08	3.0				1.2			
	C68.201	3.1	3.0	3.1	0.0	0.75	3.2	V5-51	D1-26	J3	1.5	LV1-44	J1	20
	C68.225	3.1	3.2	0.0	-0.1	0.07	2.9	V5-10	D6-13	J5	1.3	KV1-5	J2	21
	C68.236	3.2	2.9	0.0	0.0	0.05	2.2	V1-3	D1-26	J4	0.9	KV1-5	J1	22
	C68.256	2.1	2.5	0.0	0.0	0.06	3.3	V4-39	D3-10	J4	1.2	LV2-23	J2	23
	C68.263	3.1	3.1	0.0	-0.1	0.03	3.4	V3-30	D3-22	J4	1.6	KV1-5	J1	24
	C68.279	3.1	3.1	0.0	-0.1	0.12	3.3	V5-51	D5-5	J4	2.1	KV4-1	J4	25
	C68.281	3.2	3.1	0.0	0.0	0.01	3.8	V1-46	D5-5	J4	1.3	KV3-20	J1	26
	C68.285	3.2	3.1	0.0	0.0	0.01	2.0	V1-46	D5-24	J4	0.9	KV1-9	J4	27
	C68.286	2.5	2.3	0.0	0.0	0.65	1.7	V2-70	D6-19	J4	1.6	KV1D-39	J2	28
	C68.304	3.1	3.0	0.0	0.1	0.04	4.2	V3-30	D3-10	J4	1.8	LV8-61	J3	29
Cross-reactive mAbs	C68.83	3.2	3.1	3.0	3.1	0.63	2.8	V3-30	D2-15	J6	4.6	LV3-25	J2	30
	C68.88	3.2	3.3	0.0	2.8	0.13	3.6	V4-39	D3-3	J4	2.2	LV6-57	J2	31
	C68.121	3.2	3.1	3.1	1.9	>20	5.4	V3-11	D3-3	J6	2.5	LV3-25	J2	32
	C68.175	3.1	3.0	3.1	3.1	2.1	1.1	V3-23	D1-1	J4	0.3	KV1-5	J4	33
	C.68 183	3.1	3.1	3.0	3.0	>20	3.3	V3-23	D1-26	J4	1.2	KV1-5	J2	34
	C68.185	3.1	3.1	3.1	3.0	9.5	6.0	V1-46	D4-17	J5	3.1	KV3-11	J2	35
	C68.200	3.1	3.1	3.1	3.0	>20	3.1	V3-23	D1-1	J4	0.9	KV1-5	J5	36
	C68.203	3.2	3.0	3.1	3.0	14	3.0				0.9			
	C68.239	3.2	3.0	0.0	2.7	0.06	1.8	V3-23	D2-2	J2	3.0	LV3-21	J3	37
	C68.327	3.1	2.8	3.1	3.0	5.3	1.7	V3-23	D1-26	J5	1.6	KV1-12	J5	38
	C68.348	3.1	3.0	3.1	3.0	1.2	3.4	V4-4	D6-13	J4	2.1	LV2-14	J1	39

Binding activity (OD450 nm)	
0 to 0.4	
0.5 to 1.4	
1.5 to 2.5	
> 2.5	

Neutralization (IC50)	
>20 (No activity)	
5.0-20	
0.50-4.9	
0.05-.49	
0.01-0.04	

Figure 2.1. Identification and molecular characteristics of SARS-CoV-1 and SARS-CoV-2 cross-reactive mAbs.

(A) C68 mAbs binding to SARS-CoV-2 or SARS-CoV-1 recombinant spike glycoprotein by ELISA (OD450nm values). C68 antibodies that bound SARS-CoV-2 trimer and SARS-CoV-1 trimer (designated by green closed circles; SARS-CoV-2 trimer-specific mAbs shown in black closed circles). Antibodies tested at 500 ng/ml, represents the average of two technical replicates shown as background-corrected OD450nm values. Dotted line represents 3 standard deviations above the negative control Fl6v3, (190) an influenza-specific mAb. **(B)** Neutralization of spike-pseudotyped lentiviruses by C68 mAbs against SARS-CoV-2 WH-1. C68 antibodies that bound SARS-CoV-2 trimer and SARS-CoV-1 trimer are indicated (in green). IC50 values (μg/mL) were calculated by nonlinear regression analysis in the statistical software package PRISM from at least two independent experiments. Black dotted line represents the median IC50 value for the SARS-CoV-2 specific mAbs. Green line represents the median IC50 value for the cross-reactive mAbs. **(C)** Summary table representing gene family usage, somatic hypermutation percent (% SHM relative to germline), and a heatmap of functional activity of C68 mAbs. OD450 values indicate absorbance at OD450nm values where each mAb was tested at 500 ng/ml from technical replicates and background-corrected.

We next assessed the neutralization potencies of both SARS-CoV-2-specifc and cross-reactive mAbs using a pseudovirus-based neutralization assay with spike-pseudotyped lentiviruses and HEK293T-hACE2 expressing target cells (76). We calculated the 50% inhibitory concentration (IC50) values for all 42 mAbs and observed variation in neutralizing activities against the SARS-CoV-2 WH-1 pseudovirus, ranging from an IC50 of 0.01 to >20 μg/mL (**Figure 2.1C**). Generally, SARS-CoV-2 specific mAbs were more potent neutralizers (median IC50 = 0.05 μg/mL; IC50 range 0.01 μg/mL to >20 μg/mL) than cross-reactive mAbs (median IC50 = 5.3 μg/mL; IC50 range 0.06 μg/mL to >20 μg/mL; **Figure 2.1C**).

We next evaluated the genotypic properties of these mAbs, including somatic hypermutation (SHM), V(D)J gene usage and clonal diversity. We used partis, a computational tool designed to assess levels of SHM using a distance-based clustering on the inferred naive sequence, along with a hidden Markov model to infer clonality (191, 192). There was a high degree of clonal diversity among these 42 mAbs with antibodies representing 39 clonal lineages (**Figure 2.1C, S2.1 Fig; S2.1 Table**). Low levels of SHM were observed among SARS-CoV-2-

specific and cross-reactive mAbs (geomean 2.9% and 3.3% SHM relative to germline in the heavy chain genes, respectively). We observed overrepresentation of V_H3-23 among cross-reactive mAbs, and this has been shown to be a common gene family elicited from COVID-19 convalescent individuals (193–196).

Cross-reactive mAbs exhibit binding across SARS-CoV-2 variants and human and animal sarbecoviruses

To determine whether the 11 newly identified cross-reactive mAbs that bound both SARS-CoV-1 and SARS-CoV-2 exhibited breadth across SARS-CoV-2 variants, we tested binding to various recombinant SARS-CoV-2 spike proteins. C68.61, one of the RBD-specific mAbs described in our prior study that showed consistent activity against SARS-CoV-2 variants as well as SARS-CoV-1 (112) was included in this study for a total of 12 cross-reactive C68-derived mAbs. All twelve antibodies bound SARS-CoV-2 WH-1 and the Delta spike proteins with half-maximal effective concentrations (EC50s) ranging from 6 to 21 ng/mL and 5 to 28 ng/ml, respectively (**Figure 2.2A, S2.2 Fig**). Of these, 10 out of 12 mAbs, including C68.61, retained similar binding breadth across SARS-CoV-2 variants, including Omicron XBB and BQ.1.1 variants (EC50s 9 to 45 ng/ml and 11 to 62 ng/ml; **Figure 2.2A, S2.2 Fig**); only two mAbs, C68.88 and C68. 239, did not bind Omicron variants. Together, these 12 mAbs bound SARS-CoV-1 spike glycoprotein with EC50s ranging from 12 to 237 ng/ml (**Figure 2.2A**), with 10 mAbs displaying EC50s less than 25 ng/ml, which is comparable to what has previously been reported for the SARS-CoV-1 cross-reactive mAb S309 (112).

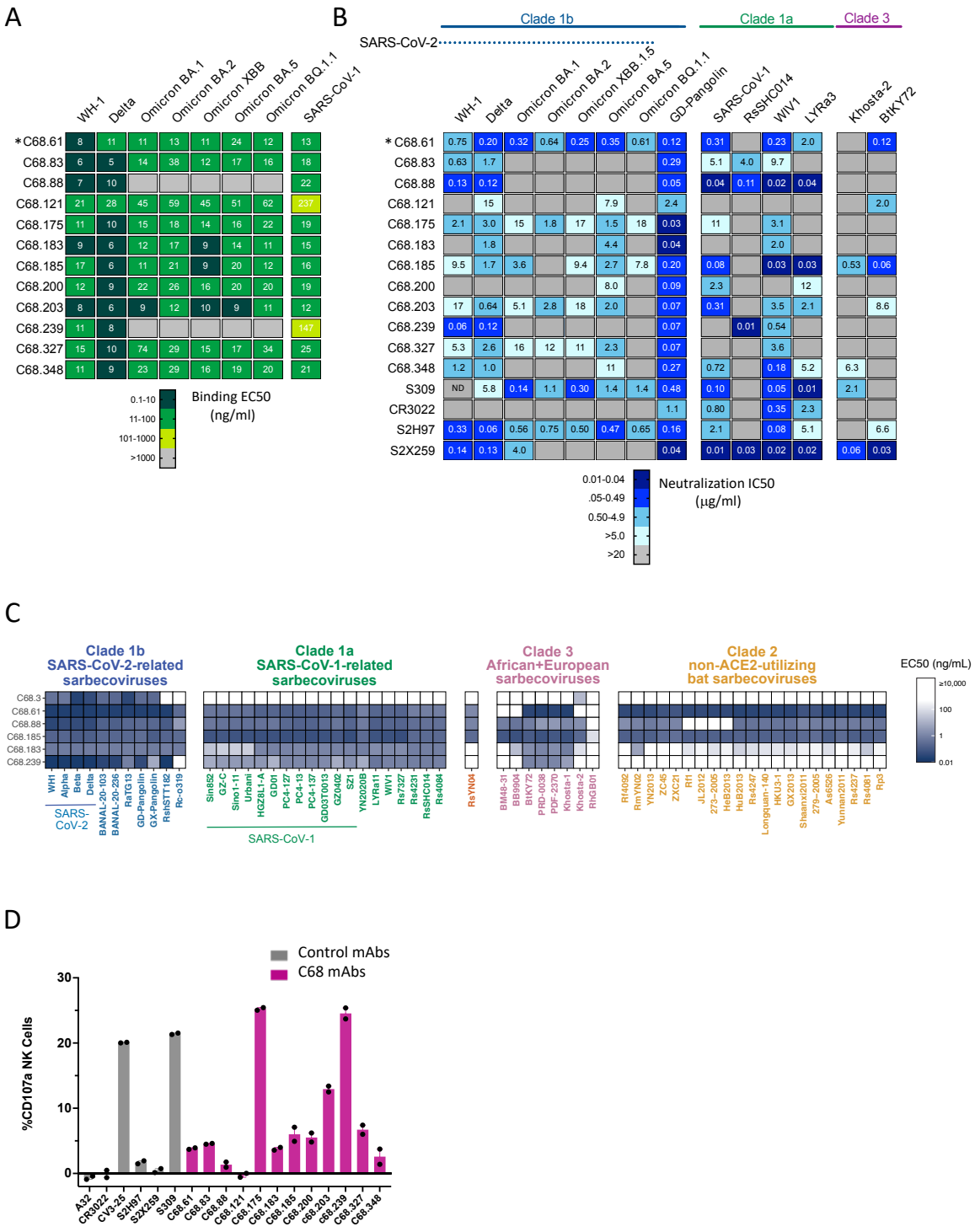

Figure 2.2. Comprehensive functional characterization of C68 cross-reactive mAbs.

(A) C68 mAbs binding to SARS-CoV-2 variants and SARS-CoV-1 recombinant spike glycoprotein by ELISA (OD450nm values). Half-maximal effective concentrations (EC50 values) calculated by nonlinear regression analysis from at least two independent replicates. *Binding activity for

C68.61 from (112). **(B)** SARS-CoV-2 variants and sarbecovirus neutralization activity. IC50 values (μg/mL) were calculated by nonlinear regression analysis from at least two independent experiments with technical replicates. Samples with IC50 values above 20 μg/mL were plotted at 20 μg/mL (no activity). *Neutralization activity for C68.61 and S309 against SARS-CoV-2 variants and SARS-CoV-1 from (112). S309 neutralizing activity against WH-1 was not determined (ND). **(C)** Pan-sarbecovirus RBD binding of select mAbs. Each antibody (row) was experimentally measured for binding to each sarbecovirus RBD (column) via a multiplexed FACS-seq titration assay with a yeast-display library of sarbecovirus RBDs. EC50 (ng/ml) value represents the geometric mean across internally replicated barcodes within the library linked to the same sarbecovirus RBD. **(D)** C68 mAbs can mediate antibody dependent cellular cytotoxicity. Cells expressing SARS-CoV-2 D614G spike cells were incubated with C68 mAbs and effector cells (PBMC) for 4h. NK cell degranulation (% CD107a+) was measured as a proxy for ADCC. The assay was run in technical duplicate with two independent PBMC donors. Background subtracted values (target cells + PBMC only) from a single donor are shown.

Using the pseudovirus-based neutralization assay described above, we assessed the neutralizing potencies of these cross-reactive mAbs against a panel of SARS-CoV-2 variants and bat SARS-like sarbecovirus strains known to utilize human ACE2 to infect cells: Pangolin GD, WIV1, RsSHC014, LYRa3 (67). WIV-1 and LyRa3 are 96% and 95% sequence similar to SARS-CoV-1 (Urbani strain) RBD whereas Pangolin GD is closely related to SARS-CoV-2 WH-1 (96% sequence similarity to RBD; **S2.3A Fig**). Among the SARS-CoV-1 related bat-derived isolates, RsSHC014 shares 82% amino acid similarity in the RBD to SARS-CoV-1 and 77% similarity to SARS-CoV-2 WH-1 RBD. We also examined neutralization against two representative clade 3 viruses that have been shown to utilize human ACE2 to infect cells *in vitro*, including Khosta-2 and the BtKY72 (K493Y/T498W mutant that confers human ACE2 binding) which share 70% and 74% similarity to SARS-CoV-1 (68, 69). We included four previously described cross-reactive mAbs with functionally defined properties and epitopes for comparison: S309, S2H97, S2X259 and CR3022 (87, 128, 131, 133).

C68.61, which was previously described as having breadth against SARS-CoV-2 variants ((112) and **Figure 2.2B**), also showed breadth against SARS-CoV-1-related sarbecoviruses WIV1 (IC50s 0.23 μg/mL) and LyRa3 (IC50s 2.0 μg/mL) (**Figure 2.2B**). C68.61 did not neutralize the more sequence divergent RsSHC014. We further examined neutralization against the more distantly-related clade 3 sarbecoviruses Khosta-2 and the BtKY72 (68, 69). C68.61 neutralized BtKY72 at an IC50 of 0.12 μg/mL but did not neutralize Khosta-2. S2H97 (129), which partially overlaps the epitope escape profile of C68.61 defined by deep mutational scanning (DMS) (112), exhibited similar cross-neutralization but reduced potency against more diverse sarbecoviruses tested in parallel.

Among the 11 other newly isolated cross-reactive C68 mAbs, we observed limited breadth and potency against SARS-CoV-2 Omicron variants. These 11 mAbs had geometric mean IC50s ranging from 4.2 to 18 μg/mL among SARS-CoV-2 viruses (**S2.3B Fig**). Among animal sarbecovirus strains, all mAbs tested were able to potently neutralize Pangolin-GD, which is highly similar in sequence to SARS-CoV-2 WH-1 RBD and is generally an easy to neutralize SARS-CoV-2-related strain, with IC50s ranging from 0.03 to 2.4 μg/mL (**Figure 2.2B**). Seven of these eleven mAbs neutralized SARS-CoV-1 with IC50s ranging from 0.04 to 11 μg/mL. Several of these mAbs also neutralized various clade 1a viruses, including some mAbs that did not neutralize SARS-CoV-1, such as C68.239. Most notably, C68.88 neutralized all four SARS-CoV-1-related viruses tested (IC50s ranging from 0.02 to 0.11 μg/mL), which was similar to some of the most potent cross-reactive mAbs described to date, such as S2X259 (130) and S309 (131, 179) tested here in parallel. C68.185 also showed similar potency against select SARS-CoV-1-related strains as S309, and neither neutralized RsSHC014 (60, 112). C68.239 neutralized RsSHC014 with IC50 of 0.01 μg/mL, effectively complementing the activity of C68.185 against clade 1a viruses. There was more limited activity against clade 3 viruses among these 11 mAbs; only C68.185 neutralized both Khosta-2 and BtKY72.

Thus, this complete set of 12 cross-reactive mAbs identified from C68 included examples with: 1) activity against nearly all SARS-CoV-1 and SARS-CoV-2 variants tested (C68.61), 2) activity against all SARS-CoV-1 clade 1a variants, but limited breadth against SARS-CoV-2 (C68.88) and 3) potent activity against select non-SARS-CoV-2 sarbecoviruses (C68.185 and C68.239). While C68.61 showed the greatest overall breadth against the full virus panel tested (neutralization of 12/14 viruses tested with geometric mean IC50 across the 12 viruses of 0.62 μg/mL; **S2.3C Fig**), the previously described S2X259 showed breadth against SARS-CoV-1-related viruses (geomean IC50 of 0.32 μg/mL against human and animal sarbecovirus strains), although it loses neutralization activity against the SARS-CoV-2 Omicron variants as previously described (130, 133).

Exceptional binding breadth of C68 mAbs across sarbecoviruses

Given the cross neutralization profiles we observed for some mAbs, we explored the extent of their cross reactivity using a yeast library displaying diverse sarbecovirus RBD proteins from across the known evolutionary clades (87). The clades, which were defined based on phylogenetic classification of their RBD sequence, share ~62-96% sequence similarity to SARS-CoV-2 RBD (87). We tested four mAbs displaying high cross-neutralization activity (C68.61, C68.88, C68.185, and C68.239) as well as one of the mAbs with more limited activity (C68.183) and the RBD mAb C68.3, which we identified previously from C68 and has broad SARS-CoV-2 activity but does not bind SARS-CoV-1 (112). The other mAbs were not run with this assay due to limitations in experimental throughput. We incubated the yeast-display library of sarbecovirus RBDs across a mAb concentration gradient, sorted yeast into bins of weak, intermediate, or strong mAb binding at each mAb concentration, and used deep sequencing to visualize the binding curve of each RBD variant, yielding an EC50 measure of binding strength of each mAb to each RBD isolate.

C68.3 displayed a narrow binding profile with functional activity (dark blue squares) mostly restricted to the SARS-CoV-2-related sarbecoviruses as well as weak binding (light blue square) to Khosta-2 (**Figure 2.2C**). The weak, limited binding of C68.3 is consistent with other SARS-CoV-2-specific mAbs that lack SARS-CoV-1 cross-reactivity (87, 185). C68.61, C68.88 and C68.185 exhibited broad binding against the more sequence divergent sarbecovirus clades, whereas C68.183 and C68.239 showed more restricted binding. Both C68.183 and C68.239 displayed restricted or weak binding against clade 2 viruses, which are ACE2-independent and display low sequence similarity (~62-65%) to SARS-CoV-2 RBD (**Figure 2.2C**). C68.61, C68.88 and C68.185 not only bound to clade 2 viruses, but also clade 3 viruses, in which only Khosta-2 strain can bind human ACE2 (**Figure 2.2C**; **S2.4A Fig**). These mAbs showed distinct binding cross-reactivity for specific RBDs and a pattern that suggests differential preference for binding to certain clades. For example, C68.61 exhibited higher binding to clade 1b RBDs (geomean EC50 0.25 ng/ml across clade 1b sarbecoviruses) than clade 1a (geomean EC50 1.9 ng/ml) RBDs whereas the opposite was true for C68.185, which bound with a higher affinity to the clade 1a RBDs than clade 1b RBDs (geomean EC50 0.66 ng/ml and 1.3 ng/ml, respectively) consistent with their differential neutralization profiles (**Figure 2.2B; S2.4A-B Fig**). Both C68.61 and C68.185 displayed the broadest binding profiles; they potently bound nearly all RBDs evaluated (EC50 values less than 10,000 ng/ml), including RBDs from ACE2-independent clade 2 viruses, suggesting they are targeting an epitope that is highly conserved across sarbecoviruses. Of note, C68.61, C68.88, C68.183, C68.185, and C68.239 all showed cross-reactive binding to the RsSHC014 RBD in the yeast assay, but only C68.88 and C68.239 showed detectable neutralization of RsSHC014 spike-pseudotyped lentivirus. The two RsSHC014-neutralizing antibodies bind to a similar class 4 epitope while the three non-neutralizers bind to the class 5 epitope (see below), suggesting that RsSHC014 might exhibit conformational dynamics that limit access to the class 5 epitope in the full spike context. In line with this, a recent cryo-electron microscopy study of RsSHC014 trimer revealed only structures with fully closed conformations

where all RBD protomers are in 'down' position (197). This is unlike SARS-CoV-2 and SARS-CoV-1 wherein at least one RBD protomer is in the "up" open conformation (8, 198, 199), and thus may impact epitope accessibility and mAb neutralization.

Several cross-reactive C68 mAbs display Fc-mediated effector function

Given that ADCC, an Fc-dependent effector function largely mediated by natural killer (NK) cells, has been associated with protection from SARS-CoV-2 infection in animal models and human studies (154, 187, 200, 201), we tested the ability of the 12 cross-reactive mAbs to trigger ADCC in primary human NK cells in the presence of SARS-CoV-2 spike expressing cells (target cells). We adapted a validated SARS-CoV-2 specific ADCC assay (gating strategy shown in **S2.5 Fig**) (150, 202, 203) to quantify NK cell activation (surface CD107a (a proxy for degranulation) and intracellular IFN-γ) against target cells expressing SARS-CoV-2 D614G spike protein. We included two spike-specific mAbs previously shown to mediate ADCC activity, CV3-25 and S309, which induced robust NK cell activation in this assay (20% and 21% CD107a+ expression, respectively; **Figure 2.2D**) (154, 187). The negative control mAbs, A32 (HIV-specific mAb) (204) and S2X259 (a SARS-CoV-2 mAb previously reported to lack ADCC activity) (129), did not show appreciable activity in this assay with less than 0.5% NK activation. Two C68 mAbs, C68.175 and C68.239, induced the most robust NK cells CD107a expression (**Figure 2.2D**) to similar levels to CV3-25 and S309, the latter of which has been shown to mediate ADCC and improve infection outcome in animal studies (154, 203). Most of the C68 mAbs demonstrated intermediate levels of CD107a expression, that were above the negative control mAbs, suggesting low level ADCC activity. These data were observed for two independent donors (**S2.6A Fig**) indicating that this phenotype is not donor dependent. CD107a expression also correlated with NK cell production of intracellular IFN-γ (**S2.6D-E Fig**), another marker for NK cell activation, and cell death of SARS-CoV-2 spike expressing target cells (**S2.6F-G Fig**). All antibodies bound target cells expressing the D614G spike above the negative control mAb (A32), except CR3022 and C68.121. Among

the antibodies that could bind target cells, mAbs like C68.88 did not mediate ADCC functions, suggesting that this was not due to absence of binding ability (**S2.6B Fig**). Consistent with this, CD107a expression did not correlate with binding activity (**S2.6C Fig**). Overall, these data demonstrate that in addition to neutralization, some C68 RBD antibodies induce robust NK cell-mediated ADCC.

Epitope profiling of cross-reactive antibodies suggest they cluster within two major epitope domains

To identify mutations that facilitate escape from antibody binding and assess the potential for antigenic variation at these sites, we employed a yeast display deep mutational scanning library encoding all possible amino-acid mutations in the RBD (87, 138, 161). This approach defines the functional epitope and generally captures key residues important for antibody-RBD interaction while also highlighting the mutations that are tolerant for viral functional activity, as mutations that decrease ACE2 binding or RBD expression in the yeast-display platform also decrease spike-mediated cell entry (162, 205). This approach has been used to map escape from structurally defined antibody classes, and for the ~2 dozen antibodies that have been mapped via this same deep mutational scanning method together with structural analysis, the escape maps have always agreed with the structural mapping (87, 129, 130, 137–139, 164, 185, 206–208). Using this approach, we classified C68 mAbs into two epitope profile groups: one which most resembles class 4-like mAbs and another which resembles class 5-like mAbs. The class 4-like mAbs include C68.88 and C68.239, which show activity against clade 1a sarbecoviruses (**Figure 2.2C**), while the class 5-like mAbs includes C68.61 and C68.185, which shows breadth across clade 1a/b sarbecoviruses and clade 3 viruses (**Figure 2.2C**).

Among the class-4 like mAbs, there is heterogeneity in the escape pathways. For example, both C68.88 and C68.239 share escape mutations centered on sites that include 374 - 377 (**Figure 2.3A**) but C68.239 has additional sites that confer escape from binding. Additionally,

these escape profiles generally aligned well with the functional data. For example, substitutions at sites S375 and T376 occurred early in Omicron variants (**Figure 2.3B**) and are predicted to facilitate escape from C68.88 and C68.239, which is consistent with the observed losses in binding and neutralization against Omicron variants (**Figure 2.2A-B**). For this reason, the epitope of these two mAbs were profiled in SARS-CoV-2 WH-1 RBD backgrounds as they retain binding activity against this viral library. C68.88 appears to target residues that are relatively conserved across SARS-CoV-1-related sarbecoviruses (**Figure 2.3B**), consistent with the observed neutralization of these viruses (**Figure 2.2C**). C68.83, C68.121 and C68.348 show more limited overlap in specific amino acids that drive escape but in general, the mAbs in this class target epitopes distal from the ACE2 binding footprint (182).

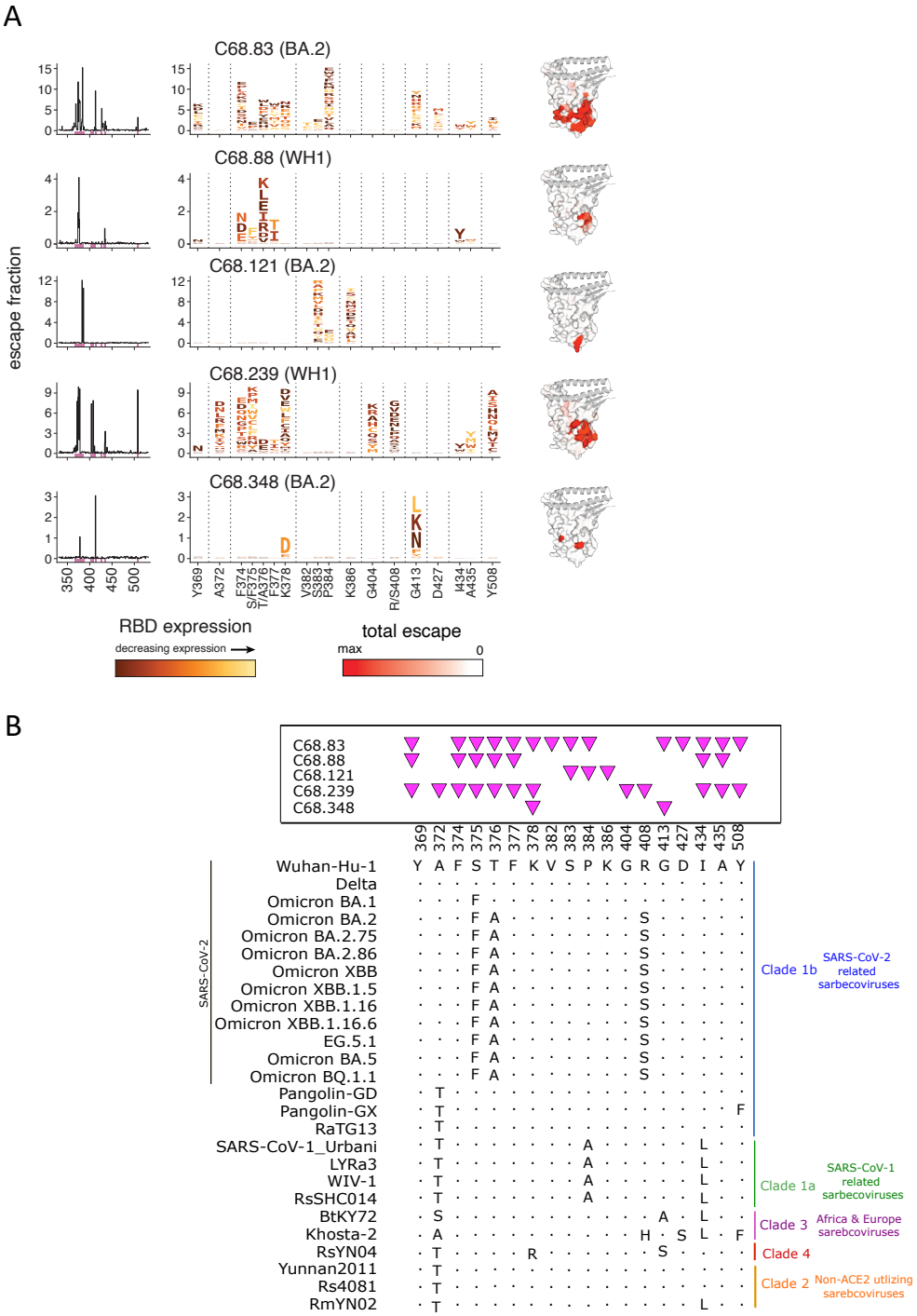

Figure 2.3. Epitope profiling by deep mutational scanning identifies a group of C68 mAbs targeting class 4 epitopes.

(A) Complete escape maps of antibody-binding escape mutations for C68 mAbs using a yeast-displayed SARS-CoV-2 RBD deep mutational scanning system (Wuhan-Hu-1 RBD DMS for C68.88 and C68.239; Omicron BA.2 RBD DMS for C68. 83, C68.121, C68.348). Residue colors

are assigned based on effect these mutations have on RBD expression (with yellow indicating mutations deleterious for RBD expression). The height of letters in the logo plots indicate level of escape by that amino acid at that site. Logo plot residue numbering is based on SARS-CoV-2 WH-1 numbering. Experiments were performed in biological duplicate using independent mutant RBD libraries (14) that correlate well (**S2.10B Fig**) so escape fractions represent the average of these two independent biological replicates. On the right, sites of escape for C68 mAbs are mapped onto the RBD structure and gradient of red coloring indicates magnitude of escape fraction at each indicated site. **(B)** Multiple sequence alignments of select SARS-CoV-2 variants and sarbecoviruses are shown corresponding to sites of escape. Residue numbering based on SARS-CoV-2 Wuhan-Hu-1 sequence with shared amino acids denoted by dots (.) and differences across sarbecoviruses relative to the reference sequence (SARS-CoV-2 Wuhan-Hu-1) indicated. Pink triangles depict the sites of escape identified by the escape maps (**Figure 2.3A**).

The second cluster of C68 mAbs target regions that are spatially distinct from the first mAb group. Many mutations at these regions are not well tolerated, indicated by decreasing RBD expression at predicted escape pathways (**Figure 2.4A**). For example, some of the mutations that allow escape from binding at sites 464-466 reduce RBD expression (yellow and orange colors; defects in expression are predictive of defects in spike-mediated entry in orthogonal DMS measurements (205); **Figure 2.4A**) and this is true for many of the predicted escape mutations for class 5-like mAbs. Whereas the class 4-like mAbs are escaped by at least some mutations that have minimal effects on SARS-CoV-2 RBD functional properties (**Figure 2.3A**; see the volume of dark-colored letters, though positions in both epitopes may experience further constraint beyond these isolated-RBD measurements due to quaternary packing in full spike trimers). As previously described, C68.61 mAb escape mutations included sites K462, E465, R466, and I468, which are conserved sites across all SARS-CoV-2 variants and some sarbecoviruses (**Figure 2.4B**).

A

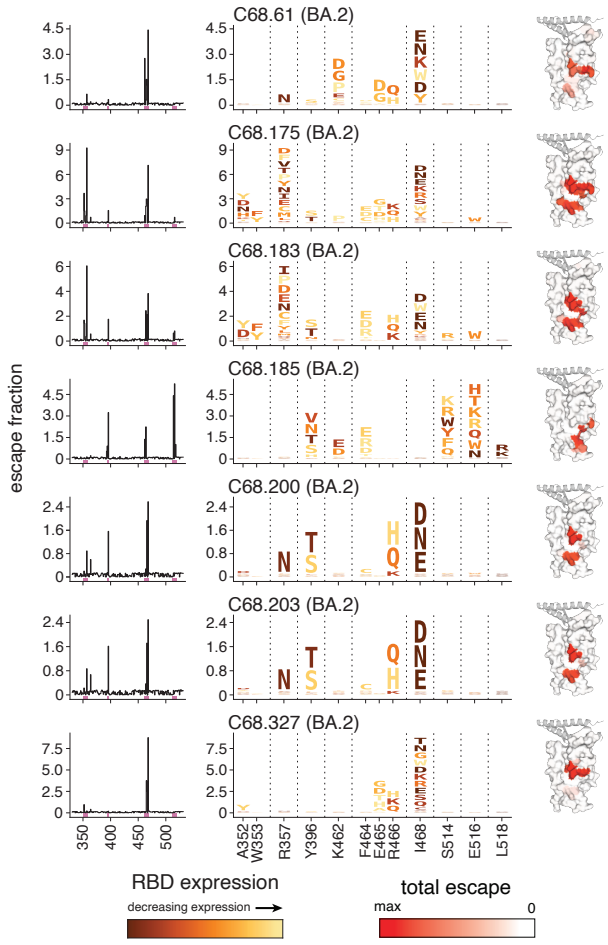
C68.61 (BA.2)
C68.175 (BA.2)
C68.183 (BA.2)
C68.185 (BA.2)
C68.200 (BA.2)
C68.203 (BA.2)
C68.327 (BA.2)
escape fraction
A352
W353
R357
Y396
K462
F464
E465
R466
I468
S514
E516
L518
RBD expression
decreasing expression
total escape
max
0

B

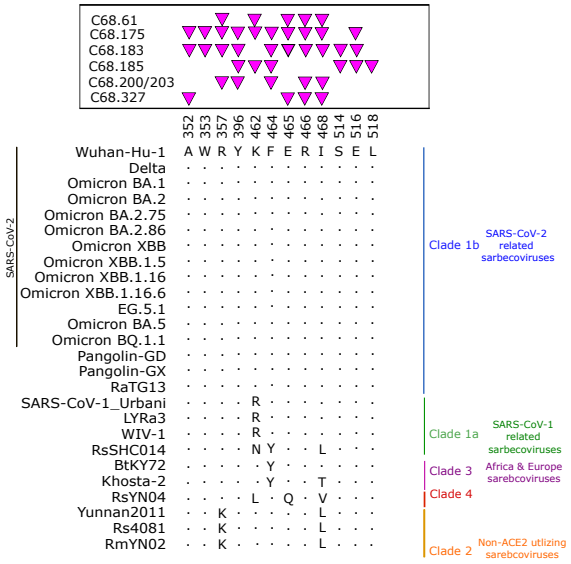
C68.61
C68.175
C68.183
C68.185
C68.200/203
C68.327
352 353 357 396 462 464 465 466 468 514 516 518
A W R Y K F E R I S E L
Wuhan-Hu-1
Delta
Omicron BA.1
Omicron BA.2
Omicron BA.2.75
Omicron BA.2.86
Omicron XBB
Omicron XBB.1.5
Omicron XBB.1.16
Omicron XBB.1.16.6
EG.5.1
Omicron BA.5
Omicron BQ.1.1
Pangolin-GD
Pangolin-GX
RaTG13
SARS-CoV-1_Urbani
LYRa3
WIV-1
RsSHC014
BtKY72
Khosta-2
RsYN04
Yunnan2011
Rs4081
RmYN02
SARS-CoV-2
Clade 1b
SARS-CoV-2 related sarbecoviruses
Clade 1a
SARS-CoV-1 related sarbecoviruses
Clade 3
Africa & Europe sarebcoviruses
Clade 4
Clade 2
Non-ACE2 utlizing sarebcoviruses

Figure 2.4. C68 mAbs target class 5 epitopes that are relatively invariant regions on the Spike Protein.

(A) Complete escape maps of antibody-binding escape mutations for C68 mAbs using a yeast-displayed SARS-CoV-2 RBD deep mutational scanning system (Omicron BA.2 RBD DMS for all class 5 mAbs). Residue colors are assigned based on effect these mutations have on RBD expression. The height of letters in the logo plots indicate escape scores. Logo plot residue numbering is based on SARS-CoV-2 Omicron BA.2. Experiments were performed in biological duplicate using independent mutant RBD libraries (14) that correlate well (**S2.10B Fig**) so escape fractions represent the average of these two independent biological replicates. On the right, sites of escape for C68 mAbs are mapped onto the RBD structure and gradient of red coloring indicates magnitude of escape fraction at each indicated site. **(B)** Multiple sequence alignments of select SARS-CoV-2 variants and sarbecoviruses are shown corresponding to sites of escape. Residue numbering based on SARS-CoV-2 Wuhan-Hu-1 sequence with shared amino acids denoted by dots (.) and differences across sarbecoviruses relative to the reference sequence (SARS-CoV-2 Wuhan-Hu-1) indicated. Pink triangles depict the sites of escape identified by the escape maps (**Figure 2.3A**).

The key C68.185 mAb-escape mutations included sites I396, K462, F464, S514, E516, and L518, and, with the exception of K462, are all highly conserved among all sarbecoviruses (**Figure 2.4A-B**). Inspection of the logo plots of mutational effects indicates that these mutations are largely not tolerated as they would be deleterious for SARS-CoV-2 RBD expression. In some instances where we observed substitutions, there was a differential effect on neutralization in different sarbecoviruses. SARS-CoV-1-related sarbecoviruses encode an arginine at position 462 as opposed to lysine in SARS-CoV-2, and we observed increased binding affinity (**S2.4A-B Fig**) and neutralization potency (**Figure 2.2B**) to the SARS-CoV-1 viruses compared to SARS-CoV-2 viruses, suggesting that the arginine at this position may be preferred for C68.185 binding. The K462N mutation found in RsHC014 may account for a loss in neutralization activity as C68.185 bound RsSHC014 RBD ~10-fold lower than SARS-CoV-1 RBD (**Figure 2.2C; S2.4 Fig**) and studies have suggested that SARS-CoV-2 RBD binding is correlated with neutralization potency (209–212). Overall, we see that these core-RBD-directed mAbs target epitopes that are

mutationally constrained with respect to RBD expression and are highly conserved across the sarbecovirus family.

We additionally chose to epitope profile a selection of C68 mAbs that broadly bind SARS-CoV-2 variants but not SARS-CoV-1 spike trimer. We selected 2 additional mAbs to epitope profile, C68.10 and C68.201, which share the heavy chain variable gene usage with C68.61 and retain XBB spike trimer binding activity (**Figure 2.1C**). Interestingly, these mAbs are not clonally related (do not share V(D)J gene rearrangement) to C68.61, yet the key alterations in the spike protein that facilitate escape for these mAbs are centered around K462 similar to C68.61 (**S2.7A Fig**). These sites are mutationally intolerant as substitutions would functionally constrain RBD expression (**Figure 2.4B; S2.7A Fig**). Because these mAbs are targeting the RBD core, we wanted to assess their pan-sarbecovirus RBD binding breadth. Despite overlapping escape maps from SARS-CoV-2, these mAbs display different binding profiles across sarbecoviruses. Both mAbs exhibit limited SARS-CoV-1-related protein reactivity (**Figure 2.1C; S2.7B Fig**) but C68.201 can additionally bind the sequence divergent clade 2 and clade 3 sarbecoviruses.

Computationally predicting RBD-bound antibody structures using AlphaFold 3

With advances in AI modeling of protein-protein interactions, we wanted to explore computational tools for modeling antibody-antigen complexes. We used the deep neural network model, AlphaFold 3 (AF3) (213, 214), which has the potential to predicts protein or complex structures based on underlying protein sequence in some cases. We tested the ability of AF3 to predict RBD-bound structures for each of the 12 mAbs presented here (**S2.8A Fig**.; sequences in **Supplemental Table 2.1**). We then compared the predicted structural epitopes to the functional epitopes (215) revealed by DMS experiments (**Figure 2.3A** and **2.4A**), which has been shown to always map precisely to within the structural epitope for multiple SARS-CoV-2 mAbs (87, 129, 137–139, 164, 185, 206–208). Overall, AF3 failed to accurately predict antibody epitopes in most of this sampling of antibody:RBD complexes. Of the 12 models, two generally place the mAb at the same epitope revealed by DMS with antibody:RBD side chain interactions that could be

plausible (C68.61:RBD and C68.203:RBD). In the other 10, the AF3 model places the antibody at an epitope that disagrees with the experimental DMS data. In these models, the antibodies were predicted by AF3 to bind the RBD's ACE2-contact surface; this would be inconsistent with the observed cross-clade sarbecovirus breadth that we observed for these antibodies, as it has previously been shown that antibodies to this surface have limited cross-reactive breadth (87, 141). Furthermore, in many cases of disagreement between AF3 prediction and DMS data, the AF3-generated RBD structure does not resemble solved RBD structures, leading to predicted epitopes that do not exist in the actual RBD (**S2.8B Fig**). Overall, we find that AF3 does not accurately predict the epitopes of these RBD mAbs, which is consistent with the reduced accuracy of protein-antibody structures observed in the original AF3 test data (216).

Resilience and exceptional mutation tolerance of C68 mAbs

To further assess the potential for escape from C68 cross-reactive mAbs, we employed a replication competent recombinant vesicular stomatitis virus system (rVSV) where viruses bearing spike in the presence of antibody select for antibody escape mutants (144, 217). rVSV with either SARS-CoV-2 or SARS-CoV-1 spikes were cultured in the presence of antibody to select for mutations, which were identified by next-generation sequencing. C68.185 drove selection for a single substitution at site L504R (SARS-CoV-1 numbering) in rVSV-SARS-CoV-1 at 10 μg/mL (**Figure 2.5A**), which is a site and residue that led to loss of antibody binding in DMS experiments (**Figure 2.4**; L518R in SARS-CoV-2 WH-1 numbering). At a lower concentration (1 μg/mL), selection occurred at additional sites centered at Y383H, R449G and Q523R (SARS-CoV-1 numbering). Two of these escape mutations were also identified by the SARS-CoV-2 DMS (Y396, K462 in SARS-CoV-2 numbering). The third substitution identified is outside of the RBD and thus not selected for in the RBD DMS experiments. For this reason, we cannot determine if this mutation directly affects mAb binding or it was selected for other stochastic reasons, or is a stochastic 'passenger' mutation in this single culture (143, 146).

A

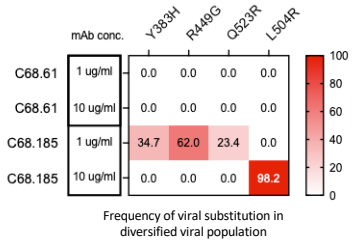

B

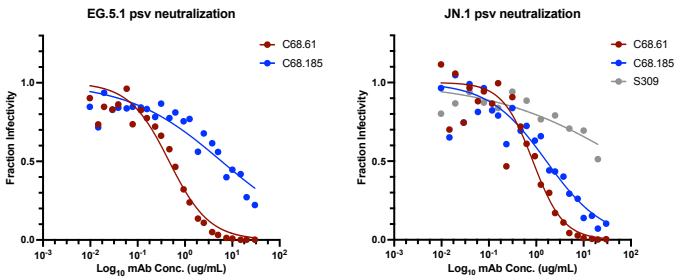

Neutralization IC50 (ug/ml)

	EG.5.1	JN.1
C68.61	0.46	0.85
C68.185	5.9	1.6
S309	ND	>20

C

C68.61 escape mutations

Genotype at S site 357, 464, 465, 466, 468

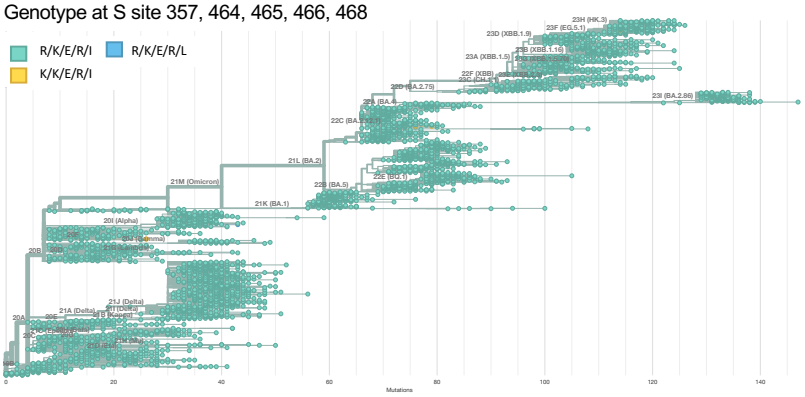

C68.185 escape mutations

Genotype at S site 396, 462, 464, 514, 516, 518

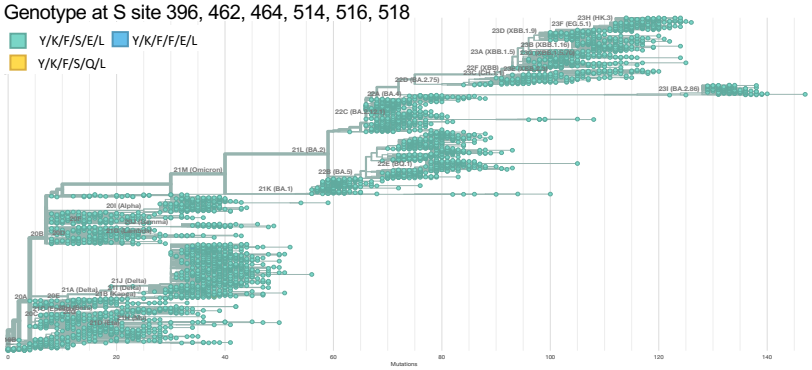

Figure 2.5. Selection experiments to identify escape mutation in the presence of SARS-Cov-1 and SARS-CoV-2 encoding VSV in cell culture and SARS-CoV-2 evolution observed in nature.

(A) C68 mAbs selection experiments in the context of SARS-CoV-1 replication competent VSV-G. Frequency of variants in viral population in the presence of C68 mAbs (variant defined as occurring at a frequency greater than 3%). **(B)** Neutralization activity of C68 mAbs (C68.61 in red and C68.185 in blue) and S309 (in grey) against recently circulating and dominant SARS-CoV-2 variant spike-pseudotyped lentiviruses. Antibodies were two-fold serially diluted and tested starting at 20 and/or 30 μg/mL. Samples with IC50 values above the tested concentration were plotted at that concentration (>20 μg/mL is no activity). **(C)** Phylogeny of SARS-CoV-2 Pangolin clade sequences containing C68 mAb RBD binding escape mutations (from **Figure 2.4A**) (Nextstrain) for C68.61 (**top panel**) and C68.185 (**bottom panel**). Circles in teal are the residues found in SARS-CoV-2 Wuhan-Hu-1 whereas viral genomes containing escape mutations are indicated by yellow/blue circles. Depicts 3900 SARS-CoV-2 viral genomes that are sampled between December 2019 and March 2024. (Nextstrain: https://nextstrain.org, CC-BY-4.0 license)

Remarkably, C68.61 did not drive escape in this replicating virus system bearing SARS-CoV-1 or SARS-CoV-2 spikes (**Figure 2.5A**). C68.61 was then tested against three SARS-CoV-2 variants spikes (WH-1, Omicron BA.2 and XBB.1.5) that it neutralized in single-cycle infection assays. This included a more recent Omicron variant XBB.1.5, which was tested because previous DMS and replication competent VSV selection studies suggest there may broadening of pathways of escape with later SARS-CoV-2 variants (144, 164). Thus, while there are amino acid mutations that are predicted to disrupt C68.61 binding to RBD (by DMS experiments), viruses with these substitutions were not selected in a replicating virus system, suggesting they may be functionally constrained sites.

Given the lack of predicted escape in cell culture among SARS-CoV-2 variants, we next evaluated the ability of two C68 broadly cross-reactive mAbs to neutralize the most recent dominant circulating variants, JN.1 and EG.5.1 (218). C68.185 exhibited moderate neutralization activity against both SARS-CoV-2 variants (EG.5.1 IC50s of 5.9 μg/mL and JN.1 IC50s of 1.6

μg/mL; **Figure 2.5B**). C68.61 retained potent neutralization activity at <1 μg/mL against both viruses with minimal fold differences in activity compared to SARS-CoV-2 WH-1 neutralization, emphasizing this antigenic site is highly conserved. We also observed dramatic losses in neutralization activity by S309 against JN.1 (IC50s >20 μg/mL), as has been observed by other studies (219), suggesting this antigenic interface is sequence diverse (220).

Antibody-escape mutations are present at a low frequency in SARS-CoV-2 evolution

To examine antigenic variation in SARS-CoV-2 spike residues that disrupt antibody binding, we used the bioinformatics tool Nextstrain to assess mutation frequency of SARS-CoV-2 spike residues (221, 222). This tool has been used throughout the pandemic to understand SARS-CoV-2 viral evolution by sampling temporal viral sequences from diverse geographic locations (**Figure 2.5C, top panel**; **S2.9 Fig**; 3900 genomes). Viral sequences that contained the C68.61 RBD binding escape mutations at sites 357, 462, 465, 466, and 468 amounted to low viral diversity with substitutions accounting for < 2% frequencies at a given time. For instance, a R357K substitution occurred but did not increase in frequency, further suggesting that this mutation may have a fitness disadvantage. We observed a similar lack of viral diversity in these regions for C68.185 (**Figure 2.5C, bottom panel; S2.9 Fig**). These epitope targets are not sites that are commonly mutated throughout SARS-CoV-2 evolution (140, 223, 224) have also not been observed in wastewater sequencing where “cryptic” mutated lineages have been found (225, 226) demonstrating that the C68.61 and C68.185 epitope has remained relatively unchanged.

DISCUSSION

Here, we have identified a collection of cross-reactive mAbs from a Delta breakthrough infection that display cross-reactive neutralizing activity against diverse sarbecoviruses with high spillover risk. Some mAbs displayed potent neutralization (half maximal inhibitory concentration

<0.05 μg/mL) against SARS-CoV-1 as well as more divergent animal sarbecoviruses from Africa and Europe. Notably, many of the isolated mAbs additionally demonstrated ADCC activity against SARS-CoV-2 spike and two mAbs exhibited activity on par with another cross-reactive mAb, S309, which has been shown to provide *in vivo* protective efficacy due to its neutralizing and non-neutralizing effector functions (154). One mAb, C68.61, showed unattenuated neutralization against all SARS-CoV-2 variants and several SARS-CoV-1 related sarbecoviruses as well as a more divergent clade 3 bat sarbecovirus. Remarkably, C68.61 did not select for escape mutants in the presence of replication competent virus and SARS-CoV-2 strains harboring C68.61 escape mutations have not increased in prevalence in nature indicating constraints on escape from this mAb. While deep mutational scanning indicates that all these mAbs target one of two regions in the RBD core, previously defined as class 4 and 5 epitopes (59, 87), there is heterogeneity in the escape pathways even among mAbs targeting a similar region.

While there was some overlap in the escape mutations among class 4 mAbs, each mAb had a unique escape and neutralization profile. For instance, C68.88 exhibits a narrowly focused epitope that partially overlaps that of C68.239, yet it shows greater cross-reactivity. While these mAbs target epitopes distal to the ACE2 binding site, these antibodies exhibit potent neutralization of a subset of SARS-CoV-2 and SARS-CoV-1 variants. Potent neutralization has been observed by some class 4 mAbs whose angle of approach partially blocks ACE2 access as well as induces S1 shedding (126, 129).

Among the class 4 mAbs previously characterized, there is diversity of contact residues that encapsulate the mAb-RBD interface that may account for functional differences observed among C68 mAbs. For instance, the structural footprint of mAb S2X35 includes residues adjacent but not overlapping the receptor binding motif whereas the contact residues for mAb S304 are further from the RBM (104). As a result, S2X35's closer proximity to the ACE2 footprint resulted in greater competition with ACE2 than S304 and this correlated with neutralization potency (104). Thus, differences in angle of approach as well as antigen affinity could also contribute to differential

functional activities including C68.239's ability to mediate potent ADCC against SARS-CoV-2. While class 4 targeting mAbs were posited as potential SARS-CoV-2 broadly neutralizing antibodies (60, 111, 129), we and others have shown that these mAbs lose activity against SARS-CoV-2 Omicron variants (126, 133). Still, their epitope is conserved across SARS-CoV-1-related and ACE2-independent sarbecoviruses tested here and we extend the functional characterization of this class of antibody by showing that a subset can display Fc-effector activation of immune cells that can eliminate infected cells. If these findings extend to a larger virus panel, these mAbs could hold promise as broad-spectrum antibodies against potential spillover sarbecoviruses (126, 129, 182).

The second cluster of C68 mAbs recognize a highly conserved cryptic epitope in RBD designated class 5. While few class 5 mAbs have been comprehensively characterized, its known that these mAbs target a conserved quaternary epitope that is accessible when spike has one-RBD-up open conformation, while occupying the space of the N-terminal domain in an adjacent protomer (87, 134, 183, 227, 228). Upon binding, tight packing of RBD-mAb interactions induces further opening of the RBD protomer (87, 228) leading to conformational changes that induce S1 shedding. Many of the identified escape mutations were predicted to be functionally intolerant, which is in agreement with published studies (112, 133, 183, 227), and may also be structurally intolerant as these residues are involved in RBD-NTD interactions (134). DMS experiments suggested that C68 mAbs bind to a similar cryptic antigenic region on the spike glycoprotein shared with the class 5 antibody S2H97, which has been shown to reduce viral load in animal studies when given prior to exposure (87). Additionally, some C68 class 5 mAbs displayed cross-reactivity with SARS-CoV-1-related sarbecoviruses and can also neutralize the more divergent African and European animal sarbecoviruses (87, 130). This breadth in sarbecovirus activity is exemplified by C68.185, which shows notable binding activity against a diverse array of sarbecovirus RBDs, as well as neutralization of clade 1a and clade 3 ACE2-dependent sarbecoviruses, suggesting the sequence of this epitope is highly conserved among members of

these viral clades. However, neutralization is weak against SARS-CoV-2 variants, perhaps because the mechanism of neutralization for this class of mAbs lacks ACE2 blocking.

While binding to spike trimer and high sequence conservation of the binding residues were largely predictive of neutralization activity, this was not always the case. For example, four of twelve mAbs that were cross reactive based on binding to SARS-CoV-1 spike trimer did not neutralize the corresponding virus. This discrepancy in binding and neutralization could be due to differences in RBD dynamics between sarbecoviruses, as has been suggested for the class 4 mAb CR3022, which binds the one-RBD-up open conformation in SARS-CoV-1 but would sterically clash with a neighboring RBD in SARS-CoV-2 (128). This may explain the ability of mAb C68.121 to bind but not neutralize sarbecoviruses, since it overlaps in contact residues with CR3022. While SARS-CoV-2, SARS-CoV-1 and other sarbecoviruses require one RBD in an “up” conformation to bind host cell receptor (8, 198, 199), studies have indicated that SARS-CoV-2 variants also alter RBD conformational dynamics (229–231). This could indirectly affect binding affinity and neutralization of mAbs whose epitopes are highly sequence conserved but may be occluded in the closed RBD conformation (232), such as C68.175 and C68.203. Another explanation for this differential effect in neutralization despite sequence conservation across sarbecoviruses may be due to epistatic shifts as the accumulation of mutations outside the antibody binding site may lead to shifts in the effect of residues on antibody function, which has been observed in other viral contexts (233, 234) as well as in SARS-CoV-2 variants (144, 164). While we performed our DMS experiments in the genetic background of the SARS-CoV-2 WH-1 or Omicron BA.2, the effects of mutations may differ in different viral contexts (144, 163).

SARS-CoV-2 evolution is likely shaped by both mutation and positive selection to evade immunity, yet the capacity to escape antibody recognition can be limited by selection to maintain functional capabilities (142). To examine this, we used a replicating virus system to select for escape for two of the mAbs that neutralized SARS-CoV-1 and SARS-CoV-2 and show activity against more diverse sarbecoviruses. In the case of C68.185, which neutralized several clade 1a

and clade 3 sarbecoviruses, escape mutants against SARS-CoV-1 virus were selected. Some of the selected mutations are highly sequence conserved across sarbecoviruses including SARS-CoV-2 emerging variants. Remarkably, there was no evidence of escape from C68.61 for either SARS-CoV-1 or SARS-CoV-2 in this same assay, including different SARS-CoV-2 variants. In agreement with this finding, SARS-CoV-2 variants that contain these spike substitutions occur at very low frequency in nature and there is no evidence of expansion of these rare mutants. Thus, mAbs like C68.61 that can functionally constrain sarbecovirus spike evolution could lead to broadly protective interventions for current and emerging SARS-CoV-1 and SARS-CoV-2 variants and inform pan-sarbecovirus vaccine strategies.

This study identified new antibodies with a range of cross-reactivity that target diverse epitopes within the core of RBD, including functionally constrained epitopes. Several of these mAbs have complementary neutralization and DMS epitope profiles that suggest they have minimal or non-overlapping escape mutations. Thus, a combination of these mAbs could form the basis for an antibody cocktail that would show activity across very diverse sarbecoviruses to be used in the event of another pandemic (123, 235).

MATERIALS AND METHODS

Human PBMC specimen

Peripheral blood mononuclear cell (PBMC) sample was collected at 30 days after a breakthrough infection from an individual, C68, who received two doses of the Pfizer-BioNTech mRNA vaccine and was subsequently infected with the Delta variant. C68 was enrolled in the study and followed prospectively as part of the Hospitalized or Ambulatory Adults with Respiratory Viral Infections cohort (study approved by the University of Washington Protocol #STUDY00000959 and Fred Hutch Cancer Center Institutional Review Boards). Written, informed consent was obtained from individual C68 at the time of enrollment in July 2021.

SARS-CoV-2 memory B cell isolation and antibody reconstruction

The methods of isolation of SARS-CoV-2 memory B cells from C68 were previously described (112, 113). In brief, cells were incubated with a cocktail of anti-CD3-BV711 (BD Biosciences, clone UCHT1), anit-CD14-BV711 (BD Biosciences, clone MφP9), anti-CD16-BV711 (BD Biosciences, clone 3G8), anti-CD19-BV510 (BD Biosciences, clone SJ25C1), anti-IgM-FITC (BD Biosciences, clone G20-127), anti-IgD-FITC (BD Biosciences, clone IA6-2) along with APC/PE-labeled Delta HexaPro spike protein (a generous gift from David Veesler) and spike S2 peptide (Acro Biosystems, cat. S2N-C52E8) for 30 minutes on ice. Single B cells defined as $CD3^-$, $CD14^-$, $CD16^-$, $CD19^+$, IgD^-, IgM^-, PE^+, APC^+ and live cells (Ghost Dye Red 780; Tonbo Biosciences cat: 13-0865-T500) were sorted (BD Biosciences, FACS AriaII) into a total of four 96-well PCR plates containing RNA storage buffer and stored at -80C. RNA storage buffer consists of RNAse OUT, 5X first-strand buffer, 0.1 M DTT, Igepal, carrier RNA, ultrapure water.

A total of 384 SARS-CoV-2 Delta trimer and/or S2 subunit specific B cells were recovered from C68. Reconstruction of antibodies was conducted as previously described (112, 113, 236–238). RT-PCR amplification of IgG antibody heavy and light chain variable regions was performed followed by nested chain-specific amplification PCRs (112, 236, 239). Two different primer sets were used to maximize recovery of antibody chain DNA (240, 241). Amplicons were sequenced and the sequences were initially assessed for the presence of an intact open-reading frame (in-frame junction and no stop codons) by comparing the sequences to IMGT V-QUEST (242, 243). Functional sequences were then subcloned into their respective IgK or IgL expression vectors and all heavy chain were expressed as IgG1 (237, 238). To determine levels of somatic hypermutation, clonality, and germline inference were performed with the partis software package (https://github.com/psathyrella/partis/ and https://arxiv.org/abs/2203.11367). Of the 384 B cells recovered, 118 had paired functional heavy and light chain sequences and of these 45 (42 newly identified mAbs characterized here and 3 RBD-targeting mAbs in (112)) were found to be RBD specific based on binding to the RBD subunit. The remaining mAbs have been characterized

here (112, 113) and were found to be NTD (17), CTD (3), S2 (29) or not binding reactive to SARS-CoV-2 antigen.

Antibody binding profiling by enzyme-linked immunosorbent assays

Antibody binding to SARS-CoV-2 or SARS-CoV-1 recombinant spike protein was performed using ELISA as previously shown (112, 244). Briefly, 384-well maxisorp plates (Nunc, Thermo Fisher Scientific) were coated with SARS-CoV-2 or SARS-CoV-1 antigen 25 uL at 1 µg/ml in 1x phosphate buffered saline (PBS) coating buffer overnight at 4°C. The recombinant spike protein included: Wuhan- Hu-1 (Sino Biologics; cat. 40589-V08H4), Delta (Sino Biologics; cat. 40589-V08H10), Omicron BA.1 (Sino Biologics; cat. 40589-V08H26), Omicron BA.2 (Sino Biologics; cat. 40589-V08H28), Omicron BA.4/BA.5 (Sino Biologics; cat. 40589-V08H32), Omicron XBB (Sino Biologics; cat. 40589-V08H40), Omicron BQ.1.1 (Sino Biologics; cat. 40589-V08H41), and SARS-CoV-1 (Acro Biosystems, CUHK-W1 strain) as well as the SARS-CoV-2 RBD subunit (Sino Biologics; cat. 40592-V08H). The following day, plates were washed 4x with 100 uL of PBS-T (1x PBS, 0.05% Tween-20) using a plate washer. Plates were then blocked in 50 uL of 3% non-fat dry milk in PBS-T for 1 hour at ambient temperature. Blocking buffer was removed and plates were incubated with 25uL monoclonal antibody dilutions for 1 hour at 37 °C. Plates were then washed and incubated with HRP-conjugated goat anti-human IgG antibody (Sigma-Aldrich) (diluted 1:2500 in PBS-T) for 1 hour at ambient temperature. Plates were washed and incubated with TMB substrate (Thermo Fisher Scientific) for ~3-5 minutes until the reaction was quenched with 1N sulfuric acid. Finally, plates were read at absorption 450 nm (BMG Labtech). For ELISAs that were used to screen for SARS-CoV-2 specificity (**Figure 2.1A**), the binding assay was performed at a single antibody dilution (500 ng/ml) and background in the 1x PBS control was subtracted to determine binding activity (OD450). Results presented were the average of technical duplicates. For experiments to determine the 50% effective concentration (EC50), ELISAs were performed at a starting concentration of 1000 ng/ml antibody and serially diluted 2-fold for at least 12 dilutions. OD450 nm values minus background from 1x PBS only

wells were averaged from technical duplicates and the final results presented are the average of two biological replicates in technical duplicate. EC50 was calculated using GraphPad Prism software (v10) by fitting a four-parameter (agonist vs response) nonlinear regression curve with the bottom fixed at 0 and the top constrained to the highest OD450 nm value observed.

Spike-pseudotyped lentiviral particle production and neutralization assays

Spike-pseudotyped lentiviral particle production was performed in 293T cells expressing high levels of ACE2 as previously described (76, 112, 244, 245). Sarbecovirus spike plasmids with spike genes specific for SARS-CoV-2 variants WH-1, Delta, Omicron BA.1, Omicron BA.2, Omicron BA.4/BA.5, as well as SARS-CoV-1 (Urbani strain), BtKY72 (K493Y/T498W mutant), Khosta-2, WIV1, LYRa3, Pangolin-GD, RsSHC014 were provided as follows: BA.4/5, XBB.1.5, BQ.1.1, EG.5.1, JN.1 and SARS-CoV-1 were generated as previously described (246); WH-1, BA.1, BA.2 were provided by Jesse Bloom (76, 245); Delta was a gift from Amit Sharma; BtKY72, Khosta-2, WIV1, LYRa3, Pangolin-GD, RsSHC014 were gifts from Pamela Bjorkman (182). Supernatant from transfected 293T cells was harvested 72-hour post-transfection and sterile filtered through a 0.2-μm filter and concentrated using Amicon Ultra Centrifugal Filters (Sigma-Aldrich). Pseudovirus was then used to infect 293T cells constitutively expressing human ACE2 (generously provided by Jesse Bloom) (76), and viral titer was determined by measuring luminescence using Bright-Glo Luciferase Assay System (Promega) at 48 hours post-infection.

In vitro spike-pseudotyped neutralization assays were performed as previously described (76, 112, 244). Briefly, 2.5e5 cells/ml of HEK293T-hACE2 cells were plated in 15 μl of complete media per well in a 384-well plate (Fisher Scientific; cat. 142761). Twelve to sixteen hours later, pseudotyped lentiviral particles were added to obtain 2-5 × 10^5 relative luciferase units (RLUs) of luminescence signal per well to an equal volume of serially diluted antibody sample. To determine the inhibitory concentration at 50% (IC50), antibody dilutions were prepared at a starting concentration of 20 or 30 μg/mL and two-fold mAb dilution curves were assessed. Antibody-

pseudovirus mix were then added to a pre-seeded plate of HEK293T-hACE2 cells. Forty-eight hours later, 30 μl of virus-mAb mixture was removed and 9 μl of Bright-Glo Luciferase Assay Reagent (Promega; cat. E2610) was added to the plated cells. Plates were then read by measuring luminescence. Background values were subtracted using the "cells only" condition as background signal. Percent neutralization was then calculated as a reduction in RLUs of each antibody-pseudovirus mix compared to cells infected with virus in the absence of antibody (cells and virus only). If the "cells and virus only" condition was 1.3x higher than the average luminescence signal from the non-neutralizing wells (highest diluted mAb plus virus condition), then the non-neutralizing wells were defined as the background signal to minimize potential variability due to edge effects. Spike-pseudotyped neutralization assays were done in technical duplicate and replicate experiments were averaged, and the fraction of infectivity was calculated. We calculated the IC50 using GraphPad Prism software by fitting a four-parameter (agonist vs response) nonlinear regression curve with the bottom fixed at 0, the top constrained to 1 and HillSlope > 1.

SARS-CoV-2 spike antibody-dependent cellular cytotoxicity assay

To measure Fc-mediated function of C68 mAbs, we adapted a validated SARS-CoV-2 specific ADCC assay (113, 150, 151, 203). CEM.NKr cells stably expressing a full length GFP-tagged SARS-CoV-2 spike (variant D614G; target cells) were generously provided by Andrés Finzi. Cryopreserved PBMCs (effector cells; acquired from Bloodworks Northwest or kindly given from Andrés Finzi) from healthy donors were thawed and rested overnight in RPMI (Gibco) supplemented with 10% FBS (Gibco), 4.0mM Glutamax (Gibco) and 1% antibiotic-antimycotic (Life Technologies). The following day, effector cells were mixed at a 10:1 ratio with target cells with C68 mAbs in a 96-well v-bottom non-TC treated plates. All C68 monoclonal antibodies were diluted in 1x PBS and tested at 5000ng/ml. This concentration of 5000ng/ml was chosen because it was the highest activity observed before reaching the prozone effect based on previous studies

(203) and in-house experiments comparing ADCC activity at different dilutions (not shown). Effector cells, target cells and antibodies were mixed and incubated with anti-CD107a-APC (clone H4A3, BioLegend) and protein transport inhibitor cocktail (1:500 dilution in 1x PBS, eBioscience). The plates were subsequently centrifuged for 1 min at 100xg, and incubated at 37°C, 5% CO_2 for 4 hrs. After incubation, cells were washed and centrifuged at 400xg for 3 minutes. Cells were stained with an antibody cocktail consisting of: viability dye (Viability Dye eFluor 780; Thermo Fisher Scientific), anti-CD3-BV711 (Clone UCHT1, Biolegend), anti-CD56-BV605 (clone 5.1H11, BioLegend), and anti-CD16-BUV395 (clone 3G8, BD Horizon) on ice for 30 minutes. Cells were washed, fixed and permeabilized (eBioscience Intracellular Fixation & Permeabilization Buffer Set) before staining for intracellular IFN-γ-PE (clone 4S.B3, BioLegend) for 20 minutes at room temperature. Cells were acquired on a Fortessa LSR instrument (Fortessa X50, BD Biosciences). ADCC was measured as the percentage of NK cells (defined as live, singlets, GFP-, CD3-, CD56+ cells) positive for CD107a or intracellular IFN-γ (gating strategy shown in S5 Fig.). Target cell death was measured as percentage of spike expressing target cells positive for cell death marker (gating strategy shown S5 Fig.). Data analysis was performed using FlowJo v10.7.1. Each experiment was performed in technical duplicates and with two independent PBMC donors. Experimental values shown are background subtracted (background defined as spike expressing target cells and effector cells in the absence of antibodies).

Epitope mapping and escape profiling by yeast display RBD DMS

To determine the epitope targets and the escape profiles of mAbs, we used a yeast library displaying RBD proteins with nearly every single amino acid mutation in the RBD of Wuhan-Hu-1 or Omicron BA.2, as previously described (87, 112, 138). First, a yeast strain expressing the unmutated RBD of Wuhan-Hu-1 or Omicron BA.2 and flow cytometry were used to identify an EC90 concentration for antibody binding to the wildtype yeast-displayed RBD construct. Then, approximately 5 OD units of yeast libraries were incubated with that EC90 concentration of mAb.

Cells were washed and incubated with 1:200 PE-conjugated goat anti-human-IgG antibody (Jackson ImmunoResearch; clone 109-115-098), and 1:100 FITC-conjugated chicken anti-Myc-tag (Immunology Consultants Lab; clone CYMC-45F). A FACS-based approach was used to identify antibody escape mutants by gating on yeast mutants with reduced antibody binding, with gates drawn on wildtype control cells labeled at 10% of the library selection mAb concentration to approximate an escape bin of 10x or greater loss of binding (**S2.10 Fig**). Approximately, 4 million RBD+ cells were sorted on a FACS AriaII.

Pre-sort and sorted antibody-escape cells were sequenced using an Illumina NovaSeq and a 16-nucleotide barcode linked to each RBD mutant was used to identify the mutant sequence. Raw sequence reads are available on NCBI Sequence Read Archive (SRA), BioProject PRJNA770094, BioSample SAMN40905401. Sequencing reads were then compiled and compared to the pre-sort population frequencies to generate the “escape fraction” visualized on logoplots. Experiments were performed in biological duplicate using independent mutant RBD libraries (161) that correlate well (**S2.10B Fig**) so escape fractions represent the average of these two independent biological replicates. Wuhan-Hu-1 RBD library backgrounds (used to profile C68.88 and C68.239) and Omicron BA.2 (used to profile C68.61, C68.83, C68.121, C68.175, C68.183, C68.185, C68.200, C68.203, C68.327, C68.348) were chosen based on initial binding experiments assessing ability to bind either Wuhan-Hu-1 RBD or Omicron BA.2 RBD expressed on the surface of yeast (not shown but aligns with ELISA binding experiments, Figure 2-2A). Final escape fraction measurements averaged across two replicates are available from GitHub: https://github.com/tstarrlab/SARS-CoV-2-RBD_Omicron_MAP_Overbaugh_v2/tree/main/results/supp_data. The entire pipeline for epitope escape profiling is available from GitHub: https://github.com/tstarrlab/SARS-CoV-2-RBD_Omicron_MAP_Overbaugh_v2.

Antibody selection experiments using replication competent VSV expressing sarbecovirus spike

To assess what escape mutants arise in the presence of C68 mAbs in the context of virus replication, we used a recombinant replication-competent vesicular stomatitis virus (rVSV) expressing the SARS-CoV-2 variants (rVSV/SARS-CoV-2/GFP) or rVSV/SARS-CoV-1/GFP spike as previously described (137, 144). Generation and titering of rVSV/SARS-CoV-2/GFP chimeric viruses using 293T cells expressing ACE2 has been previously described (144, 217).

Antibodies were incubated with rVSV at 1 million infectious units and tested at either 1 or 10 µg/mL with concentration determined by potency of a given mAb. The antibody-virus mix was incubated for 1 hour at 37°C before infecting ACE2 expressing 293Ts (Passage #1). Twenty-four hours later, supernatant was removed and replenished with fresh media containing mAb at the same antibody concentration. After an additional 24 hours, 100 uL of the virus-containing supernatant was filtered and incubated with antibody at the same concentration for 1 hour at 37 C. This virus-antibody mixture was then used to inoculate fresh 293T-ACE2 cells for a second passage with the above passaging steps repeated. After two passages, viral supernatant was harvested and viral RNA was extracted. RT-PCR was used to amplify the RBD and RBD amplicons were then tagged for sequencing analysis using Nextera TDE1 Tagment enzyme (Illumina) and then i5/i7 barcoded primers were added to tagmented cDNA using Illumina Nextera XT Index Kit v2 and KAPA HiFi HotStart ReadyMix (Roche) to barcode amplicons. The barcoded library was then pooled and sequenced. Sequencing reads were filtered and compared to the parental spike sequence with mutation counts compiled. A mutation was defined as a true variant if substitution occurred at a frequency greater than 3%.

Yeast display of sarbecovirus RBDs binding assays

To evaluate the ability to bind a panel of sarbecovirus RBDs, we used yeast libraries displaying RBDs from sarbecoviruses representing different clades as previously described (68, 87). A full list of all RBDs and sequence accession numbers is available on GitHub:

https://github.com/tstarrlab/SARSr-CoV_mAb-breadth_Overbaugh/blob/main/data/data-supp_RBD-sequences.csv. Briefly, sarbecovirus clades were phylogenetically defined based on RBD sequence, with the Hibecovirus RBD sequence (GenBank: KF636752) used to root the sarbecovirus phylogeny tree. Each sarbecovirus RBD is represented by >100 barcodes such that technical pseudo-replicates can be ascertained within each binding experiment. Antibodies were incubated with sarbecovirus libraries at five concentration points (10,000 ng/mL and four serial 25-fold dilutions to 0.0256 ng/mL; plus zero mAb condition). Approximately 1 OD units of yeast libraries were incubated with serially diluted mAb. Cells were washed and incubated with 1:200 PE-conjugated goat anti-human-IgG antibody (Jackson ImmunoResearch; clone 109-115-098), and 1:100 FITC-conjugated chicken anti-Myc-tag (Immunology Consultants Lab; clone CYMC-45F). At each concentration, approximately 1 million RBD+ cells were sorted and binned representing 4 cell populations of low and high mAb binding. Barcodes were counted within each FACS bin via Illumina sequencing, with raw sequence reads available on NCBI SRA, BioProject PRJNA714677, BioSample SAMN40905419. EC50s were calculated using the sequence data of each serially diluted bin allowing us to visualize approximate differences in affinity between different sarbecovirus RBDs. EC50 scores are the geometric mean across the independent barcodes. Violin plots show distribution of Log10 EC50 values from independent barcodes. The computational pipeline for computing sarbecovirus mAb-binding breadth is available on GitHub: https://github.com/tstarrlab/SARSr-CoV_mAb-breadth_Overbaugh.

AlphaFold 3 modeling of antibody-antigen interactions

Sequences of the heavy and light-chain of the 12 cross-reative mAbs modeled (sequences in **Supplemental Table 2.1**) and the SARS-CoV-2 WH1 RBD sequence with residues 333-526 were input as 3 separate proteins into the GUI at https://alphafoldserver.com/ as molecule type: protein, copies = 1 (213). Predictive structures were generated using AlphaFold3, with 5 predicted structures created for each mAb:RBD complex and the structure with the highest overall

confidence score (which also corresponded to the highest RBD score) was selected for further analysis. Predictive structures were aligned to the RBD chain of PDB: 6M0J (247) using the align function in Pymol version 2.5.0 (https://pymol.org), generating an RMSD value and a structural overlay for use in figures and interpretation.

ACKNOWLEDGEMENTS

We thank the Flow Cytometry Core Facility at the University of Utah Health Sciences Campus (supported by NIH 5P30CA042014-24) and the University of Utah Center for High Performance Computing (supported by NIH 1S10OD021644-01A1) for experimental support. We thank Amit Sharma (Ohio State University), Jesse Bloom (Fred Hutchinson Cancer Center), David Veesler (University of Washington) and Pamela Bjorkman (Caltech) for generously providing spike plasmids for the production of spike-pseudotyped lentiviruses. We thank all the researchers who were involved in sequencing and submitting data to GISAID. We also thank David Veesler (University of Washington) for providing Delta spike trimer to use as bait to capture spike-specific B-cells and Andrés Finzi (Université de Montréal) for the CEM.NKr CCR5+ cells. We also would like to thank the participants and the study staff of the Hospitalized or Ambulatory Adults with Respiratory Viral Infections (HAARVI) study.

Chapter 3:

Affinity maturation and enhanced neutralizing activity against SARS-CoV-2 variants and SARS-like viruses by SARS-CoV-2 elicited monoclonal antibodies

Michelle Lilly^, Felicitas Ruiz^, Will Foreman, Viren A. Baharani, Vrasha Chohan, Ashley L. Taylor, Jamie Guenthoer, Duncan Ralph, Frederick A. Matsen IV, Helen Y. Chu, Paul D. Bieniasz, Tyler N. Starr, Julie Overbaugh

Manuscript in preparation.

^Co-contributors

My contribution to this work was as the co-lead researcher of the project, and I will be co-first author (listed second) on the manuscript that results from this work. I contributed to the design of the study by adapting a B cell sort bait approach to isolate antigen specific B cells, the initial selection criteria for the amplification of antibody genes, and performed some of the neutralization assays against SARS-CoV-2 variants and other sarbecoviruses. I also carried out Alphafold 3 analysis and data compilation. Michelle Lilly contributed to the design of the study, performed antibody reconstruction, binding and some of the neutralization assays against SARS-CoV-2 variants and other sarbecoviruses.

INTRODUCTION

(introduction adapted from JO HB pilot grant with modifications)

SARS-CoV-2 vaccines have improved COVID-19 disease outcomes and neutralizing monoclonal antibodies were effective at preventing and treating early strains of SARS-CoV-2 infection (235, 248–251). Therapeutic antibodies play a crucial role in treating SARS-CoV-2 infections to minimize disease-severity. They are invaluable for individuals who cannot receive

vaccinations due to health conditions and for immunocompromised individuals who are unable to mount a protective immune response even after vaccination. However, the ongoing evolution of SARS-CoV-2 has led to the emergence of Omicron variants with numerous mutations, which have significantly diminished the efficacy of antibodies elicited by infection and vaccination, as well as therapeutic monoclonal antibodies (mAbs) (133, 140–142, 252, 253). At present, there is only one currently authorized mAb by the Food and Drug Administration to protect certain immunocompromised individuals (254), meaning the options for treatment of serious cases of COVID-19 are limited in both number and efficacy.

Because the immune response from vaccination and infection is not sterilizing, the virus replicates for days, sometimes weeks, in the face of neutralizing antibodies generated by these exposures, most of which target the receptor binding domain (RBD) in the S1 subunit of the viral spike glycoprotein (104–106, 178, 255). Not surprisingly then, the antibody escape observed for SARS-CoV-2 variants is driven mostly by mutations in the RBD, which shows remarkable ability to tolerate variation while retaining function through epistatic interactions with other mutations (140, 144, 163, 256). Many of these mutations are located at sites targeted by therapeutic mAbs, and are no longer active because they target variable regions within the RBD (133, 140–142, 252). For instance, the JN.1 variant and its sub-lineages are the dominant circulating lineages of this year and are distinguished by the D339H, R346T, F456L, and L455S mutations in RBD (218). S309 (131) was a previously authorized therapeutic mAb that exhibited broad-spectrum neutralizing activity but was recently escaped by JN.1 subvariants due, in part, to the changes in chemical properties at these substitution sites (135, 219, 257, 258).

For these reasons, there is a critical need to understand the properties of antibodies that retain breadth and potency against SARS-CoV-2 variants that target more conserved epitopes. Numerous studies have pursued this goal by identifying mAbs that exhibit broad sarbecovirus neutralizing activity, the hypothesis being these cross-reactive antibodies would target highly

conserved sarbecovirus epitopes that may represent functional constraints to viral evolution (60, 87, 112, 126, 127, 129, 131, 133–135, 185, 210, 259, 260). While a number of these antibodies have been escaped by SARS-CoV-2 Omicron variants, this extensive body of research has shown that there are conserved sarbecovirus epitopes with minimal antigenic variation. We previously identified several such antibodies in one individual that experienced a heterologous antigen exposure of SARS-CoV-2 spike through a Delta breakthrough infection (BTI) subsequent to WH-1 mRNA vaccination (112) (and Chapter 2). One of these mAbs (C68.61) target more sequence conserved regions in the core region of the RBD where there has been minimal antigenic variation in SARS-CoV-2 variants. Interestingly, we have recently discovered that C68.61 shows breadth not only across SARS-CoV-2 variants, but also against diverse sarbecovirus variants (135) (Chapter 2) and selection for resistance against SARS-CoV-2 or SARS-CoV-1 could not be driven *in vitro.*

Given the resilient functional properties of mAbs from this individual after a breakthrough infection, we sought to determine whether mAbs with even greater breadth or potency might be present after subsequent vaccinations and heterologous antigen exposure to genetically diverse SARS-CoV-2. Several studies have shown an increase in breadth and potency in plasma responses with repeated exposure to spike antigen (261, 262), as would be predicted with increased somatic hypermutation (SHM). Likewise, SARS-CoV-2 genetic diversity may provide antigenic diversity that drives the development of a more potent and or broad neutralizing antibody response. In line with this, individuals with an Omicron variant exposure developed higher and broader neutralizing titers against Omicron variants than individuals with multiple exposure to the parental mRNA strain by vaccination (140, 169, 174, 263). Thus, we isolated spike-specific B cells from a later time point in this individual, a time where the last breakthrough infection was during a period when the Omicron BA.5 lineage was the dominant circulating variant (264, 265). To maximize our chances to isolate mAbs to relevant SARS-CoV-2 variants as well as to diverse

sarbecoviruses, we used SARS-CoV-2 Omicron XBB.1.5 and SARS-CoV-1 spike glycoprotein as bait for identifying B cells of interest. We characterized the genetic (clonality, somatic hypermutation) and functional (binding and neutralization activity) properties of mAbs reconstructed from these bound B cells. In this chapter, I will present the data that we have acquired to-date to gain an improved understanding of the antibody response after an Omicron BTI.

MATERIALS AND METHODS

Participant information

Peripheral blood mononuclear cell (PBMC) sample was collected at 30 days after a breakthrough reinfection (likely Omicron BA5 based on dominant circulating variants at the time of reinfection) from an individual, C68. C68 has previously received three doses of the Pfizer-BioNTech mRNA vaccine and was previously infected with the Delta variant. Study participant C68 was enrolled in a study of convalescent adults with respiratory viral infections in the Hospitalized or Ambulatory Adults with Respiratory Viral Infections (HAARVI). This study was approved by University of Washington Protocol #STUDY00000959 and institutional review boards at the Fred Hutchinson Cancer Center.

B cell isolation approach

A PBMC sample from 30 days post-reinfection containing 11.2 million viable cells was stained on ice and sorted as described in (112, 113, 135) with modifications. In brief, cells were washed and stained on ice for 30 minutes using a cocktail of antibodies recognizing the fluorescent proteins APC or PE and the following cell markers: CD3, CD14, CD16, CD19, IgM, and IgD. PBMCs were also incubated with protein APC/PE-labeled with biotinylated SARS-CoV-2 Omicron XBB.1.5 Spike Trimer Protein (Acro Biosystems, cat. SPN-C82Ez-25ug) and biotinylated SARS-CoV-1 Spike trimer (Acro Biosystems, cat. SPN-S82E3-25ug; CUHK-W1 strain, accession#: AY278554.2). Biotinylated spike proteins were conjugated to streptavidin-fluorophores APC/PE (from BioLegend), overnight at 4°C the day before cell sorting. Cells were then washed once and

loaded onto a BD FACS Aria II cell sorter, and IgG expressing antigen-specific B cells were identified as CD3−, CD14−, CD16−, CD19+, IgD−, IgM−, PE+, APC+ and live cells (Ghost Dye Red 780; Tonbo Biosciences cat: 13-0865-T500) and were sorted into a total of four 96-well PCR plates containing RNA storage buffer and stored at −80C.

Recombinant antibody production and purification:

Amplification of variable heavy and light chain genes (VH and VL) were performed as described (112, 113, 135, 236–238). A total of 384 SARS-CoV-2 Omicron XBB.1.5 spike trimer and/or SARS-CoV-1 spike trimer specific B cells were recovered from C68. A total of 265 VH, with 253 yielding productive VH genes (VDJ rearrangement with in-frame open reading frame and with no premature stop codons) were successfully amplified from 384 samples.

The recombinant antibodies were expressed in HEK293F cells through transient transfection with equal amounts of paired heavy and light chain plasmids as described by us elsewhere (112, 113, 135). Antibody gene analysis was conducted with the B cell repertoire genetic analysis software *partis* (191, 266) to assess somatic hypermutation, clonality, and germline inference. In total, 50 VH and VL combinations were produced for testing. Of these 50 mAbs, 24 were RBD-targeting mAbs, 3 N-terminal domain (NTD) mAbs, 3 subdomains I (SD1) mAbs, and 15 S2 subunit-targeting mAbs.

ELISA binding assay

Antibody binding to SARS-CoV-2 or SARS-CoV-1 recombinant spike protein was performed using ELISA as previously described (112, 113, 135, 244). For ELISAs performed in **Figure 3.5**, all antibodies were tested at a single concentration (1000 ng/ml) with OD450 nm values representing the average of technical duplicates with background subtracted from 1x PBS only wells.

For experiments to determine the 50% effective concentration (EC50) of C68.490, ELISAs were performed at a starting concentration of 1000 ng/ml antibody and serially diluted 2-fold for at least 10 dilutions. EC50 was calculated using GraphPad Prism software by fitting a four-parameter

(agonist vs response) nonlinear regression curve with the bottom fixed at 0 and the top constrained to the highest OD450 nm value observed.

Pseudoviral Neutralization assay

Antibodies were tested against pseudotyping lentiviral particles on 293T-ACE2 expressing cells as described previously (112, 113, 135). Sarbecovirus spike plasmids with spike genes specific for SARS-CoV-2 variants, SARS-CoV-1 (Urbani strain), BtKY72 (K493Y/T498W mutant), Khosta-2, WIV1, LYRa3, Pangolin-GD, RsSHC014 were generated as previously described (113, 135). Neutralization assays were carried out with 293T-ACE2 cells stably over-expressing human ACE2 (76). To determine the inhibitory concentration at 50% (IC50) for all mAbs in **Figure 3.6**, antibody dilutions were prepared at a starting concentration of 20 µg/mL and three-fold mAb dilution curves were assessed in a 384-well format. For C68.490 (**Figure 3.9**), antibody dilutions were prepared at a starting concentration of 20 µg/mL and two-fold mAb dilution curves were assessed in a 384-well format. IC50 was calculated in PRISM statistical software by fitting a four-parameter (agonist vs response) nonlinear regression curve with the bottom fixed at 0, the top constrained to 1 and HillSlope > 1.

Alphafold antibody-antigen interaction prediction

Variable domains of the heavy and light chain antibody sequences for C68.490 and the SARS-CoV-2 WH1 RBD sequence (residues 331-531) were input as 3 separate proteins into the GUI at https://alphafoldserver.com/ as molecule type: protein, copies = 1 (213). Predictive structures were generated using AlphaFold3, with 5 predicted structures created for each mAb:RBD complex and the structure with the highest overall confidence score was selected for further analysis. For C68.490, the predictive structures were aligned to the RBD chain of PDB: 6M0J (247) using the align function in Pymol (v2.x) (https://pymol.org), generating an RMSD value and a structural overlay for use in **Figures 3.10** and **3.11**. For S2X259, the AF3 predictive structures were aligned to the experimental determined structure of Fab bound to SARS-CoV-2 WH1 RBD (7M7W) and an RMSD value was similarly calculated.

RESULTS

Isolation of broad SARS-CoV-2 and SARS-CoV-1 spike-specific monoclonal antibodies

To examine the evolution of the antibody response in C68 after additional exposures to SARS-CoV-2, we collected peripheral blood mononuclear cells (PBMCs) from C68 after an Omicron BTI (**Figure 3.1**). We previously used a "bait" approach to enrich for S2 domain- and Delta-spike trimer-specific memory B cells from C68 after this individual received two doses mRNA vaccine and experienced a Delta BTI (**Figure 3.1**) and characterized mAbs from this individual (112, 113, 135). Here, we examined a later time-point in which C68 received one additional vaccination and then experienced an Omicron BTI. To identify antigen-specific B cells, we updated our "bait" approach to enrich for memory B cells that bound to SARS-CoV-2 Omicron XBB.1.5 and or SARS-CoV-1 (CUHK-W1 strain) pre-fusion stabilized spike trimer. Previous studies indicated that approximately 6-22% of the SARS-CoV-2 antibody response after an Omicron BTI was directed at WH-1 RBD (267). While it is possible that our gating strategy would select against WH-1 specific mAbs that contribute to the antibody response, we were interested in SARS-CoV-2 broadly neutralizing and cross-reactive antibodies. Thus, in an effort to identify Omicron-specific memory B cells (MBCs) as well as MBCs with broad sarbecovirus activity we applied this heterologous bait approach.

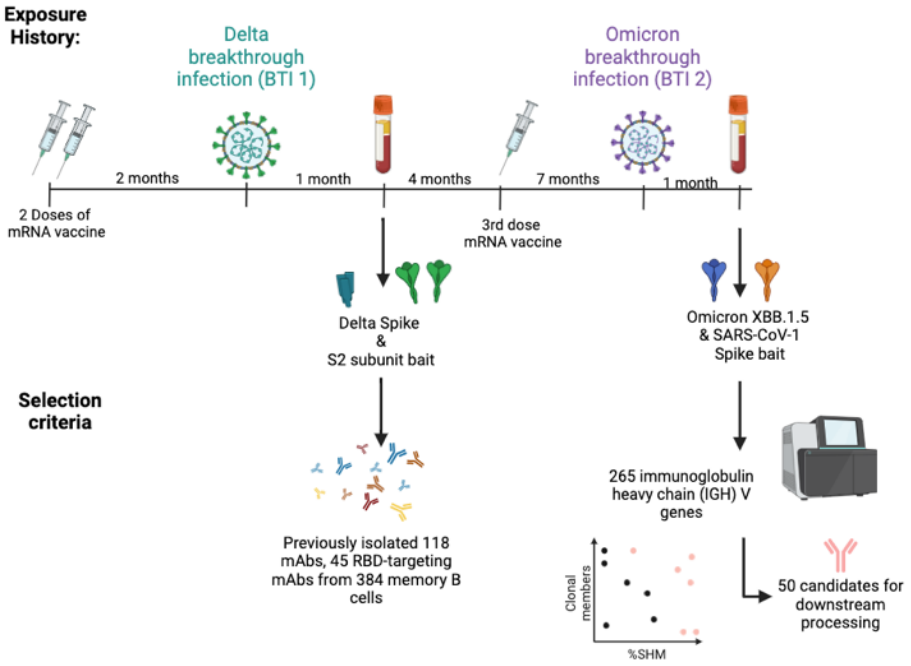

Figure 3.1. C68 exposure history and outline of screening approach for antibody isolation.

From the Delta breakthrough infection (BTI), all memory B cells that bound to Delta spike trimer and S2 domain were reconstructed and functionally characterized (Chapter 2) (112, 113, 135). For the Omicron BTI time point, all heavy chain genes were amplified, sequenced and genes analyzed for clonality and % SHM (criteria elaborated in **Figure 3.2**) to select 50 candidates for downstream antibody production and characterization. Created in BioRender. Ruiz, F. (2024) https://BioRender.com/u08o014.

We isolated 384 MBCs that bound to either SARS-CoV-2 XBB.1.5 or SARS-CoV-1 trimer (spike trimers were biotinylated with both PE and APC, so bound MBCs were PE^+ and APC^+ double positive). Given the low-throughput nature of single B cell cloning for antibody discovery, we chose to streamline our screening process and focus on select samples for further downstream analysis. Our initial antibody amplification approach (**Figure 3.1)** included using antibody heavy chain-specific primers to amplify samples and then sequencing all heavy chain genes to assess gene characteristics (clonality, SHM, in-frame VDJ rearrangement). Amplifying the VH genes allowed us to apply a single primer set for efficient identification of antibody genes. Of the 384 total MBCs, we successfully amplified 265 VH genes, with 253 yielding productive VH

genes (VDJ rearrangement with in-frame open reading frame and with no premature stop codons; **Figure 3.2**).

Our screening process included i) selecting antibody variable heavy chain (VH) genes that are clonal to mAbs identified after the Delta BTI (first BTI, Chapter 2) (112, 113, 135), ii) VH genes that are clonal to other Omicron BTI (second BTI) VH genes and iii) VH genes that exhibit high levels of SHM (**Figure 3.2**). Clonality was determined by assessing if a VH gene has the same variable, diversity and joining (V(D)J) gene segment rearrangement using *partis* (in collaboration with Duncan Ralph of the Matsen group), a BCR sequence annotation software designed for antibody sequence analysis (191, 266). We identified 16 antibody VH genes that were clonal to the Delta BTI mAbs, 8 of which were clonal to RBD-targeting mAbs. 6 VH genes were clonal to S2 or NTD-targeting mAbs and 2 VH genes were clonal to an SD1 targeting mAb. We focused on the 8 candidates that were clonal to RBD targeting mAbs from the Delta BTI time-point using this antibody isolation approach, as mAbs targeting other domains were typically non-neutralizing in the Delta BTI time point. Of the 8 VH genes that were clonal to mAbs from the 1st BTI, 1 VH gene was identical to the 1st BTI mAb C68.121, this was excluded as well. In total, we identified 7 candidates (for criteria i) related to RBD-specific neutralizing mAbs isolated from an earlier time point to analyze their genetic properties (clonality, SHM).

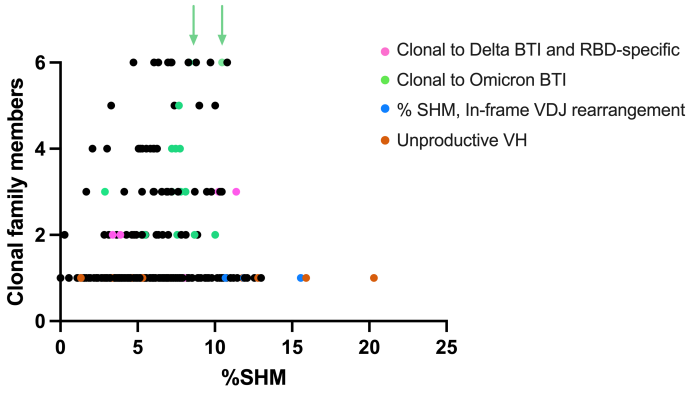

Figure 3.2. Selection criteria and gene characteristics for Omicron BTI isolated antibody variable heavy chain (VH) genes to produce.

We used *partis* to identify clonally related VH genes (based solely on VDJ gene) and assess somatic hypermutation relative to inferred germline genes. A total of 265 VH genes were successfully amplified (all shown above) and found a total of 253 to yield productive VH immunoglobin genes (in-frame VDJ rearrangement and no premature stop codons). 50 VH candidates for downstream antibody production and further characterization were chosen based on clonality to 1st BTI VH genes (pink dots), or clonality to other 2nd BTI VH genes (green), or high levels of SHM for single lineage members (blue). Within an Omicron BTI clonal family, a single representative lineage member was chosen (based on %SHM). Arrows denote an example of 2 representative lineage members chosen from the 2 clonally expanded families that have 6 clonal members. Unproductive VH immunoglobulin genes are shown in orange.

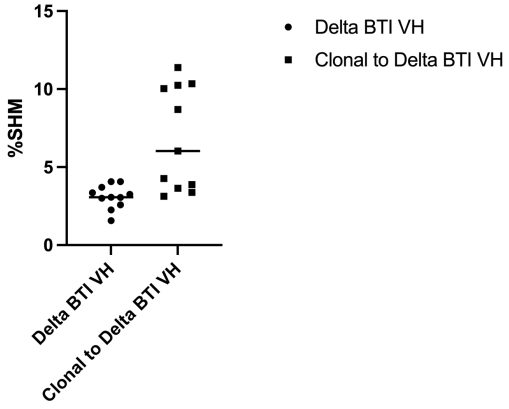

Figure 3.3. Percent SHM among Omicron VH clonal lineage members relative to Delta BTI VH.

We used *partis* to identify clonally related VH genes (based solely on VDJ gene usage) and assess somatic hypermutation relative to inferred germline genes (see **Figure 3.2**). %SHM were plotted and median values were calculated in PRISM. Depicted are the 1st BTI VH genes ("Delta BTI VH)), wherein full recombinant IgGs are known to target RBD of spike, and their clonal lineage members isolated at a later time point ("Clonal to Delta").

In our analysis of the 2nd BTI time point, we observed increased SHM levels and clonal expansion in the mAb sequences compared to the 1st BTI time point. Of the 265 VH genes analyzed from Omicron BTI, 216 diverse clonal lineages were identified, with 22 clonally related families (~85% unique clonal families). In contrast, mAbs isolated from the Delta BTI showed minimal clonal expansion with 118 mAbs representing 111 clonal families (~94% unique clonal

families) (135). Given these findings, along with other studies (176, 268, 269), we hypothesized that the presence of clonally expanded antibody sequences could be of note. We selected at least 1 representative lineage member from the 22 clonally expanded families within this time point (criteria ii) with a preference for those with high levels of %SHM, as higher SHM is associated with improved binding and neutralization activity (210, 270, 271). Among the antibody lineages related to the 1st BTI, the 2nd BTI VH genes showed higher levels of SHM (**Figure 3.3**; median 1st BTI clonal SHM= 3.1%, median 2nd BTI clonal SHM= 6.0%). Finally, to complete our selection of 50 candidate VH genes to produce and test as full IgGs, we selected unique clones (no relation to either 1st BTI VH or 2nd BTI VH clones) with high levels of SHM (criteria iii; **Figure 3.2**).

Affinity maturation garners increased binding and neutralizing activities

Of the 50 antibody candidates selected, 7 were clonal to RBD targeting mAbs from the 1st BTI and thus also likely to be RBD targeting. To assess which domains the rest of these antibodies are targeting (so that we may focus on the RBD-specific mAbs), we assessed binding by ELISA. We assessed subdomain specificities and identified 17 additional RBD-targeting mAbs, 3 N-terminal domain (NTD) mAbs, 3 subdomains I (SD1) mAbs, and 15 S2 subunit-targeting mAbs (**Figure 3.4, Figure 3.5**). We also confirmed that the 8 mAbs clonal to the 1st BTI did bind RBD antigen.

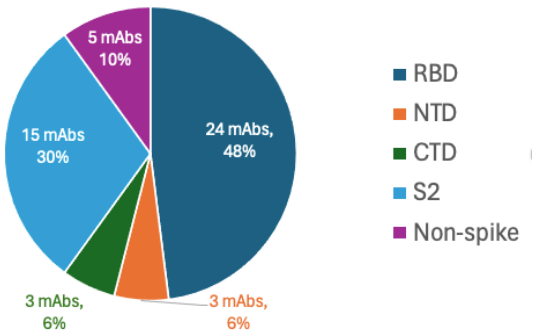

Figure 3.4. C68 reinfection mAbs are targeting different domains within the SARS-CoV-2 spike trimer.

Frequency of mAbs binding to different SARS-CoV-2 domains by ELISA. ELISA plates were coated with 25 µl per well of SARS-CoV-2 protein diluted to 1 µg/ml in PBS and incubated overnight at 4 °C. mAbs were tested in technical duplicate at a set concentration of 1000 ng/ml.

With the 24 identified RBD-specific mAbs, we assessed binding activity against a panel of SARS-CoV-2 and SARS-CoV-1 antigens by ELISA. Additionally, we wanted to determine whether subsequent antigen exposure impacted binding breadth of clonal mAbs, so we included RBD mAbs from the 1st BTI time point (**Figure 3.5**). From these 24-RBD targeting mAbs, 18 out of 24 were able to bind XBB trimer and 16 out of 24 bound SARS-CoV-1 trimer (**Figure 3.5**), which were antigens used in our B cell sort. Considering, we previously isolated 12 cross-reactive RBD mAbs out of 118 mAbs pairings from our previous antibody discovery campaign (the 1st BTI time point (135)), identifying 16 cross-reactive RBD mAbs out of 50 suggests our isolation approach did enrich for mAbs with broad and cross-reactive binding activity. Interestingly, for some Delta BTI mAb lineage members that lacked BQ.1.1 and XBB trimer reactivity, their Omicron BTI counterparts acquired binding to those SARS-CoV-2 variants (**Figure 3.5**). While we observed an increase in binding breadth against SARS-CoV-2 variants, we did not observe acquisition of binding activity against SARS-CoV-1 trimer.

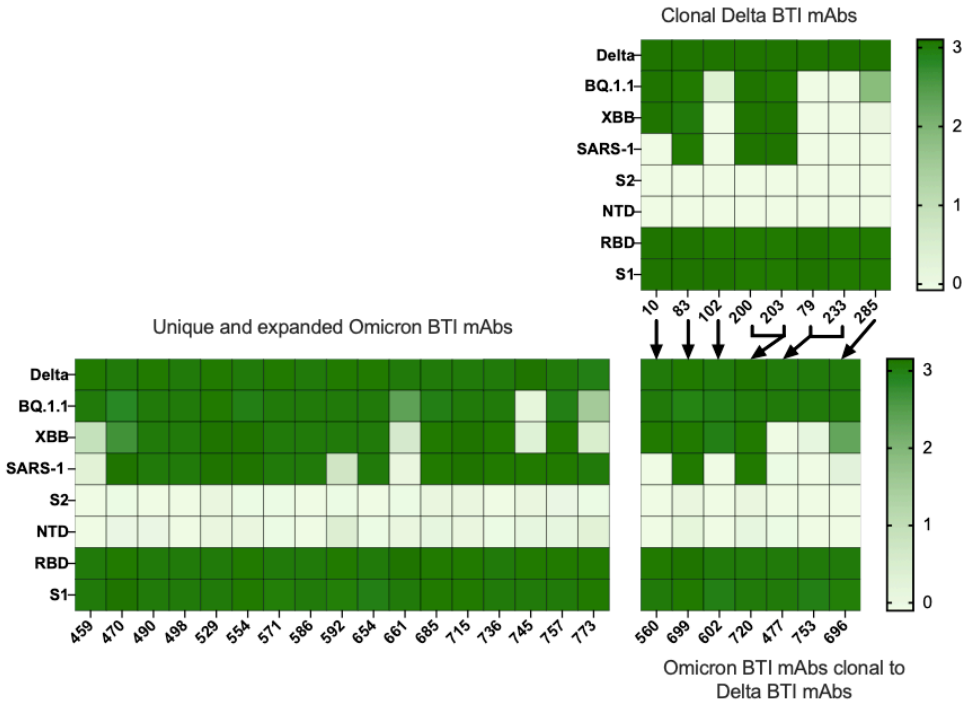

Figure 3.5. C68 Omicron BTI RBD mAbs binding profiles in comparison to clonal Delta BTI mAbs.

Heatmap showing OD450 nm ELISA binding activity of unique and clonal to the Omicron BTI time point are indicated on the left (light green indicates lack of activity while darker green indicates binding). Arrows indicate clonal lineage members on the right. ELISA plates were coated with 25 µl per well of SARS-CoV-2 protein diluted to 1 µg/ml in PBS and incubated overnight at 4 °C. mAbs were tested in technical duplicate at a set concentration of 1000 ng/ml.

To assess the impact of affinity maturation on the functionality of SARS-CoV-2 antibodies, we next compared the neutralization activity between clonal mAbs using a spike pseudotyped lentivirus neutralization assay against a panel of sarbecoviruses that utilize ACE2 for entry (205). The 7 clonal RBD mAbs representing six clonal families were examined (clonal families 1-6; **Figure 3.6**). In most instances, 2nd BTI mAbs had either no change or increased sarbecovirus neutralization compared to their clonal lineage members from the 1st BTI time point (**Figure 3.6**). For example, C68.477 and C68.753 acquired the ability to neutralize Omicron BA.5 and BQ.1.1 compared to their clonal counterpart for the 1st BTI, C68.79 and C68.233. Likewise, C68.699 and

C68.720 are cross-reactive mAbs that not only acquired enhanced neutralization against SARS-CoV-1 relative to their clonal counterparts, C68.83 and C68.200, but also cross-neutralized multiple SARS-related viruses more potently. In total, six of seven 2nd BTI mAbs displayed lower (at least 2-fold) geometric mean IC50s (**Figure 3.7**) and exhibited enhanced breadth and potency relative to lineage members isolated at an earlier time point.

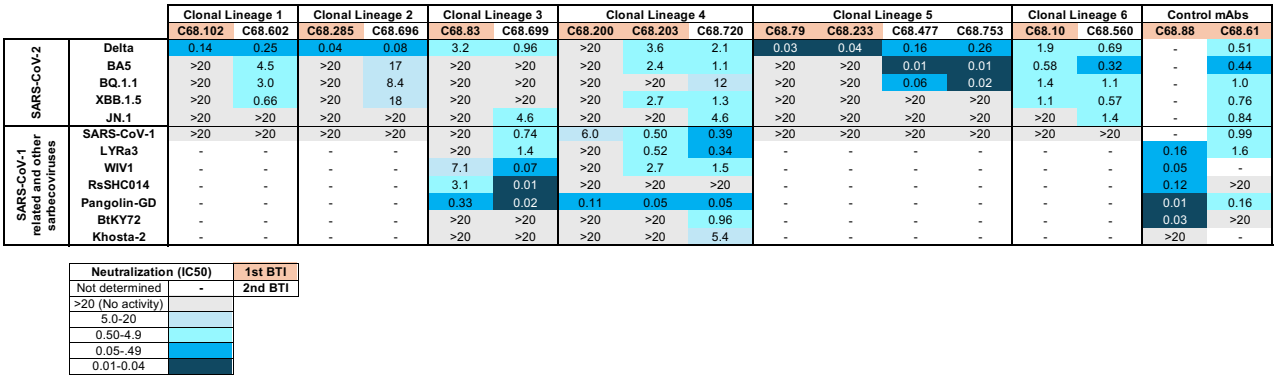

Figure 3.6. Affinity matured C68 mAbs display enhanced neutralization activity.
Heatmap showing the neutralization IC50s (half maximal inhibitory concentration) of the clonal C68 antibodies against a panel of sarbecoviruses. IC50 values are averaged from 2–3 experiments performed in technical duplicate. Values are color coded so that the darker shade of blue correlates with IC50 potency. White/grey indicates not tested or no activity (values greater than the tested concentration). All mAbs were tested starting at 20 ug/ml in 3-fold dilutions over a six-point dilution series. IC50 values were calculated with GraphPad Prism, with a four-parameter non-linear regression model. C68.88 and C68.61 are positive control mAbs that have activity across sarbecoviruses.

Statistics for all sarbecovirus neutralization		
mAb ID	Geomean	95% CI
C68.102	8.7	(73, 1)
C68.602	3.1	(20, 0.48)
C68.285	7.2	(100, 0.52)
C68.696	6.6	(65, 0.68)
C68.83	9.6	(22, 4.2)

C68.699	1.6	(9.5, 0.26)
C68.200	12	(31, 4.5)
C68.203	3.4	(12, 1)
C68.720	1.5	(4.4, 0.54)
C68.79	6.8	(110, 0.43)
C68.233	7.1	(100, 0.49)
C68.477	0.88	(38, 0.02)
C68.753	0.87	(38, 0.02)
C68.10	3.0	(15, 0.6)
C68.560	1.3	(5.8, 0.27)
C68.88	0.13	(2.2, 0.01)
C68.61	1.3	(4, 0.43)

Figure 3.7. Geometric mean IC50s of C68 mAbs along with 95% confidence interval (CI). Geometric means of the IC50 values were calculated with GraphPad Prism along a 95% CI. Indicated in pink are mAbs from the 1st BTI time point and in white are mAbs from the 2nd BTI time point. C68.88 and C68.61 are positive control mAbs that have activity across sarbecoviruses.

We also evaluated the neutralizing ability of the 2nd BTI mAbs that were selected to represent clonal families present at the 2nd BTI, but not found in the 1st BTI (clonal families 7-21) against SARS-CoV-2 Omicron XBB.1.5 and SARS-CoV-1 spike-pseudotyped lentivirus (pseudoviruses bearing the screening spike). With the exception of C68.459 and C68.661, all mAbs were capable of neutralizing one or both screening pseudoviruses with moderate to potent activity (**Figure 3.8**). Against SARS-CoV-2 XBB.1.5, IC50s ranged from non-neutralizing to 0.57 ug/ml (average IC50 = 9.7 ug/ml). Interestingly, all mAbs more potently neutralized SARS-CoV-1 than XBB.1.5 with IC50s ranging from non-neutralizing to 0.02 ug/ml (average IC50 = 4.2 ug/ml). While these antibody responses were elicited in a viral context that did not include XBB.1.5 or SARS-CoV-1, RBD-targeting mAbs isolated from this individual cross-neutralized either or both viruses.

C68.459 and C68.661's lack of neutralizing activity against either screening virus could be explained by their limited binding activity to the corresponding spike trimer. Both of these mAbs bound BQ.1.1 trimer exhibited little to no binding to XBB or SARS-CoV-1 trimer (**Figure 3.5**). Key residues that differ between Omicron XBB, Omicron BQ.1.1 and SARS-CoV-1 spike trimer include sites 445, 446 and 490 which are sites where mutations convergently arise in multiple SARS-CoV-2 variant lineages and may be targeted by these two C68 mAbs (140).

		Neutralization data (IC50)	
Clonal Family	**mAb**	**SARS-CoV-2 XBB.1.5**	**SARS-CoV-1 (Urbani strain)**
6	C68.470	>20	0.60
	C68.773	>20	0.36
7	C68.459	>20	>20
8	C68.490	1.3	0.020
9	C68.498	0.89	0.36
10	C68.529	8.3	1.9
11	C68.554	3.5	0.46
12	C68.571	3.6	1.1
13	C68.586	1.4	1.0
14	C68.592	0.57	>20
15	C68.654	7.2	0.35
16	C68.661	>20	>20
17	C68.685	14	1.9
18	C68.715	13	1.9
19	C68.736	0.58	0.29
20	C68.745	>20	0.32
21	C68.757	10	1.0

Neutralization data (IC50)	
Not determined	-
>20 (No activity)	
5.0-20	
0.50-4.9	
0.05-.49	
0.01-0.04	

Figure 3.8. Characterizing the functional properties of C68 Omicron mAbs.
Neutralization IC50 (ug/ml) for each mAb against pseudoviruses bearing the screening spike. Antibodies were serially diluted and tested at a starting dilution concentration of 20 ug/ml and diluted 3-fold over 6 dilutions. Data indicate the cumulative IC50 from represent duplicate measurements from two independent experiments. IC50 values (ug/mL) were then calculated by nonlinear regression analysis using Graphpad Prism. IC50 values greater than the highest tested concentration were set to the highest concentration for this calculation.

Functional characterization of a broad and potent cross-neutralizing mAb C68.490

We isolated several antibodies that cross-neutralized SARS-CoV-1, but only C68.490 potently neutralized (< 0.1 ug/ml) such that we sought to assess neutralization against other SARS-like viruses. C68.490 potently neutralized all ACE2-utilizing sarbecovirus clades in our virus panel (**Figure 3.9**), including BtKY72 from clade 3 and RsSHC014 from clade 1A, which have less than 75% sequence similarity to SARS-CoV-2 WH-1. C68.490 exhibited broad specificity to sarbecoviruses in all clades on par with the cross-reactive mAb S2X259 (129), but surpassed its neutralization activity against SARS-CoV-2 Omicron BA.2 and above variants. We observed minimal folds in reduction against a recently circulating Omicron subvariants JN.1 and EG.5.1, which have caused severe reduction in neutralization in other broadly neutralizing mAbs, like S309 (131, 135). For all Omicron variants tested, we observed IC50s of 3 ug/ml or less, a similar neutralization profile as the class 5 core RBD-targeting mAb C68.61 (112, 113, 135).

C68.490 displayed approximately an 8-fold reduction in neutralizing activity against Omicron BA.2 compared to BA.1, meaning alterations in spike between BA.1 and BA.2 may partially impact neutralization. In analyzing the mutations that occur in the RBD between Omicron BA.1 and Omicron BA.2, there are three mutations: T376A, D405N, and R408S (264). These mutations may account for the reduced neutralization pattern against Omicron sub-lineages starting at BA.2. Of note, these are also carried in Omicron subvariants including the recently circulating JN.1 variant; neutralization of this variant was intermediate to BA.1 and BA.2.

		C68.490	S2X259	C68.61
SARS-CoV-2	WH-1	0.10	0.09	0.67
	Delta	0.23	0.20	0.24
	BA.1	0.26	1.4	0.57
	BA.2	2.2	>20	1.0
	BA.5	1.0	>20	0.53
	BQ.1.1	1.3	>20	1.0
	XBB.1.5	1.7	>20	0.80
	EG.5.1	0.84	-	0.46
	JN.1	0.59	-	0.46
SARS-CoV-1 related and other sarbecoviruses	SARS-CoV-1	0.01	0.01	0.37
	Pangolin-GD	0.03	0.02	0.06
	WIV1	0.02	0.04	1.1
	RsSHC014	0.02	0.04	>20
	LYRa3	0.02	0.06	6.5
	BtKY72	0.04	0.05	0.14
	Khosta-2	0.09	0.31	>20

Neutralization (IC50)	
Not determined	-
>20 (No activity)	
5.0-20	
0.50-4.9	
0.05-.49	
0.01-0.04	

Figure 3.9. Broad and potent neutralization to sarbecoviruses in all clades by C68.490. Neutralization of pseudotyped Omicron subvariants including recently circulating JN.1 and EG.5.1 as well as sarbecoviruses identified in various animal reservoirs. Antibodies were serially diluted and tested at a starting dilution concentration of 20 ug/ml and diluted 2-fold over at least 10 dilutions. IC50 values (ug/mL) were then calculated by nonlinear regression analysis using PRISM from the average of at least two independent experiments with technical replicates. IC50 values greater than the highest tested concentration were set to the highest concentration for this calculation.

Computational approaches for determining C68.490 interaction with SARS-CoV-2 WH-1 RBD

To further dissect the key residues involved in C68.490s recognition of SARS-CoV-2 RBD protein, we used Alphafold3 (AF3; Google DeepMind and Isomorphic Labs collaboration, version Beta) a protein folding deep learning system that models protein–protein interactions (213, 214, 272). Acquiring experimental structural data is technically challenging and time intensive.

Advances in applying computational tools for modeling antibody-antigen complexes may facilitate expedited pathways for understanding these interactions (272).

The latest version of Alphafold, AF3, exhibited improved success at modeling antibody-antigen interactions than previous iterations. AF3 is estimated to have a ~75% success rate at modeling protein-protein interfaces that have been experimentally defined, although the accuracy rate for antibody-antigen interactions is expected to be lower (213). Still, coupling our functional dataset (informs which residues on the viral surface are relevant for antibody binding) with computational approaches (predictions of residues at the antigen and antibody interface) can provide insights into the molecular interactions at the antibody-antigen interface.

Using AF3's interactive web-service (https://alphafoldserver.com/), we generated predicted structures of S2X259. S2X259 is a monoclonal with an experimentally determined structure and the residues on the viral surface contributing to escape from antibody recognition have been defined by deep mutational scanning approaches (129). The experimentally determined structure of S2X259 bound to WH-1 RBD (WH-1 in grey, S2X259 in blue) aligned well with the AF3 predicted-structure (WH-1 in pink, S2X259 in green), with a root-mean-square distance (RMSD) value of 0.461 (**Figure 3.10**, panel A). This indicates a low level of structural deviation of this modeled antibody-antigen complex relative to the experimentally determined complex. We then compared the S2X259-RBD AF3 predicted-structure to the WH-1 RBD structure displaying the predicted escape mutations by DMS. The predicted antibody-antigen interactions defined by AF3 generally aligned well and were near residues identified by DMS (**Figure 3.10**, panel B).

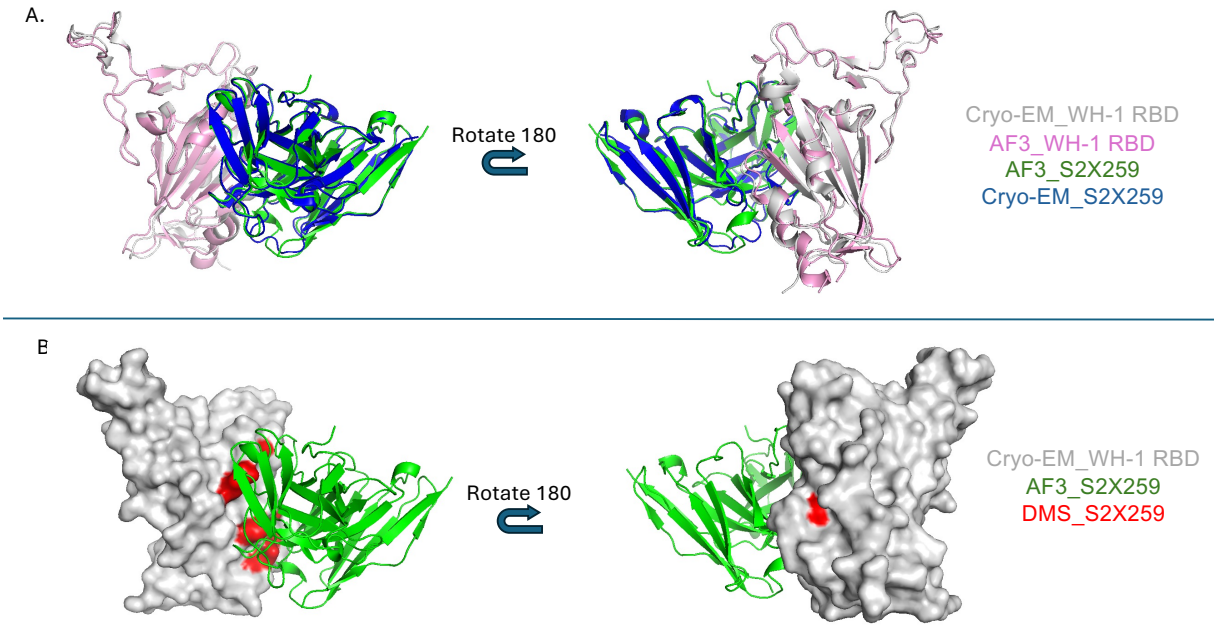

Figure 3.10. Comparing S2X259 structurally defined by predicted antibody-antigen interaction with SARS-CoV-2 WH-1 RBD.

Panel A) We superimposed the experimentally determined structure of S2X259 (PDB: 7M7W) bound to WH-1 RBD (WH-1 in grey, S2X259 in blue) with the AF3 predicted-structure (WH-1 in pink, S2X259 in green), using "cartoon" representation in Pymol. In this comparison, both the predicted antibody-antigen complex structure are compared to the experimentally determined structure using the "align" function in Pymol. Panel B) With a space-filled WH-1 RBD structure, we highlighted the escape sites of S2X259 defined by RBD DMS in red. We aligned the escape profile to the AF3 predicted structure of S2X259 bound to WH-1 RBD.

We assessed AF3's ability to predict structures for C68.490 bound to WH-1 RBD, in comparison to predicted antigen interactions by DMS. The escape pathways for C68.490 identified by DMS, provided by Will Foreman and Tyler Starr (preliminary data, private correspondence) suggest escape occurs at sites K378, P384 and K386. We first superimposed a reference SARS-CoV-2 WH-1 RBD structure (PDB: 6M0J) to the AF3 predicted structure of C68.490 bound to WH-1 RBD. First, the predicted RBD structure aligned well to the reference RBD sequence (RMSD= 0.418) (**Figure 3.11**, panel A), this was a quality control check as we

previously applied Alphafold with mixed results due in large part to incorrect RBD modeling (see **Chapter 3;** (135)). We then aligned the AF3 predicted structure of C68.490 bound to WH-1 RBD with a space-filled WH-1 RBD structure depicting the escape profile for C68.490. Yet again, we see that C68.490 is predicted to interact with RBD near residues relevant for antibody recognition identified by DMS (**Figure 3.11**, panel B).

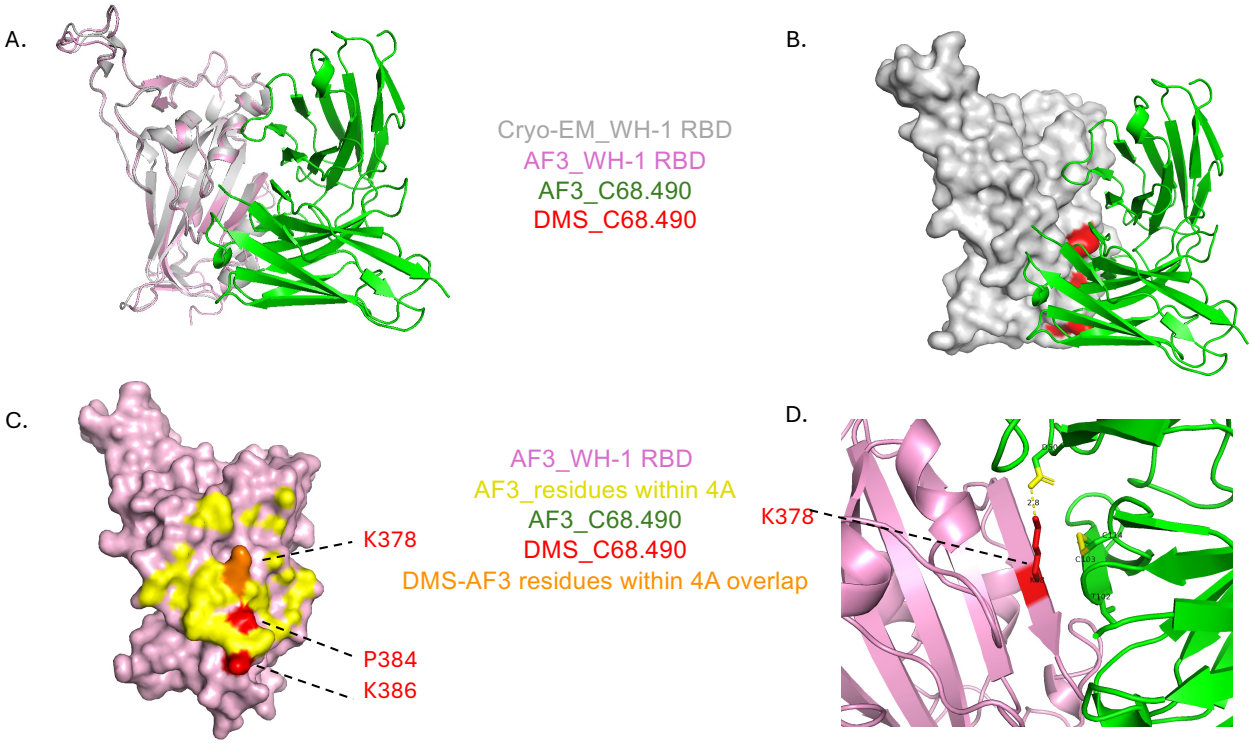

Figure 3.11. Comparing predicted C68.490-RBD interaction with experimentally determined antibody recognition sites defined by DMS.

Panel A) We superimposed the experimentally defined structure of WH-1 RBD (WH-1 in grey) with the AF3 predicted-structure (WH-1 in pink, C68.490 in green), using “cartoon representation” in Pymol. Panel B) With a space-filled WH-1 RBD structure, we highlighted the escape sites of C68.490 defined by RBD DMS in red. We aligned the escape profile to the AF3 predicted structure of C68.490 bound to WH-1 RBD. Panel C) To identify residues that may be in close contact in the AF3 antibody-antigen interface, we used the “select within” command in Pymol to select close contact residues between WH-1 RBD and C68.490 (residues within 4Å; highlighted in yellow and displayed on the RBD). Residues that overlap with sites identified by DMS are shown in orange, with the 3 DMS escape sites labeled. Panel D) Residues on C68.490 that may be in close contact

with site K378 (escape site on the viral RBD) were identified with the “select within” command in Pymol (residues within 4Å; highlighted in yellow and displayed on C68.490 predicted structure) and labeled.

To interrogate the plausible residues in this antibody-antigen interface, we applied a 4Å distance cutoff to assess residues that may be in close contact (273). We identified close to 2 dozen residues on the viral RBD that are within 4Å (**Figure 3.11**, panel C), but only one residue (K378) overlaps with the DMS dataset. It is possible that a number of these predicted sites could be antibody-contact sites, despite not appearing in the escape dataset, as some mutations in this interface may not strongly disrupt antibody binding (137). Also, our strict distance cutoff would not identify potential proximal contact sites (between 4-10 Å). Based on both the preliminary DMS functional epitope profiling and sites identified by antigen-antibody modeling, C68.490 appears to target residues in the SARS-CoV-2 RBD class 4 epitope. We also identified a potential antibody site in close contact to K378, particularly residue D50 (complementarity-determining region 2) on the light chain that could form a salt-bridge with K378 (**Figure 3.11**, panel D).

Overall, AF3 did predict antibody-antigen contact sites in the antibody epitope that to a limited extent overlapped with the experimental dataset. We also identified plausible contact sites on the antibody, though, experimental data will be needed to corroborate identified residues in the paratope as AF3s predictions of intermolecular interactions can be inaccurate, particularly between antibody-antigen complexes.

DISCUSSION

To address the diminished effectiveness of therapeutic monoclonal antibodies against SARS-CoV-2 Omicron sub-lineages, some studies have pursued identifying and characterizing monoclonals elicited by exposure to Omicron variants. Other studies have focused on discovering antibodies with broad sarbecovirus reactivity that may target conserved regions that are

functionally constrained and less likely to evolve. The preliminary findings outlined in this chapter demonstrate the potential of applying both methods for the identification of broadly cross-reactive mAbs. We characterized the antibody response of an individual who experienced a heterologous antigen exposure of WH-1, Delta and Omicron spike through vaccination and multiple vaccine-breakthrough infections. We identified RBD-targeting antibody lineages that were clonally related to an earlier time point and these mAbs neutralized multiple sarbecoviruses more potently or broadly than some of their lineage members. We also identified multiple cross-reactive antibodies with enhanced binding and neutralizing activity against Omicron variants and other animal-derived sarbecoviruses. Notably, one mAb exhibits broad sarbecovirus neutralizing activity and is highly potent against recently circulating Omicron variants highlighting its potential application against emerging SARS-CoV-2 variants and zoonotic sarbecoviruses.

Characterization of mAbs isolated after multiple exposures to SARS-CoV-2 including an Omicron breakthrough infection, illustrated a largely polyclonal response with antibodies originating from multiple B cell lineages. We observed high clonal diversity and a small percentage of clonally expanded families detected at both time points, consistent with previous studies (274). mAbs isolated from the 2nd BTI time point had significantly more VH nucleotide mutations compared with lineage members isolated from an earlier time point, consistent with studies that clonal evolution (higher SHM levels) can result in enhanced functional properties like broader and increased neutralization activity (275).

Lack of isolation of affinity matured or clonal sequences relative to the first BTI for all lineages could be due to multiple factors in our experimental approach. The first, we adjusted our antigen-specific memory B cell isolation approach with the goal of selecting for more broad and cross-reactive mAbs. Using an Omicron spike and SARS-CoV-1 spike trimer could have selected against clonal memory B cells mAbs that exhibited minimal levels of affinity maturation and thus minimal changes in binding affinity (for instance memory B cells that are WH-1 or Delta specific exhibited little to no enhancement in binding breadth) that would not be picked up in our

experimental approach. Also, some studies have found that ~6-22% of the memory B response is WH-1 specific after Omicron BTI subsequent to a WH-1 vaccine (169, 267) or Omicron bivalent vaccination exposure (267), so while it is possible that by updating our bait approach we could have missed these minimally affinity matured B cell lineages, this may represent a small frequency of the antibody subset. We also used a single primer set to amplify the top 50 candidate samples, thus additional antibody discovery of novel and clonal mAbs is possible.

Whether or not the Omicron and SARS-CoV-1-binding memory B cells were reactivated by a 3rd dose of wild-type vaccine (which occurred between breakthrough infections) or breakthrough infection or are the result of *de novo* responses is unclear given our experimental design. Memory B cells are stable for several months post-vaccination (275) and infection (274, 276) and they can be broadly-neutralizing (i.e. Omicron BA1 exposure can elicit antibodies that neutralize Omicron XBB) and cross-neutralizing (elicit core RBD mAbs that exhibit SARS-CoV-1 binding activity). Thus, additional antibody discovery efforts that target mAbs after each exposure would help to fully understand the evolution of the antibody response in this individual with multiple SARS-CoV-2 exposures.

In characterizing the antibody response after exposure to Omicron BTI, we identified a neutralizing antibody that is highly potent against current Omicron variants and broadly neutralizes across multiple clades of sarbecoviruses. Our modeling of the predicted contact interface between C68.490:RBD and preliminary escape mutations by DMS (Foreman and Starr, personal communication) suggested that this mAbs targets the more sequence conserved RBD core region (RBD class 4 mAb). The epitopes of class 4 antibodies target regions that are conserved across sarbecovirus strains, which explains C68.490's ability to neutralize across sarbecovirus clades. Unlike other class 4 mAbs (126, 133), C68.490 retains potent activity against Omicron variants such as the recently circulating JN.1 variant. The JN.1 sublineages that have emerged (JN.1.11.1, KP.3) harbor mutations outside of the predicted escape sites and is thus predicted to maintain neutralizing activities as we observed here for JN.1.

We applied computational approaches to further understand the antibody-antigen interactions. In comparison with the experimentally determined viral residues pertinent for C68.490 recognition, we found antibody C68.490 engages a similar RBD interface as predicted by DMS profiling. Although AF3 can greatly expedite our understanding of antibody-antigen interactions, these predictions can fail (213) and they do not directly indicate the functional residues relevant for neutralization or the viral mutations that escape these interactions. Yet, DMS escape profiling can also be limited by library design and escape mutations may be strain specific (215). A combination of both approaches can be useful for predicting the functional and structural contact sites between antibody-antigen and provide insights into viral pathways of escape from antibody recognition. Additionally, understanding the molecular basis of these antibody-antigen interactions can be used to then guide the design of affinity matured antibodies.

Overall, subsequent exposures through vaccination or infection elicited antibodies enhanced neutralizing potency and breadth relative to clonally related antibodies from a previous time point. Additionally, our experimental approach did enrich for broadly active antibodies. In particular, C68.490 displayed one of the broadest neutralization profiles against ACE2-utilizing sarbecoviruses with spillover risk of any C68 mAb isolated to date. This strategy could be applied in other exposure contexts, such as more recently circulating Omicron variants, to discover additional cross-reactive antibodies against evolving viruses.

Chapter 4:

Conclusions

4.1 Implications for pan-coronavirus vaccine efforts, future directions

Cross-reactive broadly neutralizing sarbecovirus antibodies can develop in SARS-CoV-2 convalescent and vaccinated individual's but typically account for a fraction of elicited antibodies (142). Pan-coronavirus vaccine efforts to elicit cross-reactive antibody responses to conserved epitopes between sarbecovirus strains has included immunizing animal models with diverse sarbecovirus RBDs. While these studies have elicited multi-sarbecovirus clade reactivity in binding and neutralization (277, 278), serum responses typically have poor reactivity against evolving SARS-CoV-2. The goal of this thesis was to investigate cross-neutralizing antibody responses in SARS-CoV-2 exposure contexts and how these responses may change after additional heterologous antigen exposure. The studies presented in this thesis investigated the functional properties of cross-reactive neutralizing antibodies that developed in response to diverse antigen and characterization of these responses that could contribute to the development of a protective pan-coronavirus vaccine.

In this thesis, I showed that a broad range of cross-reactive monoclonals antibodies could be elicited in SARS-CoV-2 infection contexts and, through collaborative studies, that these mAbs target different epitopes within the RBD core. In chapter 2, while the class 4-like mAbs we discovered were exceptionally potent, their breadth is limited. Conversely, the class 5-like mAbs displayed breadth against multiple clades of sarbecoviruses but their potency was limited. In chapter 3, in the same individual with an Omicron breakthrough infection subsequent to the Delta breakthrough, we identified C68.490, a broadly active class-4 antibody that displays activity against every single sarbecovirus variant tested by neutralization. While it exhibits a 10-fold loss

in activity against evolving SARS-CoV-2 compared to its activity against SARS-CoV-2 parental strain WH-1, this is nonetheless quite broad and potent compared to other described antibodies.

These antibodies we isolated from this one individual collectively represent a polyclonal response with less than 10% somatic hypermutation, genetic diversity and diversity in the epitope targets. These near-germline levels of SHM suggests the developmental pathway of these responses could be elicited by vaccination. Importantly, a vaccine will likely require the elicitation of a polyclonal response with mAbs targeting multiple epitopes to obtain a protective pan-coronavirus response.

Given what we have learned about the antibody response over the course of the pandemic, including the studies in this thesis, and the advances made in methods and technologies to tackle infectious disease with antibody-based therapeutics, the following chapter will consider a number of future directions.

4.2 Characterizing affinity matured and novel SARS-CoV-2 monoclonal antibodies

Various studies have been conducted to understand the SARS-CoV-2 antibody responses over time, and their durability against SARS-CoV-2 evolution. Several studies have described isolating and characterizing cross-reactive antibodies (87, 123, 128, 129, 131, 140, 184) from SARS-CoV-1 and SARS-CoV-2 vaccine and infection elicited contexts. Yet, most of these cross-reactive antibodies lose activity against SARS-CoV-2 variants, like Omicron, and were isolated prior to Omicron exposure. Given that individuals that have heterologous exposure to SARS-CoV-2, by vaccination (vaccinated with different spike antigens) (159) or breakthrough infection with Omicron variants (175), developed increased overall neutralizing activity against Omicron variants. These would plausible contexts to understand the development of broadly neutralizing antibodies.

Thus, two questions naturally arise that can be addressed concurrently: what is the affinity maturation pathway of previously isolated cross-reactive antibodies and are there novel

antibodies elicited overtime and after additional exposure to Omicron antigen by vaccination or infection? We would examine the memory B cell compartment overtime in individual C68 to understand the affinity maturation of previously isolated antibodies and how these mutations may contribute to neutralization breadth and potency. This would also allow us to isolate novel broad antibodies and characterize their development. Our group is poised to address this because we have access to longitudinal PBMC samples from individual C68, whose SARS-CoV-2-specific antibody responses we have studied in detail (112, 113, 135), including additional exposure to SARS-CoV-2 antigen (see **Figure 4.1**).

Chapter 3 represents our initial efforts to understand the affinity maturation of cross-reactive antibodies after additional heterologous Omicron spike exposure in this individual. We isolated SARS-CoV-1 and or SARS-CoV-2 cross-reactive memory B cells using a bait approach. Due to limited timing, we chose to perform RT-PCRs and amplification of the variable region of the heavy chain immunoglobulin genes to select antibody lineages that were clonal to the Delta breakthrough infection (chapter 2) to reconstruct antibodies for functional characterization. While we found affinity matured versions of a subset of cross-reactive antibodies, it is worth noting that we used a single primer set to amplify the VH antibody gene fragments. Thus, the use of alternative primer sets (237, 279) could yield additional affinity matured antibody genes, though this can be low-throughput.

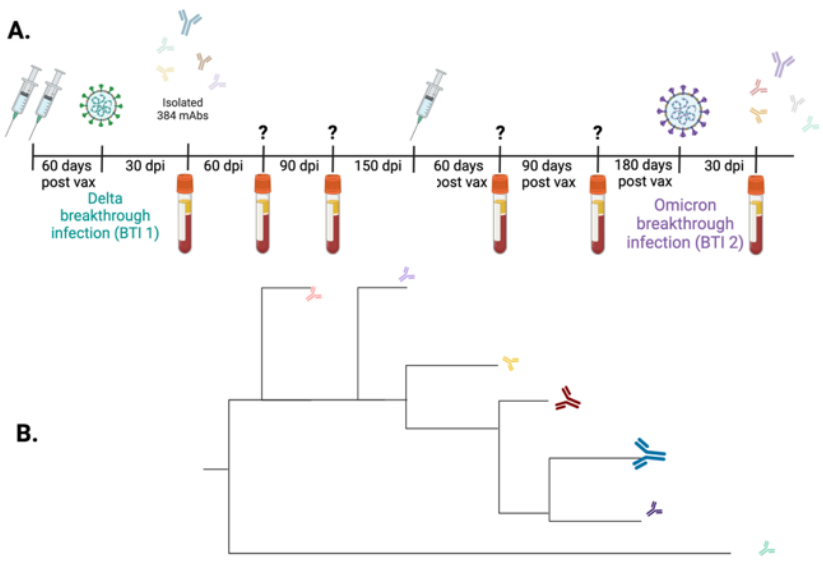

Figure 4.1. C68 longitudinal sample availability and example of lineage tracing developmental pathway for broadly reactive mAbs.
(A) Available longitudinal PBMC samples from C68 post SARS-CoV-2 infection and vaccination. (B) Single-cell RNA sequencing of the B cell repertoire coupled with antibody lineage tracing using the software package *partis* (191), could infer clonality and the likely developmental pathway of isolated antibodies. Created in BioRender. Ruiz, F. (2024) https://BioRender.com/u08o014.

To understand the development of affinity matured and *de novo* cross-reactive antibodies over time and in the setting of SARS-CoV-2 reinfection in high-throughput, I suggest performing single cell B cell receptor (BCR) sequencing of C68's antibody repertoire using longitudinal PBMC samples. Single cell RNA sequencing approaches using 10X Genomics would generate paired sequencing data to reconstruct antibodies. For this experiment, I would perform bulk isolation of IgG+ memory B cells by fluorescence activated cell sorting. To examine the evolution of the B-cell lineages from antibody repertoire sequencing, we would collaborate with the Matsen group to analyze BCR libraries using the software package *partis* (191). We (280, 281) and others (282) have previously performed longitudinal antibody sequencing and used *partis* for antibody lineage tracing.

Lineage tracing from longitudinal timepoints could inform the inferred developmental pathway of affinity matured antibodies overtime, as well as the development of diversified or non-clonal antibodies following additional SARS-CoV-2 exposure. Thus, we could not only isolate

affinity matured and novel antibodies from longitudinal samples, we could also assess what mutations in the antibody sequence contribute to neutralization. In particular, if we find affinity matured lineage members of C68.61 and C68.490 (which target different epitopes), they may exhibit enhanced neutralization activity and could contribute to a broad-spectrum antibody cocktail that would be readily deployable in the event of an outbreak. These results could also offer a detailed dissection of the B cell response, and specifically the maturation of cross-reactive immunity generated overtime and following additional SARS-CoV-2 antigen exposure that could guide strategies to mimic the affinity maturation of the antibody response.

4.3 Use of synthetic biology and protein engineering to affinity mature cross-reactive monoclonal antibodies

There is the possibility that we would not find affinity matured versions of C68 mAbs because these cross-reactive responses constitute a small subset of the antibody response (140) and may not persist overtime. In chapter 3, we found an antibody sequence in the Delta breakthrough infection time point that had not acquired mutations in the Omicron breakthrough infection time point. We also found very little clonality between the two time points. Thus, alternative approaches may be needed to improve the affinity of monoclonals towards sarbecovirus spike trimer.

Advances in synthetic biology with yeast surface display coupled with deep mutational scanning tools have increasingly been employed throughout the SARS-CoV-2 pandemic to understand viral pathways that escape antibody recognition (87, 112, 129, 135, 138–142) and for antibody discovery efforts (283, 284). Yeast surface display techniques can also be used for the engineered affinity maturation of antibodies by introducing random V(D)J mutations into the antibody of interest and using fluorescence-activated cell sorting or magnetic bead binding to SARS-CoV-2 antigen to select for high affinity antibody variants (285). This form of directed evolution by introducing random single V(D)J mutations can lead to no change in affinity, subtle

changes or unproductive antibodies, thus multiple rounds of mutation and selection are conducted that can be quickly screened through using this high-throughput approach (286).

Yeast surface display technology was used by Laura Walker's group to engineer affinity matured versions of multiple SARS-CoV-2 neutralizing antibodies and led to the identification of antibody variants that exhibited improvements in both SARS-CoV-2 spike binding affinity and neutralization potency (210). Additionally, they engineered antibodies that exhibited >10-fold improvement in neutralization against SARS-CoV-1 and related sarbecoviruses relative to the parental mAb.

Thus, I would apply this approach to engineer antibodies with higher affinity towards a recently circulating variant like SARS-CoV-2 JN.1 or an animal sarbeocvirus. Our cross-reactive mAbs, C68.490 and C68.61, display potent activity against sarbecoviruses found in animal reservoirs but have reduced or weak neutralization against SARS-CoV-2 variants. These efforts could increase affinity of mAbs towards SARS-CoV-2 variants. Thus, yeast display technologies can be used to engineer antibodies to enhance binding affinity, neutralization potency and breadth against SARS-CoV-2 and or animal sarbecoviruses. Antibodies that are targeting functionally conserved epitopes and non-overlapping epitopes that are affinity matured towards SARS-CoV-2 could be combined with another mAb resilient to SARS-CoV-2 evolution, such as the recently identified VIR-7229 (287), and could be considered a promising component for next-generation antibody therapeutics against future SARS-CoV-2 evolution. Antibodies that are affinity matured towards an animal sarbecovirus can form the basis of a pan-sarbecovirus antibody cocktail that can be stockpiled for pandemic preparedness.

4.4 Structural studies of C68 Fabs bound to SARS-CoV-2 and other sarbecovirus trimers to understand RBD interactions and conservation of epitope residues

To better identify which residues contribute to the pan-sarbecovirus inhibitory activity of C68 mAbs, like C68.61 and C68.490, we would next determine the residues involved at the

binding interface using cryo–electron microscopy of spike trimer bound to C68 antigen-binding fragments (Fabs). This would identify the critical residues relevant to antigen recognition. Additionally, understanding these interactions is important to understanding C68 mAbs mechanism of restriction not only against SARS-CoV-2 but against other sarbecoviruses found in nature.

Conformational differences can exist between sarbecovirus spike trimers in the open confirmation such that the RBD protomers can be in different angles or a different number of RBDs may be up in the open confirmation whereby affecting antibody recognition. Such is the case for the antibody 47D11 bound to spike trimer (288). Feldry and colleagues found that the 47D11 Fabs could bind each of the three RBD protomers of SARS-CoV-1 spike trimer but Fabs could only bind two RBD protomers in the partially open conformation of SARS-CoV-2 spike trimer. Additionally, they observed a potential stabilizing salt bridge between the light chain of 47D11 and SARS-CoV-1 spike trimer, which is an electrostatic interaction not observed with SARS-CoV-2. This may partially explain why 47D11 binds to the SARS-CoV-1 spike with higher affinity than SARS-CoV-2 spike. Conformational differences in the spike trimer affecting antibody recognition to SARS-CoV-2 and SARS-CoV-1 spike trimer have been observed with other cross-reactive mAbs (128, 289). Thus, differences in amino acid residues between sarbecovirus spike trimers can affect intermolecular interactions between antibody and trimer, which effect functional properties of antibodies, and can be resolved with structural methods.

In most cases, structurally defined epitopes align with and partially explains the escape maps and epitope profiling using DMS (137). Yet, others have previously shown that not all structurally defined contact sites contribute to the functional epitope, and thus DMS escape mutations occur only at a subset of sites (137, 215, 290). While DMS can identify sites and residues on the viral surface that are relevant for antibody binding, these residues are limited to those that escape antibody recognition and may be context or strain dependent (215), so escape profiles may vary across diverse sarbecovirus strains. Since, we have mapped the escape

profiles of C68 mAbs using SARS-CoV-2 WH-1 deep mutational scanning libraries, I would recommend additionally structurally defining the epitope of these mAbs bound to a currently circulating strain of SARS-CoV-2 and a highly sequence divergent clade 3 sarbecovirus spike trimer, like Khosta-2 spike trimer. The rationale being, that while we know the escape profile in the context of SARS-CoV-2 WH-1, the potential pathways of escape maybe altered and widened in different SARS-CoV-2 variants and in different sarbecoviruses. Thus, there is a need to understand the structural epitope in these different viral backgrounds to assess antibody-antigen contact sites and aid in predicting neutralization (or escape) against these viruses.

As noted above, structural contacts may explain how some C68 cross-reactive mAbs accommodate residues that are substituted between SARS-CoV-2 and other sarbecoviruses. For example, RBD DMS identified K462 in SARS-CoV-2 as a site of escape for C68.61and this residue is substituted to R462 in SARS-CoV-1 and SARS-related viruses (112). Arginine and Lysine are both polar amino acids and C68.61 retains neutralization activity against both viruses (in chapter 2). Yet, in the case of Khosta-2 that contains the same R462 as SARS-CoV-1, C68.61 loses binding and consequently neutralization against this sarbecovirus despite no other amino acid changes in contact residues identified by RBD DMS. Structural studies with another clade 3 sarbecovirus like Khosta-1 (which shares 68% sequence identity to Khosta-2) or BtkY72 could reveal the potential differences in binding mode and the electrostatic interactions that are formed that allows this mAb to accommodate residues altered between sarbecoviruses.

At this moment, a crystal structure or electron micrograph of antibody Fabs bound to clade 3 sarbecovirus trimer do not exist. Few cryo-electron microscopy structures exist of non-SARS-CoV-2 sarbecovirus trimers likely because this is a low-throughput and technically challenging technique. Only last year was there a cryo-EM structure of the clade 3 sarbecovirus PRD-0038 RBD bound to its host *Rhinolophus* ACE2 (88). In this paper, Lee and colleagues found several substitutions and deletions in the PRD-0038 RBD relative to SARS-CoV-2 and SARS-CoV-1 that led to new electrostatic interactions and RBD remodeling and may explain PRD-0038 RBDs

inability to bind human ACE2. They also resolved the prefusion structure of PRD-0038 trimer using cryo-EM and found primarily closed PRD-0038 Spike trimers which could be due to glycosylation differences between PRD-0038 and SARS-CoV-2 (230, 291). Understanding these conformational changes is relevant because conformational states modulate the accessibility of certain epitopes. Thus, it is pivotal to not only understand the residues relevant for C68 mAbs to interact with SARS-CoV-2 spike trimer but also other sarbecoviruses.

Ultimately, this structural information can contribute to immunogen design such as structure-based immunogen design (292). In structure-based vaccine design, the antibody-antigen binding sites are used to design immunogens to these antibody responses. The C68.61, C68.490 and other C68 antibody lineages should be considered an attractive template for vaccine design given their near-germline levels of SHM (<10 %SHM) (112, 135). Considering that class 4 and class 5 RBD targeting antibodies appear to be subdominant compared to other antibody classes, immunofocusing may be one approach to try and elicit these responses. Immunofocusing is an approach to direct the antibody response toward certain epitopes by occluding or masking other epitopes. Peter Kim's group recently published a preprint applying this immunofocusing approach towards eliciting S2x259-like antibodies (a cross-reactive, class 4 targeting antibody) (293). By harnessing the relevant contact sites defined by the structural (experimental structural determination) and functional (binding residues identified by DMS) epitope of S2x259, they used protein engineering to focus the response and succeeded in eliciting increased cross-reactive responses. This approach could be extended to eliciting C68.61- and C68.490-like cross-reactive antibodies that may be durable not only against SARS-CoV-2 variants but also other animal sarbecoviruses.

4.5 Conclusion

Eliciting cross-reactive neutralizing antibodies that target conserved sarbecovirus epitopes is a major goal of pan-coronavirus vaccine efforts. Antibodies that exhibit durable

neutralizing activity against diverse sarbecoviruses appear to be rare. Studying the contexts in which these responses develop and how antibodies affinity mature after additional antigen exposure can inform how to elicit these protective responses and identify broad neutralizing antibodies that could readily be deployed in the event of an outbreak. It's clear that core RBD epitopes may represent functionally conserved epitopes that may be targeted by resilient and broad neutralizing antibodies, like the class 4 and class 5 mAbs described in this thesis. Focusing the immune response towards these epitopes may have broader implications for eliciting not only SARS-CoV-2 vaccines durable to evolving virus but also pan-sarbecovirus immunity. Additionally, these antibodies display potent neutralization against animal sarbecovirues and could be stockpiled for pandemic preparedness.

References

1. T. G. Ksiazek, *et al.*, A novel coronavirus associated with severe acute respiratory syndrome. *N. Engl. J. Med.* **348**, 1953–1966 (2003).
2. C. Drosten, *et al.*, Identification of a novel coronavirus in patients with severe acute respiratory syndrome. *N. Engl. J. Med.* **348**, 1967–1976 (2003).
3. P. Zhou, *et al.*, A pneumonia outbreak associated with a new coronavirus of probable bat origin. *Nature* **579**, 270–273 (2020).
4. F. Wu, *et al.*, A new coronavirus associated with human respiratory disease in China. *Nature* **579**, 265–269 (2020).
5. A. M. Zaki, S. van Boheemen, T. M. Bestebroer, A. D. M. E. Osterhaus, R. A. M. Fouchier, Isolation of a novel coronavirus from a man with pneumonia in Saudi Arabia. *N. Engl. J. Med.* **367**, 1814–1820 (2012).
6. World Health Organization 2023 data.who.int. *WHO Coronavirus (COVID-19) dashboard > Cases [Dashboard]*. Available at: https://data.who.int/dashboards/covid19/cases [Accessed 20 August 2024].
7. H. F. Boncristiani, M. F. Criado, E. Arruda, “Respiratory Viruses” in *Encyclopedia of Microbiology*, M. Schaechter, Ed. (Elsevier, 2009), pp. 500–518.
8. A. C. Walls, *et al.*, Structure, Function, and Antigenicity of the SARS-CoV-2 Spike Glycoprotein. *Cell* **181**, 281-292.e6 (2020).
9. J. ter Meulen, *et al.*, Human monoclonal antibody combination against SARS coronavirus: synergy and coverage of escape mutants. *PLoS Med.* **3**, e237 (2006).
10. J. Sui, *et al.*, Evaluation of human monoclonal antibody 80R for immunoprophylaxis of severe acute respiratory syndrome by an animal study, epitope mapping, and analysis of spike variants. *J. Virol.* **79**, 5900–5906 (2005).
11. T. C. Greenough, *et al.*, Development and characterization of a severe acute respiratory syndrome-associated coronavirus-neutralizing human monoclonal antibody that provides effective immunoprophylaxis in mice. *J. Infect. Dis.* **191**, 507–514 (2005).
12. L. Du, Y. Yang, X. Zhang, F. Li, Recent advances in nanotechnology-based COVID-19 vaccines and therapeutic antibodies. *Nanoscale* **14**, 1054–1074 (2022).
13. P. Mlcochova, *et al.*, SARS-CoV-2 B.1.617.2 Delta variant replication and immune evasion. *Nature* **599**, 114–119 (2021).
14. M. Levine-Tiefenbrun, *et al.*, Viral loads of Delta-variant SARS-CoV-2 breakthrough infections after vaccination and booster with BNT162b2. *Nat. Med.* **27**, 2108–2110 (2021).
15. R. Gupta, L. A. Purcell, D. Corti, H. W. Virgin, Pandemic preparedness strategies must go beyond vaccines. *Sci. Transl. Med.* **15**, eadd3055 (2023).
16. Fields B, Knipe D, and Howley P, *Field’s Virology, 7th Edition,* (Lippincott Williams & Wilkins, 2020).
17. D. A. Wilkinson, L. Joffrin, C. Lebarbenchon, P. Mavingui, Analysis of partial sequences of the RNA-dependent RNA polymerase gene as a tool for genus and subgenus classification of coronaviruses. *J. Gen. Virol.* **101**, 1261–1269 (2020).
18. A. Llanes, *et al.*, Betacoronavirus Genomes: How Genomic Information has been Used to Deal with Past Outbreaks and the COVID-19 Pandemic. *Int. J. Mol. Sci.* **21** (2020).
19. P. V’kovski, A. Kratzel, S. Steiner, H. Stalder, V. Thiel, Coronavirus biology and replication: implications for SARS-CoV-2. *Nat. Rev. Microbiol.* **19**, 155–170 (2021).

20. F. Pene, *et al.*, Coronavirus 229E-related pneumonia in immunocompromised patients. *Clin. Infect. Dis.* **37**, 929–932 (2003).
21. J. D. Cherry, P. Krogstad, SARS: the first pandemic of the 21st century. *Pediatr. Res.* **56**, 1–5 (2004).
22. Centers for Disease Control and Prevention, CDC SARS Response Timeline. *Centers for Disease Control and Prevention*. Available at: https://archive.cdc.gov/www_cdc_gov/about/history/sars/timeline.htm. [Accessed 3 June 2024].
23. Z. Shi, Z. Hu, A review of studies on animal reservoirs of the SARS coronavirus. *Virus Res.* **133**, 74–87 (2008).
24. Y. Guan, *et al.*, Isolation and characterization of viruses related to the SARS coronavirus from animals in southern China. *Science* **302**, 276–278 (2003).
25. V. D. Menachery, *et al.*, SARS-like WIV1-CoV poised for human emergence. *Proc. Natl. Acad. Sci. U. S. A.* **113**, 3048–3053 (2016).
26. X.-Y. Ge, *et al.*, Isolation and characterization of a bat SARS-like coronavirus that uses the ACE2 receptor. *Nature* **503**, 535–538 (2013).
27. B. He, *et al.*, Identification of diverse alphacoronaviruses and genomic characterization of a novel severe acute respiratory syndrome-like coronavirus from bats in China. *J. Virol.* **88**, 7070–7082 (2014).
28. E. de Wit, N. van Doremalen, D. Falzarano, V. J. Munster, SARS and MERS: recent insights into emerging coronaviruses. *Nat. Rev. Microbiol.* **14**, 523–534 (2016).
29. Z. Zhu, *et al.*, From SARS and MERS to COVID-19: a brief summary and comparison of severe acute respiratory infections caused by three highly pathogenic human coronaviruses. *Respir. Res.* **21**, 224 (2020).
30. R. Goyal, *et al.*, Comparative highlights on MERS-CoV, SARS-CoV-1, SARS-CoV-2, and NEO-CoV. *EXCLI J.* **21**, 1245–1272 (2022).
31. CSR, MERS outbreaks. *World Health Organization, Eastern Mediterranean Region*. Available at: https://www.emro.who.int/health-topics/mers-cov/mers-outbreaks.html [Accessed 3 June 2024].
32. J. Cui, F. Li, Z.-L. Shi, Origin and evolution of pathogenic coronaviruses. *Nat. Rev. Microbiol.* **17**, 181–192 (2019).
33. T. Carvalho, F. Krammer, A. Iwasaki, The first 12 months of COVID-19: a timeline of immunological insights. *Nat. Rev. Immunol.* **21**, 245–256 (2021).
34. T. Burki, First shared SARS-CoV-2 genome: GISAID vs virological.org. *Lancet Microbe* **4**, e395 (2023).
35. Coronavirus Disease (COVID-19) Situation Reports - archive page. Available at: https://www.who.int/emergencies/diseases/novel-coronavirus-2019/situation-reports/situation-reports-archive [Accessed 7 November 2024].
36. X. He, *et al.*, Temporal dynamics in viral shedding and transmissibility of COVID-19. *Nat. Med.* **26**, 672–675 (2020).
37. Y. Wan, J. Shang, R. Graham, R. S. Baric, F. Li, Receptor Recognition by the Novel Coronavirus from Wuhan: an Analysis Based on Decade-Long Structural Studies of SARS Coronavirus. *J. Virol.* **94** (2020).
38. A. G. Wrobel, Mechanism and evolution of human ACE2 binding by SARS-CoV-2 spike. *Curr. Opin. Struct. Biol.* **81**, 102619 (2023).
39. S. Borkotoky, D. Dey, Z. Hazarika, Interactions of angiotensin-converting enzyme-2 (ACE2) and SARS-CoV-2 spike receptor-binding domain (RBD): a structural perspective. *Mol. Biol. Rep.* **50**, 2713–2721 (2023).
40. F. Li, Structure, Function, and Evolution of Coronavirus Spike Proteins. *Annu Rev Virol* **3**, 237–261 (2016).

41. I. Sola, F. Almazán, S. Zúñiga, L. Enjuanes, Continuous and Discontinuous RNA Synthesis in Coronaviruses. *Annu Rev Virol* **2**, 265–288 (2015).
42. M. R. Denison, R. L. Graham, E. F. Donaldson, L. D. Eckerle, R. S. Baric, Coronaviruses: an RNA proofreading machine regulates replication fidelity and diversity. *RNA Biol.* **8**, 270–279 (2011).
43. D. Kim, *et al.*, The architecture of SARS-CoV-2 transcriptome. *Cell* **181**, 914-921.e10 (2020).
44. B. Malone, N. Urakova, E. J. Snijder, E. A. Campbell, Structures and functions of coronavirus replication-transcription complexes and their relevance for SARS-CoV-2 drug design. *Nat. Rev. Mol. Cell Biol.* **23**, 21–39 (2022).
45. R. L. Graham, J. S. Sparks, L. D. Eckerle, A. C. Sims, M. R. Denison, SARS coronavirus replicase proteins in pathogenesis. *Virus Res.* **133**, 88–100 (2008).
46. D. Forni, R. Cagliani, M. Sironi, Recombination and positive selection differentially shaped the diversity of Betacoronavirus subgenera. *Viruses* **12**, 1313 (2020).
47. H. L. Wells, *et al.*, The coronavirus recombination pathway. *Cell Host Microbe* **31**, 874–889 (2023).
48. C. Hulo, *et al.*, ViralZone: a knowledge resource to understand virus diversity. *Nucleic Acids Res.* **39**, D576-82 (2011).
49. Family: Coronaviridae. Available at: https://ictv.global/report/chapter/coronaviridae/coronaviridae [Accessed 24 August 2024].
50. S. Zhou, *et al.*, SARS-CoV-2 E protein: Pathogenesis and potential therapeutic development. *Biomed. Pharmacother.* **159**, 114242 (2023).
51. J. Mu, *et al.*, SARS-CoV-2 N protein antagonizes type I interferon signaling by suppressing phosphorylation and nuclear translocation of STAT1 and STAT2. *Cell Discov* **6**, 65 (2020).
52. C. Fenwick, *et al.*, Changes in SARS-CoV-2 spike versus nucleoprotein antibody responses impact the estimates of infections in population-based seroprevalence studies. *J. Virol.* **95**, e01828-20 (2021).
53. S. R. Soares, *et al.*, Antibody response to the SARS-CoV-2 spike and nucleocapsid proteins in patients with different COVID-19 clinical profiles. *Viruses* **15**, 898 (2023).
54. D. Li, J. Li, Immunologic testing for SARS-CoV-2 infection from the antigen perspective. *J. Clin. Microbiol.* **59**, JCM.02160-20 (2021).
55. M. A. Tortorici, D. Veesler, Structural insights into coronavirus entry. *Adv. Virus Res.* **105**, 93–116 (2019).
56. B. J. Bosch, R. van der Zee, C. A. M. de Haan, P. J. M. Rottier, The coronavirus spike protein is a class I virus fusion protein: structural and functional characterization of the fusion core complex. *J. Virol.* **77**, 8801–8811 (2003).
57. J. M. White, A. E. Ward, L. Odongo, L. K. Tamm, Viral membrane fusion: A dance between proteins and lipids. *Annu. Rev. Virol.* **10**, 139–161 (2023).
58. M. E. Hamdy, *et al.*, Mutations of the SARS-CoV-2 spike glycoprotein detected in cats and their effect on its structure and function. *Front. Cell. Infect. Microbiol.* **12**, 875123 (2022).
59. C. O. Barnes, *et al.*, SARS-CoV-2 neutralizing antibody structures inform therapeutic strategies. *Nature* **588**, 682–687 (2020).
60. C. A. Jette, *et al.*, Broad cross-reactivity across sarbecoviruses exhibited by a subset of COVID-19 donor-derived neutralizing antibodies. *Cell Rep.* **36**, 109760 (2021).
61. S. M.-C. Gobeil, *et al.*, D614G Mutation Alters SARS-CoV-2 Spike Conformation and Enhances Protease Cleavage at the S1/S2 Junction. *Cell Rep.* **34**, 108630 (2021).
62. Y. Wang, *et al.*, Conformational dynamics of the Beta and Kappa SARS-CoV-2 spike proteins and their complexes with ACE2 receptor revealed by cryo-EM. *Nat. Commun.* **12**, 7345 (2021).
63. M. McCallum, *et al.*, Structural basis of SARS-CoV-2 Omicron immune evasion and receptor engagement. *Science* **375**, 864–868 (2022).

64. R. J. G. Hulswit, *et al.*, Human coronaviruses OC43 and HKU1 bind to 9-O-acetylated sialic acids via a conserved receptor-binding site in spike protein domain A. *Proc. Natl. Acad. Sci. U. S. A.* **116**, 2681–2690 (2019).
65. G. Lu, *et al.*, Molecular basis of binding between novel human coronavirus MERS-CoV and its receptor CD26. *Nature* **500**, 227–231 (2013).
66. Q. Xiong, *et al.*, Close relatives of MERS-CoV in bats use ACE2 as their functional receptors. *Nature* **612**, 748–757 (2022).
67. M. Letko, A. Marzi, V. Munster, Functional assessment of cell entry and receptor usage for SARS-CoV-2 and other lineage B betacoronaviruses. *Nat Microbiol* **5**, 562–569 (2020).
68. T. N. Starr, *et al.*, ACE2 binding is an ancestral and evolvable trait of sarbecoviruses. *Nature* **603**, 913–918 (2022).
69. S. M. Roelle, N. Shukla, A. T. Pham, A. M. Bruchez, K. A. Matreyek, Expanded ACE2 dependencies of diverse SARS-like coronavirus receptor binding domains. *PLoS Biol.* **20**, e3001738 (2022).
70. H. Guo, *et al.*, Isolation of ACE2-dependent and -independent sarbecoviruses from Chinese horseshoe bats. *bioRxiv* 2023.03.02.530738 (2023).
71. W. Li, *et al.*, Angiotensin-converting enzyme 2 is a functional receptor for the SARS coronavirus. *Nature* **426**, 450–454 (2003).
72. H. Guo, *et al.*, ACE2-Independent Bat Sarbecovirus Entry and Replication in Human and Bat Cells. *MBio* **13**, e0256622 (2022).
73. P. Eifart, *et al.*, Role of endocytosis and low pH in murine hepatitis virus strain A59 cell entry. *J. Virol.* **81**, 10758–10768 (2007).
74. L. Zhang, *et al.*, ACE2-independent sarbecovirus cell entry is supported by TMPRSS2-related enzymes and reduces sensitivity to antibody-mediated neutralization. *bioRxiv* 2024.04.18.590061 (2024).
75. S. N. Seifert, *et al.*, An ACE2-dependent Sarbecovirus in Russian bats is resistant to SARS-CoV-2 vaccines. *PLoS Pathog.* **18**, e1010828 (2022).
76. K. H. D. Crawford, *et al.*, Protocol and Reagents for Pseudotyping Lentiviral Particles with SARS-CoV-2 Spike Protein for Neutralization Assays. *Viruses* **12** (2020).
77. M. F. Boni, *et al.*, Evolutionary origins of the SARS-CoV-2 sarbecovirus lineage responsible for the COVID-19 pandemic. *Nat Microbiol* **5**, 1408–1417 (2020).
78. M. M. Becker, *et al.*, Synthetic recombinant bat SARS-like coronavirus is infectious in cultured cells and in mice. *Proc. Natl. Acad. Sci. U. S. A.* **105**, 19944–19949 (2008).
79. T. Tamura, *et al.*, Virological characteristics of the SARS-CoV-2 XBB variant derived from recombination of two Omicron subvariants. *Nat. Commun.* **14**, 2800 (2023).
80. C. Chakraborty, *et al.*, The SARS-CoV-2 Omicron recombinant subvariants XBB, XBB.1, and XBB.1.5 are expanding rapidly with unique mutations, antibody evasion, and immune escape properties - an alarming global threat of a surge in COVID-19 cases again? *Int. J. Surg.* **109**, 1041–1043 (2023).
81. W. Li, *et al.*, Bats are natural reservoirs of SARS-like coronaviruses. *Science* **310**, 676–679 (2005).
82. S. K. P. Lau, *et al.*, Severe acute respiratory syndrome coronavirus-like virus in Chinese horseshoe bats. *Proc. Natl. Acad. Sci. U. S. A.* **102**, 14040–14045 (2005).
83. H. L. Wells, *et al.*, The evolutionary history of ACE2 usage within the coronavirus subgenus Sarbecovirus. *Virus Evol* **7**, veab007 (2021).
84. J. F. Drexler, *et al.*, Genomic characterization of severe acute respiratory syndrome-related coronavirus in European bats and classification of coronaviruses based on partial RNA-dependent RNA polymerase gene sequences. *J. Virol.* **84**, 11336–11349 (2010).
85. C. C. S. Tan, *et al.*, Surveillance of 16 UK native bat species through conservationist networks uncovers coronaviruses with zoonotic potential. *bioRxiv* 2023.01.17.524183 (2023).

86. J. M. Crook, *et al.*, Metagenomic identification of a new sarbecovirus from horseshoe bats in Europe. *Sci. Rep.* **11**, 14723 (2021).
87. T. N. Starr, *et al.*, SARS-CoV-2 RBD antibodies that maximize breadth and resistance to escape. *Nature* **597**, 97–102 (2021).
88. J. Lee, *et al.*, Broad receptor tropism and immunogenicity of a clade 3 sarbecovirus. *Cell Host Microbe* **31**, 1961-1973.e11 (2023).
89. Y. Tao, S. Tong, Complete Genome Sequence of a Severe Acute Respiratory Syndrome-Related Coronavirus from Kenyan Bats. *Microbiol Resour Announc* **8** (2019).
90. S. Alkhovsky, *et al.*, SARS-like Coronaviruses in Horseshoe Bats (Rhinolophus spp.) in Russia, 2020. *Viruses* **14** (2022).
91. L. J. Stockman, R. Bellamy, P. Garner, SARS: systematic review of treatment effects. *PLoS Med.* **3**, e343 (2006).
92. J. ter Meulen, *et al.*, Human monoclonal antibody as prophylaxis for SARS coronavirus infection in ferrets. *Lancet* **363**, 2139–2141 (2004).
93. J. Sui, *et al.*, Potent neutralization of severe acute respiratory syndrome (SARS) coronavirus by a human mAb to S1 protein that blocks receptor association. *Proc. Natl. Acad. Sci. U. S. A.* **101**, 2536–2541 (2004).
94. B. L. Haagmans, A. D. M. Osterhaus, SARS. *Vaccines for Biodefense and Emerging and Neglected Diseases* 671 (2009).
95. M. Spruth, *et al.*, A double-inactivated whole virus candidate SARS coronavirus vaccine stimulates neutralising and protective antibody responses. *Vaccine* **24**, 652–661 (2006).
96. D. Deming, *et al.*, Vaccine efficacy in senescent mice challenged with recombinant SARS-CoV bearing epidemic and zoonotic spike variants. *PLoS Med.* **3**, e525 (2006).
97. W.-C. Cao, W. Liu, P.-H. Zhang, F. Zhang, J. H. Richardus, Disappearance of antibodies to SARS-associated coronavirus after recovery. *N. Engl. J. Med.* **357**, 1162–1163 (2007).
98. J.-T. Lin, *et al.*, Safety and immunogenicity from a phase I trial of inactivated severe acute respiratory syndrome coronavirus vaccine. *Antivir. Ther.* **12**, 1107–1113 (2007).
99. D. Goldblatt, G. Alter, S. Crotty, S. A. Plotkin, Correlates of protection against SARS-CoV-2 infection and COVID-19 disease. *Immunol. Rev.* **310**, 6–26 (2022).
100. P. B. Gilbert, *et al.*, Immune correlates analysis of the mRNA-1273 COVID-19 vaccine efficacy clinical trial. *Science* **375**, 43–50 (2022).
101. Y. Wu, *et al.*, A noncompeting pair of human neutralizing antibodies block COVID-19 virus binding to its receptor ACE2. *Science* **368**, 1274–1278 (2020).
102. T. F. Rogers, *et al.*, Isolation of potent SARS-CoV-2 neutralizing antibodies and protection from disease in a small animal model. *Science* **369**, 956–963 (2020).
103. P. Bégin, *et al.*, Author Correction: Convalescent plasma for hospitalized patients with COVID-19: an open-label, randomized controlled trial. *Nat. Med.* **28**, 212 (2022).
104. L. Piccoli, *et al.*, Mapping Neutralizing and Immunodominant Sites on the SARS-CoV-2 Spike Receptor-Binding Domain by Structure-Guided High-Resolution Serology. *Cell* **183**, 1024-1042.e21 (2020).
105. A. J. Greaney, *et al.*, Comprehensive mapping of mutations in the SARS-CoV-2 receptor-binding domain that affect recognition by polyclonal human plasma antibodies. *Cell Host Microbe* **29**, 463-476.e6 (2021).
106. W. Dejnirattisai, *et al.*, The antigenic anatomy of SARS-CoV-2 receptor binding domain. *Cell* **184**, 2183-2200.e22 (2021).
107. F. Bianchini, *et al.*, Human neutralizing antibodies to cold linear epitopes and subdomain 1 of the SARS-CoV-2 spike glycoprotein. *Sci Immunol* eade0958 (2023).
108. Z. Wang, *et al.*, Analysis of memory B cells identifies conserved neutralizing epitopes on the N-terminal domain of variant SARS-Cov-2 spike proteins. *Immunity* **55**, 998-1012.e8 (2022).

109. L. Liu, *et al.*, Antibodies targeting a quaternary site on SARS-CoV-2 spike glycoprotein prevent viral receptor engagement by conformational locking. *Immunity* **56**, 2442-2455.e8 (2023).
110. L. Liu, *et al.*, Potent neutralizing antibodies against multiple epitopes on SARS-CoV-2 spike. *Nature* **584**, 450–456 (2020).
111. Y. Chen, *et al.*, Broadly neutralizing antibodies to SARS-CoV-2 and other human coronaviruses. *Nat. Rev. Immunol.* **23**, 189–199 (2023).
112. J. Guenthoer, *et al.*, Identification of broad, potent antibodies to functionally constrained regions of SARS-CoV-2 spike following a breakthrough infection. *Proc. Natl. Acad. Sci. U. S. A.* **120**, e2220948120 (2023).
113. J. Guenthoer, *et al.*, The S2 subunit of spike encodes diverse targets for functional antibody responses to SARS-CoV-2. *PLoS Pathog.* **20**, e1012383 (2024).
114. P. Zhou, *et al.*, Broadly neutralizing anti-S2 antibodies protect against all three human betacoronaviruses that cause deadly disease. *Immunity* **56**, 669-686.e7 (2023).
115. M. M. Sauer, *et al.*, Structural basis for broad coronavirus neutralization. *Nat. Struct. Mol. Biol.* **28**, 478–486 (2021).
116. D. Pinto, *et al.*, Broad betacoronavirus neutralization by a stem helix-specific human antibody. *Science* **373**, 1109–1116 (2021).
117. P. Shah, G. A. Canziani, E. P. Carter, I. Chaiken, The case for S2: The potential benefits of the S2 subunit of the SARS-CoV-2 spike protein as an immunogen in fighting the COVID-19 pandemic. *Front. Immunol.* **12**, 637651 (2021).
118. P. Zhou, *et al.*, A human antibody reveals a conserved site on beta-coronavirus spike proteins and confers protection against SARS-CoV-2 infection. *Sci. Transl. Med.* **14**, eabi9215 (2022).
119. C. Dacon, *et al.*, Broadly neutralizing antibodies target the coronavirus fusion peptide. *Science* **377**, 728–735 (2022).
120. C. O. Barnes, *et al.*, Structures of Human Antibodies Bound to SARS-CoV-2 Spike Reveal Common Epitopes and Recurrent Features of Antibodies. *Cell* **182**, 828-842.e16 (2020).
121. S.-M. Lok, An NTD supersite of attack. *Cell Host Microbe* **29**, 744–746 (2021).
122. G. Cerutti, *et al.*, Potent SARS-CoV-2 neutralizing antibodies directed against spike N-terminal domain target a single supersite. *Cell Host Microbe* **29**, 819-833.e7 (2021).
123. J. Hansen, *et al.*, Studies in humanized mice and convalescent humans yield a SARS-CoV-2 antibody cocktail. *Science* **369**, 1010–1014 (2020).
124. B. E. Jones, *et al.*, The neutralizing antibody, LY-CoV555, protects against SARS-CoV-2 infection in nonhuman primates. *Sci. Transl. Med.* **13** (2021).
125. M. Cox, *et al.*, SARS-CoV-2 variant evasion of monoclonal antibodies based on in vitro studies. *Nat. Rev. Microbiol.* **21**, 112–124 (2023).
126. K.-Y. A. Huang, *et al.*, Structural basis for a conserved neutralization epitope on the receptor-binding domain of SARS-CoV-2. *Nat. Commun.* **14**, 311 (2023).
127. Y. Cao, *et al.*, Rational identification of potent and broad sarbecovirus-neutralizing antibody cocktails from SARS convalescents. *Cell Rep.* **41**, 111845 (2022).
128. M. Yuan, *et al.*, A highly conserved cryptic epitope in the receptor binding domains of SARS-CoV-2 and SARS-CoV. *Science* **368**, 630–633 (2020).
129. M. A. Tortorici, *et al.*, Broad sarbecovirus neutralization by a human monoclonal antibody. *Nature* **597**, 103–108 (2021).
130. W. N. Chia, *et al.*, Potent pan huACE2-dependent sarbecovirus neutralizing monoclonal antibodies isolated from a BNT162b2-vaccinated SARS survivor. *Sci Adv* **9**, eade3470 (2023).
131. D. Pinto, *et al.*, Cross-neutralization of SARS-CoV-2 by a human monoclonal SARS-CoV antibody. *Nature* **583**, 290–295 (2020).

132. C. Fan, *et al.*, Neutralizing monoclonal antibodies elicited by mosaic RBD nanoparticles bind conserved sarbecovirus epitopes. *Immunity* **55**, 2419-2435.e10 (2022).
133. E. Cameroni, *et al.*, Broadly neutralizing antibodies overcome SARS-CoV-2 Omicron antigenic shift. *Nature* **602**, 664–670 (2022).
134. J. L. Jensen, *et al.*, Targeting the Spike Receptor Binding Domain Class V Cryptic Epitope by an Antibody with Pan-Sarbecovirus Activity. *J. Virol.* **97**, e0159622 (2023).
135. F. Ruiz, *et al.*, Delineating the functional activity of antibodies with cross-reactivity to SARS-CoV-2, SARS-CoV-1 and related sarbecoviruses. *PLoS Pathog.* **20**, e1012650 (2024).
136. L. B. Shrestha, N. Tedla, R. A. Bull, Broadly-Neutralizing Antibodies Against Emerging SARS-CoV-2 Variants. *Front. Immunol.* **12**, 752003 (2021).
137. A. J. Greaney, *et al.*, Mapping mutations to the SARS-CoV-2 RBD that escape binding by different classes of antibodies. *Nat. Commun.* **12**, 4196 (2021).
138. A. J. Greaney, *et al.*, Complete Mapping of Mutations to the SARS-CoV-2 Spike Receptor-Binding Domain that Escape Antibody Recognition. *Cell Host Microbe* **29**, 44-57.e9 (2021).
139. T. N. Starr, A. J. Greaney, A. S. Dingens, J. D. Bloom, Complete map of SARS-CoV-2 RBD mutations that escape the monoclonal antibody LY-CoV555 and its cocktail with LY-CoV016. *Cell Rep Med* **2**, 100255 (2021).
140. Y. Cao, *et al.*, Imprinted SARS-CoV-2 humoral immunity induces convergent Omicron RBD evolution. *Nature* **614**, 521–529 (2023).
141. Y. Cao, *et al.*, Omicron escapes the majority of existing SARS-CoV-2 neutralizing antibodies. *Nature* **602**, 657–663 (2022).
142. Y. Cao, *et al.*, BA.2.12.1, BA.4 and BA.5 escape antibodies elicited by Omicron infection. *Nature* (2022). https://doi.org/10.1038/s41586-022-04980-y.
143. Y. Weisblum, *et al.*, Escape from neutralizing antibodies by SARS-CoV-2 spike protein variants. *Elife* **9** (2020).
144. L. Witte, *et al.*, Epistasis lowers the genetic barrier to SARS-CoV-2 neutralizing antibody escape. *Nat. Commun.* **14**, 302 (2023).
145. K. Westendorf, *et al.*, LY-CoV1404 (bebtelovimab) potently neutralizes SARS-CoV-2 variants. *Cell Rep.* **39**, 110812 (2022).
146. A. Baum, *et al.*, Antibody cocktail to SARS-CoV-2 spike protein prevents rapid mutational escape seen with individual antibodies. *Science* **369**, 1014–1018 (2020).
147. T. Zohar, *et al.*, Compromised humoral functional evolution tracks with SARS-CoV-2 mortality. *Cell* **183**, 1508-1519.e12 (2020).
148. M. J. Gorman, *et al.*, Fab and Fc contribute to maximal protection against SARS-CoV-2 following NVX-CoV2373 subunit vaccine with Matrix-M vaccination. *Cell Rep Med* **2**, 100405 (2021).
149. E. Brunet-Ratnasingham, *et al.*, Integrated immunovirological profiling validates plasma SARS-CoV-2 RNA as an early predictor of COVID-19 mortality. *Sci Adv* **7**, eabj5629 (2021).
150. S. P. Anand, *et al.*, Longitudinal analysis of humoral immunity against SARS-CoV-2 Spike in convalescent individuals up to 8 months post-symptom onset. *Cell Rep Med* **2**, 100290 (2021).
151. A. Tauzin, *et al.*, A single dose of the SARS-CoV-2 vaccine BNT162b2 elicits Fc-mediated antibody effector functions and T cell responses. *Cell Host Microbe* **29**, 1137-1150.e6 (2021).
152. I. Ullah, *et al.*, Live imaging of SARS-CoV-2 infection in mice reveals that neutralizing antibodies require Fc function for optimal efficacy. *Immunity* **54**, 2143-2158.e15 (2021).
153. E. S. Winkler, *et al.*, Human neutralizing antibodies against SARS-CoV-2 require intact Fc effector functions for optimal therapeutic protection. *Cell* **184**, 1804-1820.e16 (2021).

154. J. B. Case, *et al.*, Resilience of S309 and AZD7442 monoclonal antibody treatments against infection by SARS-CoV-2 Omicron lineage strains. *Nat. Commun.* **13**, 3824 (2022).
155. A. Schäfer, *et al.*, Antibody potency, effector function, and combinations in protection and therapy for SARS-CoV-2 infection in vivo. *J. Exp. Med.* **218** (2021).
156. G. Beaudoin-Bussières, A. Finzi, Deciphering Fc-effector functions against SARS-CoV-2. *Trends Microbiol.* (2024). https://doi.org/10.1016/j.tim.2024.01.005.
157. R. Viana, *et al.*, Rapid epidemic expansion of the SARS-CoV-2 Omicron variant in southern Africa. *Nature* **603**, 679–686 (2022).
158. A. Wilhelm, *et al.*, Limited neutralisation of the SARS-CoV-2 Omicron subvariants BA.1 and BA.2 by convalescent and vaccine serum and monoclonal antibodies. *EBioMedicine* **82**, 104158 (2022).
159. J. E. Bowen, *et al.*, Omicron spike function and neutralizing activity elicited by a comprehensive panel of vaccines. *Science* **377**, 890–894 (2022).
160. W. Dejnirattisai, *et al.*, SARS-CoV-2 Omicron-B.1.1.529 leads to widespread escape from neutralizing antibody responses. *Cell* **185**, 467-484.e15 (2022).
161. T. N. Starr, *et al.*, Deep Mutational Scanning of SARS-CoV-2 Receptor Binding Domain Reveals Constraints on Folding and ACE2 Binding. *Cell* **182**, 1295-1310.e20 (2020).
162. B. Dadonaite, *et al.*, Spike deep mutational scanning helps predict success of SARS-CoV-2 clades. *Nature* **631**, 617–626 (2024).
163. A. L. Taylor, T. N. Starr, Deep mutational scans of XBB.1.5 and BQ.1.1 reveal ongoing epistatic drift during SARS-CoV-2 evolution. *PLoS Pathog.* **19**, e1011901 (2023).
164. T. N. Starr, *et al.*, Deep mutational scans for ACE2 binding, RBD expression, and antibody escape in the SARS-CoV-2 Omicron BA.1 and BA.2 receptor-binding domains. *PLoS Pathog.* **18**, e1010951 (2022).
165. A. Moulana, *et al.*, Compensatory epistasis maintains ACE2 affinity in SARS-CoV-2 Omicron BA.1. *Nat. Commun.* (2022).
166. J. Ito, *et al.*, Convergent evolution of SARS-CoV-2 Omicron subvariants leading to the emergence of BQ.1.1 variant. *Nat. Commun.* **14**, 2671 (2023).
167. A. Yisimayi, *et al.*, Repeated Omicron exposures override ancestral SARS-CoV-2 immune imprinting. *Nature* **625**, 148–156 (2024).
168. F. Muecksch, *et al.*, Increased memory B cell potency and breadth after a SARS-CoV-2 mRNA boost. *Nature* **607**, 128–134 (2022).
169. J. Quandt, *et al.*, Omicron BA.1 breakthrough infection drives cross-variant neutralization and memory B cell formation against conserved epitopes. *Sci Immunol* eabq2427 (2022).
170. F. Jian, *et al.*, Evolving antibody response to SARS-CoV-2 antigenic shift from XBB to JN.1. *Nature* 1–3 (2024).
171. S. Yang, *et al.*, Antigenicity and infectivity characterization of SARS-CoV-2 BA.2.86. *bioRxiv* (2023). https://doi.org/10.1101/2023.09.01.555815.
172. H. D. Stacey, M. S. Miller, Repeated seasonal influenza vaccination: How much is too much of a good thing? *J. Infect. Dis.* **222**, 173–175 (2020).
173. K. van der Straten, *et al.*, Antigenic cartography using sera from sequence-confirmed SARS-CoV-2 variants of concern infections reveals antigenic divergence of Omicron. *Immunity* **55**, 1725-1731.e4 (2022).
174. Collier Ai-ris Y., *et al.*, Immunogenicity of BA.5 Bivalent mRNA Vaccine Boosters. *N. Engl. J. Med.* **388**, 565–567 (2023).
175. Y.-J. Park, *et al.*, Imprinted antibody responses against SARS-CoV-2 Omicron sublineages. *Science* **378**, 619–627 (2022).
176. M. Chernyshev, *et al.*, Vaccination of SARS-CoV-2-infected individuals expands a broad range of clonally diverse affinity-matured B cell lineages. *Nat. Commun.* **14**, 2249 (2023).
177. V. D. Menachery, *et al.*, A SARS-like cluster of circulating bat coronaviruses shows potential for human emergence. *Nat. Med.* **21**, 1508–1513 (2015).

178. D. F. Robbiani, *et al.*, Convergent antibody responses to SARS-CoV-2 in convalescent individuals. *Nature* **584**, 437–442 (2020).
179. M. Yuan, *et al.*, Structural and functional ramifications of antigenic drift in recent SARS-CoV-2 variants. *Science* **373**, 818–823 (2021).
180. X. Tian, *et al.*, Potent binding of 2019 novel coronavirus spike protein by a SARS coronavirus-specific human monoclonal antibody. *Emerg. Microbes Infect.* **9**, 382–385 (2020).
181. M. F. Jennewein, *et al.*, Isolation and characterization of cross-neutralizing coronavirus antibodies from COVID-19+ subjects. *Cell Rep.* **36**, 109353 (2021).
182. A. A. Cohen, *et al.*, Mosaic RBD nanoparticles protect against challenge by diverse sarbecoviruses in animal models. *Science* **377**, eabq0839 (2022).
183. S. Wang, *et al.*, Three SARS-CoV-2 antibodies provide broad and synergistic neutralization against variants of concern, including Omicron. *Cell Rep.* **39**, 110862 (2022).
184. D. R. Martinez, *et al.*, A broadly cross-reactive antibody neutralizes and protects against sarbecovirus challenge in mice. *Sci. Transl. Med.* **14**, eabj7125 (2022).
185. Y.-J. Park, *et al.*, Antibody-mediated broad sarbecovirus neutralization through ACE2 molecular mimicry. *Science* **375**, 449–454 (2022).
186. Office of the Commissioner, Coronavirus (COVID-19) Update: FDA Authorizes Additional Monoclonal Antibody for Treatment of COVID-19. *U.S. Food and Drug Administration* (2021). Available at: https://www.fda.gov/news-events/press-announcements/coronavirus-covid-19-update-fda-authorizes-additional-monoclonal-antibody-treatment-covid-19 [Accessed 18 March 2024].
187. G. Beaudoin-Bussières, *et al.*, A Fc-enhanced NTD-binding non-neutralizing antibody delays virus spread and synergizes with a nAb to protect mice from lethal SARS-CoV-2 infection. *Cell Rep.* **38**, 110368 (2022).
188. D. Li, *et al.*, In vitro and in vivo functions of SARS-CoV-2 infection-enhancing and neutralizing antibodies. *Cell* **184**, 4203-4219.e32 (2021).
189. M. Yuan, *et al.*, A broad and potent neutralization epitope in SARS-related coronaviruses. *Proc. Natl. Acad. Sci. U. S. A.* **119**, e2205784119 (2022).
190. D. Corti, *et al.*, A neutralizing antibody selected from plasma cells that binds to group 1 and group 2 influenza A hemagglutinins. *Science* **333**, 850–856 (2011).
191. D. K. Ralph, F. A. Matsen IV, Inference of B cell clonal families using heavy/light chain pairing information. *arXiv [q-bio.GN]* (2022).
192. D. K. Ralph, F. A. Matsen 4th, Likelihood-Based Inference of B Cell Clonal Families. *PLoS Comput. Biol.* **12**, e1005086 (2016).
193. C. Kreer, *et al.*, Longitudinal Isolation of Potent Near-Germline SARS-CoV-2-Neutralizing Antibodies from COVID-19 Patients. *Cell* **182**, 843-854.e12 (2020).
194. Y. Wang, *et al.*, A large-scale systematic survey reveals recurring molecular features of public antibody responses to SARS-CoV-2. *Immunity* **55**, 1105-1117.e4 (2022).
195. M. Yuan, *et al.*, Structural basis of a shared antibody response to SARS-CoV-2. *Science* **369**, 1119–1123 (2020).
196. X. Jin, *et al.*, Global characterization of B cell receptor repertoire in COVID-19 patients by single-cell V(D)J sequencing. *Brief. Bioinform.* **22** (2021).
197. A. L. Tse, *et al.*, Distinct pathway for evolution of enhanced receptor binding and cell entry in SARS-like bat coronaviruses. *bioRxivorg* 2024.06.24.600393 (2024).
198. D. Wrapp, *et al.*, Cryo-EM structure of the 2019-nCoV spike in the prefusion conformation. *Science* **367**, 1260–1263 (2020).
199. M. Gui, *et al.*, Cryo-electron microscopy structures of the SARS-CoV spike glycoprotein reveal a prerequisite conformational state for receptor binding. *Cell Res.* **27**, 119–129 (2017).

200. A. Addetia, *et al.*, Therapeutic and vaccine-induced cross-reactive antibodies with effector function against emerging Omicron variants. *bioRxiv* 2023.01.17.523798 (2023).
201. A. Zhang, *et al.*, Beyond neutralization: Fc-dependent antibody effector functions in SARS-CoV-2 infection. *Nat. Rev. Immunol.* 1–16 (2022).
202. C. A. Fielding, *et al.*, SARS-CoV-2 host-shutoff impacts innate NK cell functions, but antibody-dependent NK activity is strongly activated through non-spike antibodies. *Elife* **11** (2022).
203. G. Beaudoin-Bussières, J. Richard, J. Prévost, G. Goyette, A. Finzi, A new flow cytometry assay to measure antibody-dependent cellular cytotoxicity against SARS-CoV-2 Spike-expressing cells. *STAR Protoc* **2**, 100851 (2021).
204. C. M. Finnegan, W. Berg, G. K. Lewis, A. L. DeVico, Antigenic properties of the human immunodeficiency virus envelope during cell-cell fusion. *J. Virol.* **75**, 11096–11105 (2001).
205. B. Dadonaite, *et al.*, A pseudovirus system enables deep mutational scanning of the full SARS-CoV-2 spike. *Cell* **186**, 1263-1278.e20 (2023).
206. T. N. Starr, *et al.*, Prospective mapping of viral mutations that escape antibodies used to treat COVID-19. *Science* **371**, 850–854 (2021).
207. J. Dong, *et al.*, Genetic and structural basis for SARS-CoV-2 variant neutralization by a two-antibody cocktail. *Nat Microbiol* **6**, 1233–1244 (2021).
208. A. C. Hunt, *et al.*, Multivalent designed proteins neutralize SARS-CoV-2 variants of concern and confer protection against infection in mice. *Sci. Transl. Med.* **14**, eabn1252 (2022).
209. A. A. Cohen, *et al.*, Mosaic nanoparticles elicit cross-reactive immune responses to zoonotic coronaviruses in mice. *Science* **371**, 735–741 (2021).
210. C. G. Rappazzo, *et al.*, Broad and potent activity against SARS-like viruses by an engineered human monoclonal antibody. *Science* **371**, 823–829 (2021).
211. M. J. Bolton, *et al.*, IgG3 subclass antibodies recognize antigenically drifted influenza viruses and SARS-CoV-2 variants through efficient bivalent binding. *Proc. Natl. Acad. Sci. U. S. A.* **120**, e2216521120 (2023).
212. B. L. Hie, *et al.*, Efficient evolution of human antibodies from general protein language models. *Nat. Biotechnol.* **42**, 275–283 (2024).
213. J. Abramson, *et al.*, Accurate structure prediction of biomolecular interactions with AlphaFold 3. *Nature* **630**, 493–500 (2024).
214. J. Jumper, *et al.*, Highly accurate protein structure prediction with AlphaFold. *Nature* **596**, 583–589 (2021).
215. A. S. Dingens, D. Arenz, H. Weight, J. Overbaugh, J. D. Bloom, An Antigenic Atlas of HIV-1 Escape from Broadly Neutralizing Antibodies Distinguishes Functional and Structural Epitopes. *Immunity* **50**, 520-532.e3 (2019).
216. J. A. Ruffolo, C. Guerra, S. P. Mahajan, J. Sulam, J. J. Gray, Geometric potentials from deep learning improve prediction of CDR H3 loop structures. *Bioinformatics* **36**, i268–i275 (2020).
217. F. Schmidt, *et al.*, Measuring SARS-CoV-2 neutralizing antibody activity using pseudotyped and chimeric viruses. *J. Exp. Med.* **217** (2020).
218. S. Yang, *et al.*, Fast evolution of SARS-CoV-2 BA.2.86 to JN.1 under heavy immune pressure. *Lancet Infect. Dis.* **24**, e70–e72 (2024).
219. P. Li, *et al.*, Distinct patterns of SARS-CoV-2 BA.2.87.1 and JN.1 variants in immune evasion, antigenicity, and cell-cell fusion. *MBio* e0075124 (2024).
220. P. Qu, *et al.*, Immune evasion, infectivity, and fusogenicity of SARS-CoV-2 BA.2.86 and FLip variants. *Cell* **187**, 585-595.e6 (2024).
221. J. Hadfield, *et al.*, Nextstrain: real-time tracking of pathogen evolution. *Bioinformatics* **34**, 4121–4123 (2018).

222. P. Sagulenko, V. Puller, R. A. Neher, TreeTime: Maximum-likelihood phylodynamic analysis. *Virus Evol* **4**, vex042 (2018).
223. F. Jian, *et al.*, Convergent evolution of SARS-CoV-2 XBB lineages on receptor-binding domain 455-456 synergistically enhances antibody evasion and ACE2 binding. *PLoS Pathog.* **19**, e1011868 (2023).
224. D. Focosi, R. Quiroga, S. McConnell, M. C. Johnson, A. Casadevall, Convergent Evolution in SARS-CoV-2 Spike Creates a Variant Soup from Which New COVID-19 Waves Emerge. *Int. J. Mol. Sci.* **24**, 2264 (2023).
225. D. A. Gregory, *et al.*, Genetic diversity and evolutionary convergence of cryptic SARS-CoV-2 lineages detected via wastewater sequencing. *PLoS Pathog.* **18**, e1010636 (2022).
226. S. Karthikeyan, *et al.*, Wastewater sequencing reveals early cryptic SARS-CoV-2 variant transmission. *Nature* **609**, 101–108 (2022).
227. R. Rouet, *et al.*, Broadly neutralizing SARS-CoV-2 antibodies through epitope-based selection from convalescent patients. *Nat. Commun.* **14**, 687 (2023).
228. X. Wang, *et al.*, A potent human monoclonal antibody with pan-neutralizing activities directly dislocates S trimer of SARS-CoV-2 through binding both up and down forms of RBD. *Signal Transduct Target Ther* **7**, 114 (2022).
229. A. G. Wrobel, *et al.*, Evolution of the SARS-CoV-2 spike protein in the human host. *Nat. Commun.* **13**, 1178 (2022).
230. S. Zhang, *et al.*, Loss of Spike N370 glycosylation as an important evolutionary event for the enhanced infectivity of SARS-CoV-2. *Cell Res.* **32**, 315–318 (2022).
231. Q. E. Zhang, *et al.*, SARS-CoV-2 Omicron XBB lineage spike structures, conformations, antigenicity, and receptor recognition. *Mol. Cell* **84**, 2747-2764.e7 (2024).
232. R. Henderson, *et al.*, Controlling the SARS-CoV-2 spike glycoprotein conformation. *Nat. Struct. Mol. Biol.* **27**, 925–933 (2020).
233. N. C. Wu, *et al.*, Diversity of Functionally Permissive Sequences in the Receptor-Binding Site of Influenza Hemagglutinin. *Cell Host Microbe* **21**, 742-753.e8 (2017).
234. H. K. Haddox, A. S. Dingens, S. K. Hilton, J. Overbaugh, J. D. Bloom, Mapping mutational effects along the evolutionary landscape of HIV envelope. *Elife* **7** (2018).
235. D. M. Weinreich, *et al.*, REGEN-COV Antibody Combination and Outcomes in Outpatients with Covid-19. *N. Engl. J. Med.* **385**, e81 (2021).
236. Z. A. Yaffe, *et al.*, Reconstruction of a polyclonal ADCC antibody repertoire from an HIV-1 non-transmitting mother. *iScience* **26**, 106762 (2023).
237. T. Tiller, *et al.*, Efficient generation of monoclonal antibodies from single human B cells by single cell RT-PCR and expression vector cloning. *J. Immunol. Methods* **329**, 112–124 (2008).
238. J. Huang, *et al.*, Isolation of human monoclonal antibodies from peripheral blood B cells. *Nat. Protoc.* **8**, 1907–1915 (2013).
239. C. Simonich, *et al.*, A diverse collection of B cells responded to HIV infection in infant BG505. *Cell Rep Med* **2**, 100314 (2021).
240. N. A. Doria-Rose, *et al.*, New Member of the V1V2-Directed CAP256-VRC26 Lineage That Shows Increased Breadth and Exceptional Potency. *J. Virol.* **90**, 76–91 (2016).
241. H.-X. Liao, *et al.*, High-throughput isolation of immunoglobulin genes from single human B cells and expression as monoclonal antibodies. *J. Virol. Methods* **158**, 171–179 (2009).
242. M.-P. Lefranc, *et al.*, IMGT, the international ImMunoGeneTics information system. *Nucleic Acids Res.* **37**, D1006-12 (2009).
243. M.-P. Lefranc, *et al.*, IMGT®, the international ImMunoGeneTics information system® 25 years on. *Nucleic Acids Res.* **43**, D413-22 (2015).
244. M. E. Garrett, *et al.*, High-resolution profiling of pathways of escape for SARS-CoV-2 spike-binding antibodies. *Cell* **184**, 2927-2938.e11 (2021).

245. A. G. Farrell, *et al.*, Receptor-Binding Domain (RBD) Antibodies Contribute More to SARS-CoV-2 Neutralization When Target Cells Express High Levels of ACE2. *Viruses* **14** (2022).
246. M. Benlarbi, *et al.*, Temperature-dependent Spike-ACE2 interaction of Omicron subvariants is associated with viral transmission. *bioRxiv* 2024.01.20.576353 (2024).
247. J. Lan, *et al.*, Structure of the SARS-CoV-2 spike receptor-binding domain bound to the ACE2 receptor. *Nature* **581**, 215–220 (2020).
248. R. Copin, *et al.*, The monoclonal antibody combination REGEN-COV protects against SARS-CoV-2 mutational escape in preclinical and human studies. *Cell* **184**, 3949-3961.e11 (2021).
249. A. Gupta, *et al.*, Early Treatment for Covid-19 with SARS-CoV-2 Neutralizing Antibody Sotrovimab. *N. Engl. J. Med.* **385**, 1941–1950 (2021).
250. D. M. Weinreich, *et al.*, REGN-COV2, a Neutralizing Antibody Cocktail, in Outpatients with Covid-19. *N. Engl. J. Med.* **384**, 238–251 (2021).
251. Chen Peter, *et al.*, SARS-CoV-2 Neutralizing Antibody LY-CoV555 in Outpatients with Covid-19. *N. Engl. J. Med.* **384**, 229–237 (2021).
252. FDA, FACT SHEET FOR HEALTHCARE PROVIDERS: EMERGENCY USE AUTHORIZATION FOR BEBTELOVIMAB in (2022).
253. Q. Wang, *et al.*, Alarming antibody evasion properties of rising SARS-CoV-2 BQ and XBB subvariants. *Cell* **186**, 279-286.e8 (2023).
254. U.S. Food and Drug Administration (FDA), FACT SHEET FOR HEALTHCARE PROVIDERS: EMERGENCY USE AUTHORIZATION OF PEMGARDA. (03/2024). Available at: https://www.fda.gov/media/177067/download [Accessed 25 July 2024].
255. H. Qi, B. Liu, X. Wang, L. Zhang, The humoral response and antibodies against SARS-CoV-2 infection. *Nat. Immunol.* **23**, 1008–1020 (2022).
256. T. N. Starr, *et al.*, Shifting mutational constraints in the SARS-CoV-2 receptor-binding domain during viral evolution. *Science* **377**, 420–424 (2022).
257. Z. Liu, *et al.*, Neutralization of SARS-CoV-2 BA.2.86 and JN.1 by CF501 adjuvant-enhanced immune responses targeting the conserved epitopes in ancestral RBD. *Cell Rep Med* **5**, 101445 (2024).
258. P. Li, *et al.*, Neutralization escape, infectivity, and membrane fusion of JN.1-derived SARS-CoV-2 SLip, FLiRT, and KP.2 variants. *Cell Rep.* **43**, 114520 (2024).
259. L. Cui, *et al.*, A cryptic site in class 5 epitope of SARS-CoV-2 RBD maintains highly conservation across natural isolates. *iScience* **27** (2024).
260. H. Liu, *et al.*, Cross-Neutralization of a SARS-CoV-2 Antibody to a Functionally Conserved Site Is Mediated by Avidity. *Immunity* **53**, 1272-1280.e5 (2020).
261. Q. Wang, *et al.*, SARS-CoV-2 neutralising antibodies after a second BA.5 bivalent booster. *Lancet* **402**, 1827–1828 (2023).
262. Q. Wang, *et al.*, XBB.1.5 monovalent mRNA vaccine booster elicits robust neutralizing antibodies against XBB subvariants and JN.1. *Cell Host Microbe* **32**, 315-321.e3 (2024).
263. C. Kurhade, *et al.*, Low neutralization of SARS-CoV-2 Omicron BA.2.75.2, BQ.1.1 and XBB.1 by parental mRNA vaccine or a BA.5 bivalent booster. *Nat. Med.* **29**, 344–347 (2023).
264. E. B. Hodcroft, CoVariants: SARS-CoV-2 Mutations and Variants of Interest. *Covariants.org* (2021). Available at: https://covariants.org/ [Accessed 23 July 2024].
265. UW Virology COVID-19 Dashboard. Available at: https://depts.washington.edu/labmed/covid19/ [Accessed 24 July 2024].
266. D. K. Ralph, F. A. Matsen 4th, Consistency of VDJ Rearrangement and Substitution Parameters Enables Accurate B Cell Receptor Sequence Annotation. *PLoS Comput. Biol.* **12**, e1004409 (2016).

267. A. Addetia, *et al.*, Neutralization, effector function and immune imprinting of Omicron variants. *Nature* **621**, 592–601 (2023).
268. G. J. Keitany, *et al.*, Multimodal, broadly neutralizing antibodies against SARS-CoV-2 identified by high-throughput native pairing of BCRs from bulk B cells. *Cell Chem Biol* (2023). https://doi.org/10.1016/j.chembiol.2023.07.011.
269. M. Mor, *et al.*, Multi-clonal SARS-CoV-2 neutralization by antibodies isolated from severe COVID-19 convalescent donors. *PLoS Pathog.* **17**, e1009165 (2021).
270. M. Rapp, *et al.*, Modular basis for potent SARS-CoV-2 neutralization by a prevalent VH1-2-derived antibody class. *Cell Rep.* **35**, 108950 (2021).
271. M. Korenkov, *et al.*, Somatic hypermutation introduces bystander mutations that prepare SARS-CoV-2 antibodies for emerging variants. *Immunity* **56**, 2803-2815.e6 (2023).
272. R. Yin, B. G. Pierce, Evaluation of AlphaFold antibody-antigen modeling with implications for improving predictive accuracy. *Protein Sci.* **33**, e4865 (2024).
273. R. Yin, B. Y. Feng, A. Varshney, B. G. Pierce, Benchmarking AlphaFold for protein complex modeling reveals accuracy determinants. *Protein Sci.* **31**, e4379 (2022).
274. M. Sakharkar, *et al.*, Prolonged evolution of the human B cell response to SARS-CoV-2 infection. *Sci Immunol* **6** (2021).
275. R. R. Goel, *et al.*, mRNA vaccines induce durable immune memory to SARS-CoV-2 and variants of concern. *Science* **374**, abm0829 (2021).
276. K. W. Cohen, *et al.*, Longitudinal analysis shows durable and broad immune memory after SARS-CoV-2 infection with persisting antibody responses and memory B and T cells. *Cell Rep Med* **2**, 100354 (2021).
277. R. A. Hills, *et al.*, Proactive vaccination using multiviral Quartet Nanocages to elicit broad anti-coronavirus responses. *Nat. Nanotechnol.* **19**, 1216–1223 (2024).
278. A. A. Cohen, *et al.*, Mosaic sarbecovirus nanoparticles elicit cross-reactive responses in pre-vaccinated animals. *bioRxivorg* (2024).
279. J. F. Scheid, *et al.*, Sequence and structural convergence of broad and potent HIV antibodies that mimic CD4 binding. *Science* **333**, 1633–1637 (2011).
280. C. A. Simonich, *et al.*, Kappa chain maturation helps drive rapid development of an infant HIV-1 broadly neutralizing antibody lineage. *Nat. Commun.* **10**, 2190 (2019).
281. M. M. Shipley, *et al.*, Functional development of a V3/glycan-specific broadly neutralizing antibody isolated from a case of HIV superinfection. *Elife* **10** (2021).
282. J. Lubow, *et al.*, Single B cell transcriptomics identifies multiple isotypes of broadly neutralizing antibodies against flaviviruses. *PLoS Pathog.* **19**, e1011722 (2023).
283. M. I. Mustafa, A. A. Alzebair, A. Mohammed, Development of Recombinant Antibody by Yeast Surface Display Technology. *Curr Res Pharmacol Drug Discov* **6**, 100174 (2024).
284. F. R. Cross, *et al.*, Expanding and improving nanobody repertoires using a yeast display method: Targeting SARS-CoV-2. *J. Biol. Chem.* **299**, 102954 (2023).
285. B. Ban, R. C. Blake 2nd, D. A. Blake, Yeast Surface Display Platform for Rapid Selection of an Antibody Library via Sequential Counter Antigen Flow Cytometry. *Antibodies (Basel)* **11** (2022).
286. M. Schoof, *et al.*, An ultrapotent synthetic nanobody neutralizes SARS-CoV-2 by stabilizing inactive Spike. *Science* **370**, 1473–1479 (2020).
287. L. E. Rosen, *et al.*, A potent pan-sarbecovirus neutralizing antibody resilient to epitope diversification. *Cell* (2024).
288. J. Fedry, *et al.*, Structural insights into the cross-neutralization of SARS-CoV and SARS-CoV-2 by the human monoclonal antibody 47D11. *Sci Adv* **7** (2021).
289. N. C. Wu, *et al.*, A natural mutation between SARS-CoV-2 and SARS-CoV determines neutralization by a cross-reactive antibody. *PLoS Pathog.* **16**, e1009089 (2020).
290. C. R. Carr, *et al.*, Deep mutational scanning reveals functional constraints and antibody-escape potential of Lassa virus glycoprotein complex. *Immunity* **57**, 2061-2076.e11 (2024).

291. A. C. Walls, *et al.*, Unexpected receptor functional mimicry elucidates activation of Coronavirus fusion. *Cell* **176**, 1026-1039.e15 (2019).
292. B. S. Graham, M. S. A. Gilman, J. S. McLellan, Structure-Based Vaccine Antigen Design. *Annu. Rev. Med.* **70**, 91–104 (2019).
293. T. U. J. Bruun, J. Do, P. A.-B. Weidenbacher, A. Utz, P. S. Kim, Engineering a SARS-CoV-2 vaccine targeting the receptor-binding domain cryptic-face via immunofocusing. *ACS Cent. Sci.* **10**, 1871–1884 (2024).

Supplementary Material

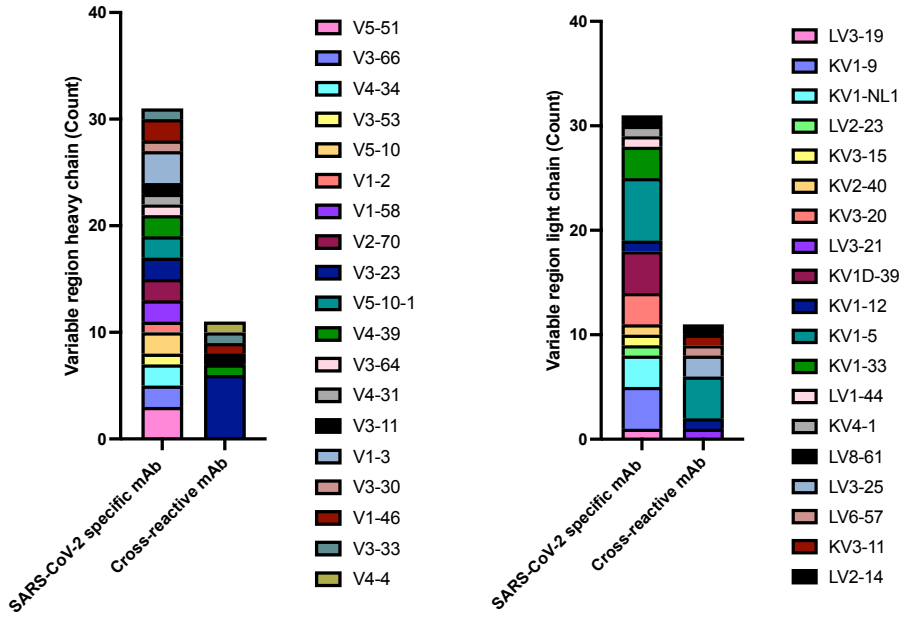

Supplementary Figure 2.1. Antibody heavy and light chain V-gene family characteristics.

Counts for the heavy and light chain V-gene segments among C68 RBD mAbs (related to **Figure 2.1C**) based on *partis* computational software analysis. Antibody heavy (left panel) and light (right panel) chain amino acid sequences found in **S2.1 Table**.

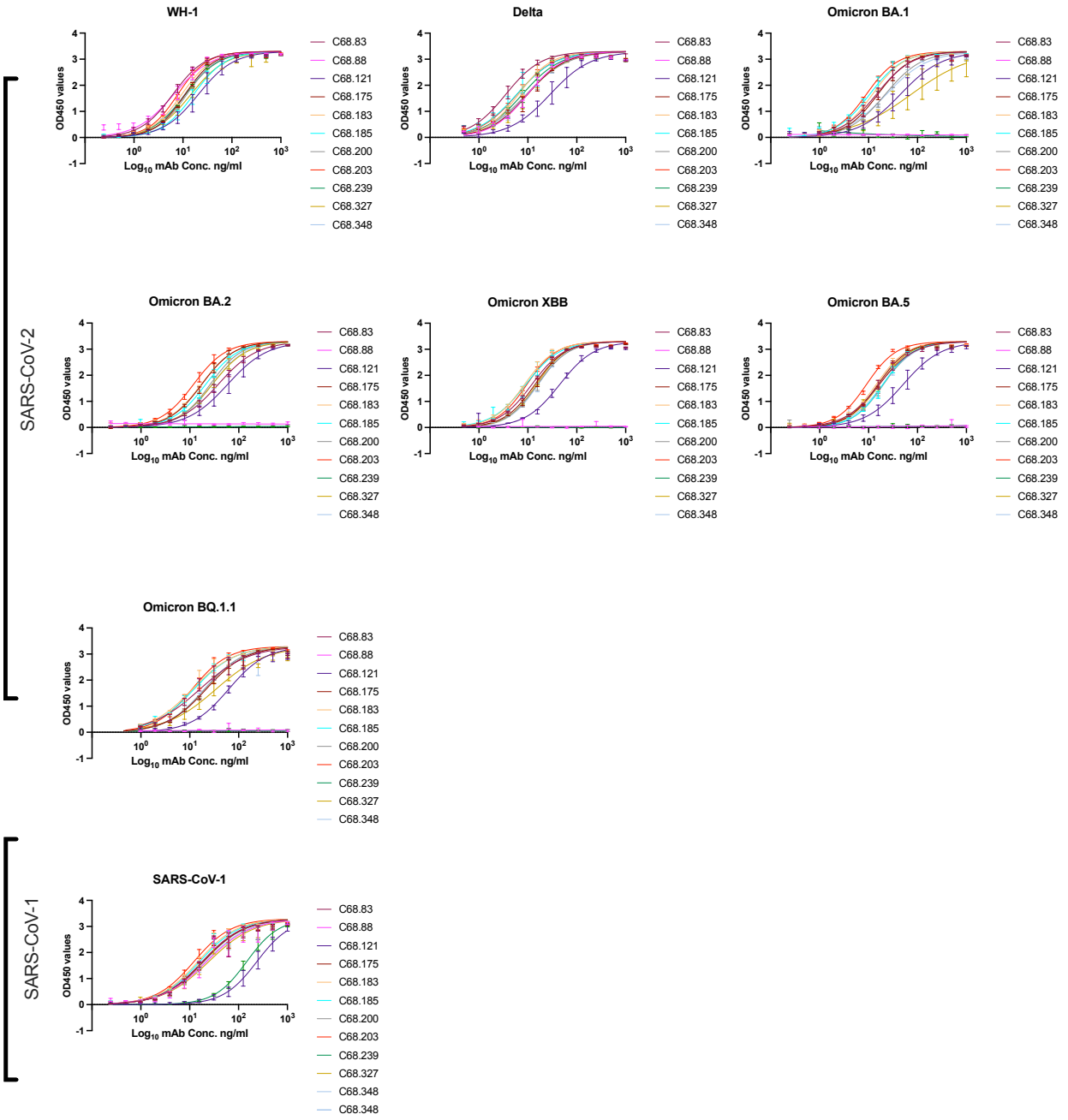

Supplementary Figure 2.2. Binding curves for C68 mAbs to SARS-CoV-2 variants and SARS-CoV-1 recombinant spike glycoprotein by ELISA.

Binding of C68 mAbs to SARS-CoV-2 WH-1, SARS-CoV-2 variants (Delta, Omicron BA.1, Omicron BA.2, Omicron XBB, Omicron BA.4/BA.5, Omicron BQ.1.1) or SARS-CoV-1 recombinant spike trimers. The concentration of each mAb (ng/mL) is plotted on a log10 scale versus absorbance (OD450nm values). Half-maximal effective concentrations (EC_{50} values) calculated by nonlinear regression analysis from at least two independent technical replicates. Each mAb

was serially diluted 2-fold for 11-12 total dilutions. Curves represent nonlinear regression fits with error bars that indicate SEM.

A

	WH-1	Delta	Omicron BA.1	Omicron BA.2	Omicron XBB.1.5	Omicron BA.5	Omicron BQ.1.1	GD-Pangolin	SARS-CoV-1	RsSHC014	WIV1	LYRa3	Khosta-2	BtKY72
% Sequence identity to SARS-CoV-2 WH-1 RBD	-	99	93	92	89	92	90	96	74	77	77	75	68	73
% Sequence identity to SARS-CoV-1 RBD	74	75	72	71	71	71	72	75	-	82	96	95	70	74

B

Statistics for SARS-CoV-2 variants neutralization		
	Geomean	95% CI
C68.61	0.40	(0.25, 0.64)
C68.83	8.6	(2.2, 34)
C68.88	4.7	(0.47, 46)
C68.121	17	(12, 23)
C68.175	5.0	(1.7, 14)
C68.183	11	(4.6, 29)
C68.185	5.8	(2.6, 13)
C68.200	18	(13, 24)
C68.203	5.3	(1.6, 18)
C68.239	4.2	(0.35, 50)
C68.327	7.5	(3.4, 17)
C68.348	8.0	(2.2, 29)
S309	1.4	(0.3, 6.6)
CR3022	20	(20, 20)
S2H97	0.39	(0.17, 0.86)
S2X259	3.8	(0.43, 34)

Statistics for all sarbecovirus neutralization		
	Geomean	95% CI
C68.61	0.62	(0.24, 1.6)
C68.83	7.4	(3.2, 17)
C68.88	1.1	(0.19, 6.4)
C68.121	13	(8.4, 21)
C68.175	5.3	(1.9, 15)
C68.183	8.2	(3, 23)
C68.185	1.1	(0.26, 4.3)
C68.200	11	(4.4, 25)
C68.203	3.6	(1.3, 9.9)
C68.239	2.7	(0.52, 14)
C68.327	7.2	(2.9, 18)
C68.348	4.4	(1.6, 12)
S309	0.90	(0.23, 3.5)
CR3022	8.3	(3.5, 20)
S2H97	0.95	(0.32, 2.8)
S2X259	0.32	(0.05, 1.9)

Supplementary Figure 2.3. Sarbecovirus percent sequence identity relative to SARS-CoV-2 or SARS-CoV-1 RBD and neutralization statistics.

(A) Sarbecovirus percent sequence identity to SARS-CoV-2 WH-1 RBD or SARS-CoV-1 RBD. (B) Geometric means (geomeans) of the IC50s and 95% confidence interval (95% CI) across SARS-CoV-2 variants only (left panel) and all tested sarbecoviruses (right panel) tested in **Figure 2.2B**.

A

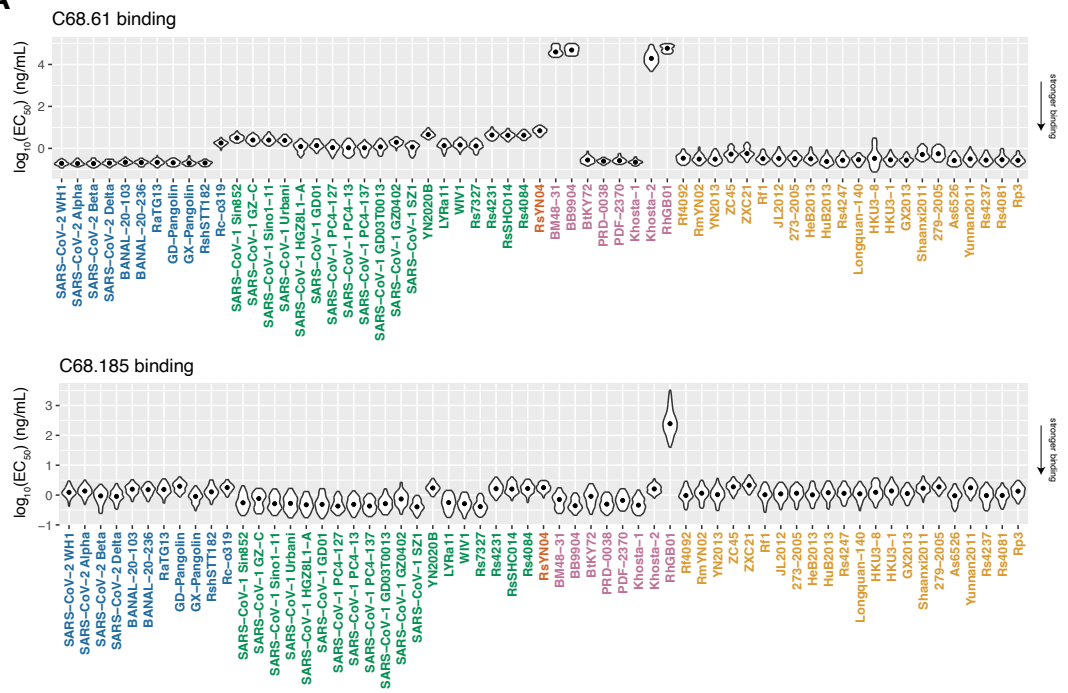

B

	Clade 1b SARS-CoV-2 related sarbecoviruses	
	Geomean	**95% CI**
C68.61	0.25	(0.39,0.16)
C68.185	1.3	(1.6,1.1)
	Clade 1a SARS-CoV-2 related sarbecoviruses	
	Geomean	**95% CI**
C68.61	1.9	(2.5,1.4)
C68.185	0.66	(0.85,0.52)

Supplementary Figure 2.4. Violin plots showing Log10 EC50 values from pan-coronavirus RBD yeast display assay.

(A) We assessed the cross-reactivity of C68.61 (upper panel) and C68.185 (lower panel) (data from **Figure 2.2C**) with 61 RBDs from sarbecovirus clades (indicated by different colors where clade 1b SARS-CoV-2-related sarbecoviruses are in blue, clade 1a SARS-CoV-1-related sarbecoviruses are in green, clade 2 ACE2-independent sarbecoviruses in yellow, clade 3 African/European sarbecoviruses in purple, and clade 4 sarbecoviruses in orange) analyzed by flow cytometry. The lower the EC50 (log10 ng/ml), the stronger binding response. Represents data from at least two independent experiments. (B) Geometric means of the EC50s (ng/ml; data from **Figure 2.2C**) and 95% confidence interval (95% CI) across clade 1b SARS-CoV-2-related sarbecoviruses and clade 1a SARS-CoV-1-related sarbecoviruses tested.

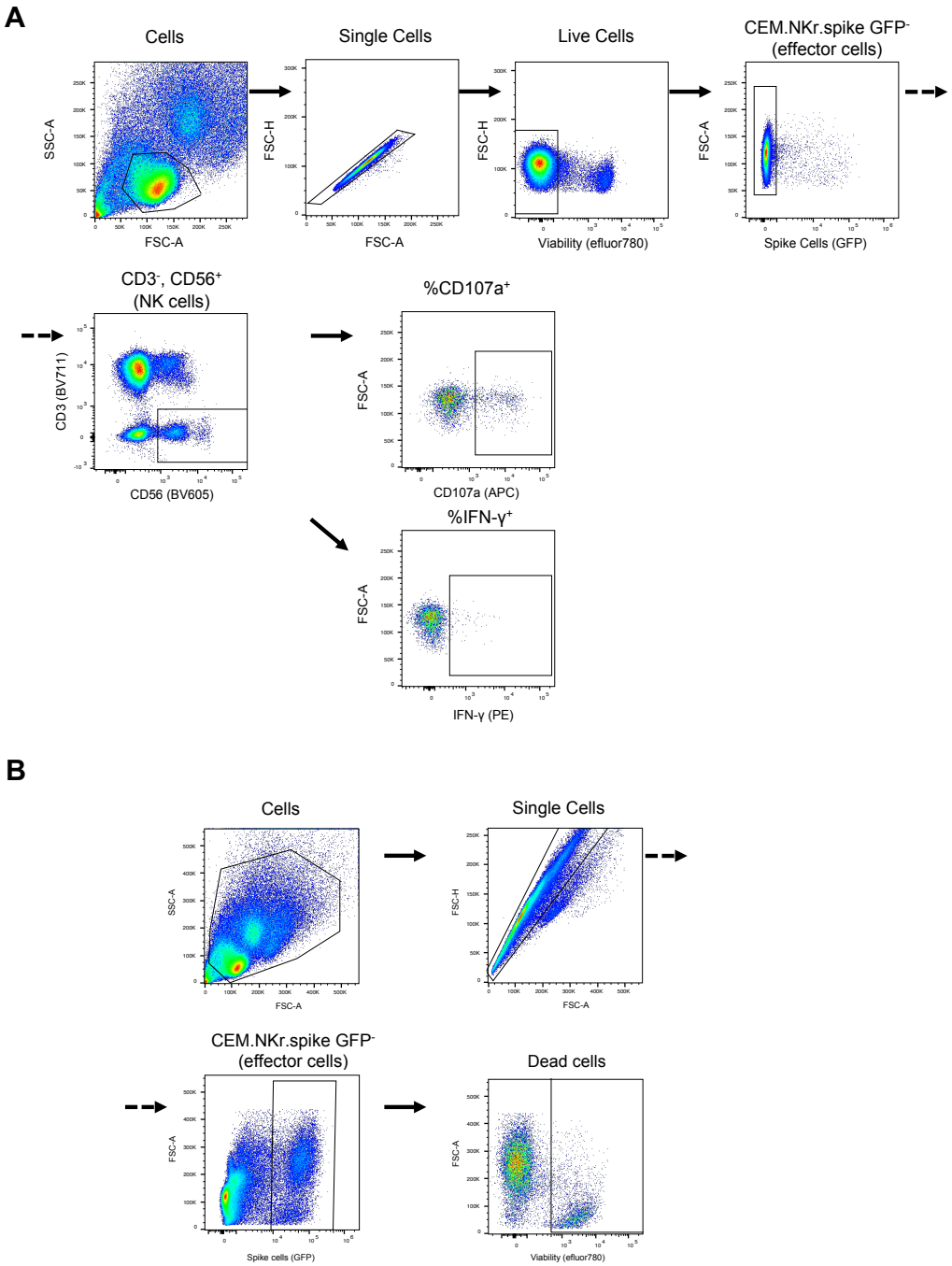

Supplementary Figure 2.5. Gating strategy for ADCC.

(A) The ability of candidate mAbs to trigger ADCC was determined by flow cytometry. NK cell (gated as live, single cells, CEM.NKr.spike$^-$, CD3$^-$, CD56$^+$ cells) activation was measured by

surface expression of CD107a (a proxy for degranulation) and intracellular IFN-γ (113). (B) Representative gating strategy for CEM.NKr.spike cell death.

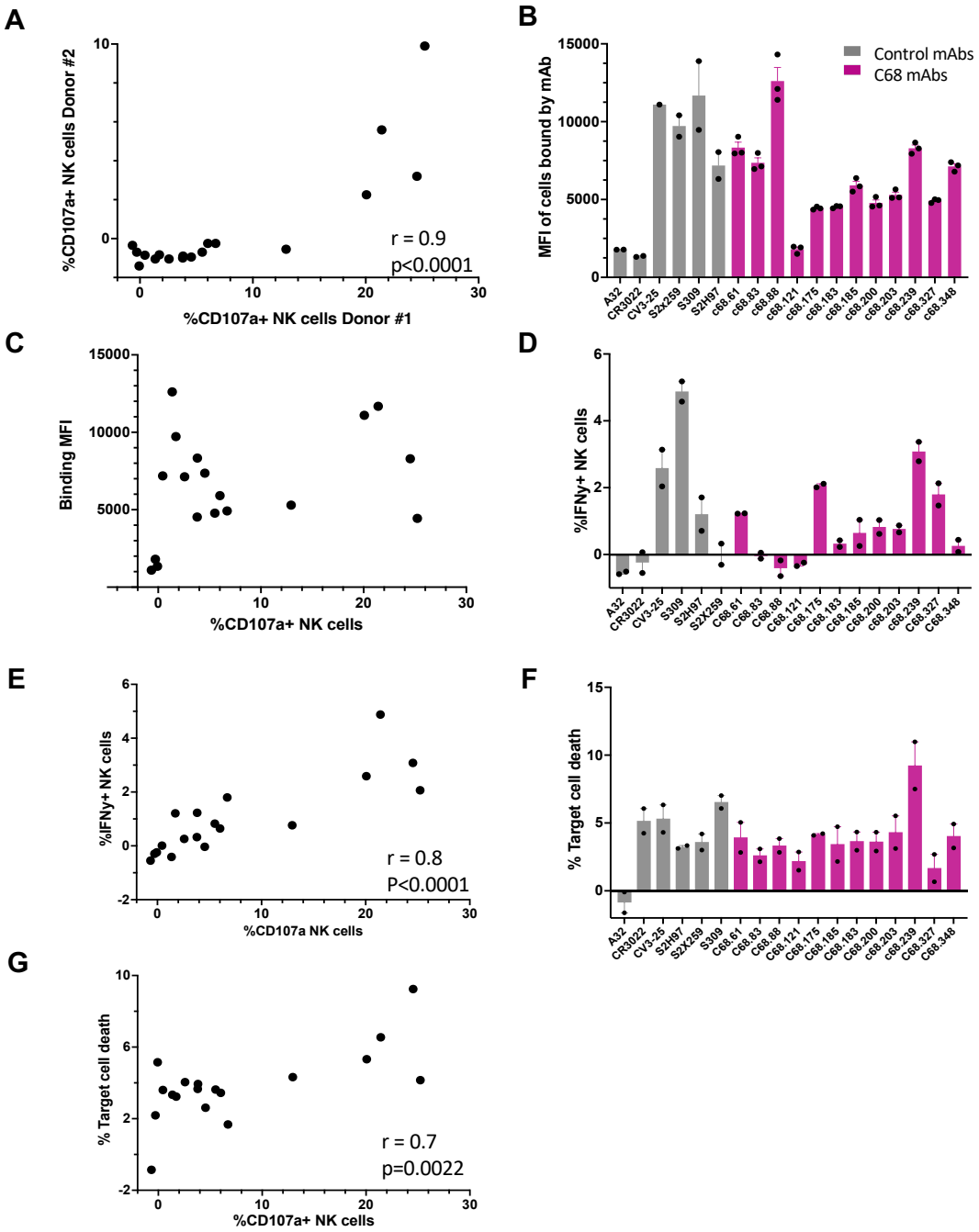

Supplementary Figure 2.6. Assessment of Fc-mediated functions of C68 mAbs.

(A) Correlation plot of the ability of C68 mAbs and control mAbs (control mAbs: S309, CV3-25, A32, S2H97, S2H97) to trigger NK cell activation (%CD107a+) from two independent PBMC donors using Pearson's correlation. (B) Measurement of the degree of binding to CEM.NKr cells expressing D614G SARS-CoV-2 spike (target cells). Control mAbs are shown in grey and C68 mAbs in pink. (C) Correlation plot between the degree of binding to target cells and the ability to trigger NK cell activation (%CD107a+). Pearson's correlation analysis showed no association between NK cell activation (%CD107a+) and MFI ($r = 0.3$, $p = 0.2$). (D) Assessment of the ability of C68 mAbs to trigger NK cell activation (%intracellular IFN-γ). (E) Correlation between the ability of C68 mAbs to trigger NK cell activation as measured by percent cell surface CD107a or percent intracellular IFN-γ. (F) Percent of cell death within the target cell population. (G) Correlation plot between target cell death and %CD107a expression. Correlation plots between NK activation measurements (%CD107a, %intracellular IFN-γ, %target cell death) and binding of targets cells by mAbs (MFI) were assessed by Pearson correlation using PRISM. Results represent assays run in technical duplicate with background subtracted values, data shown from a single donor (for B-G).

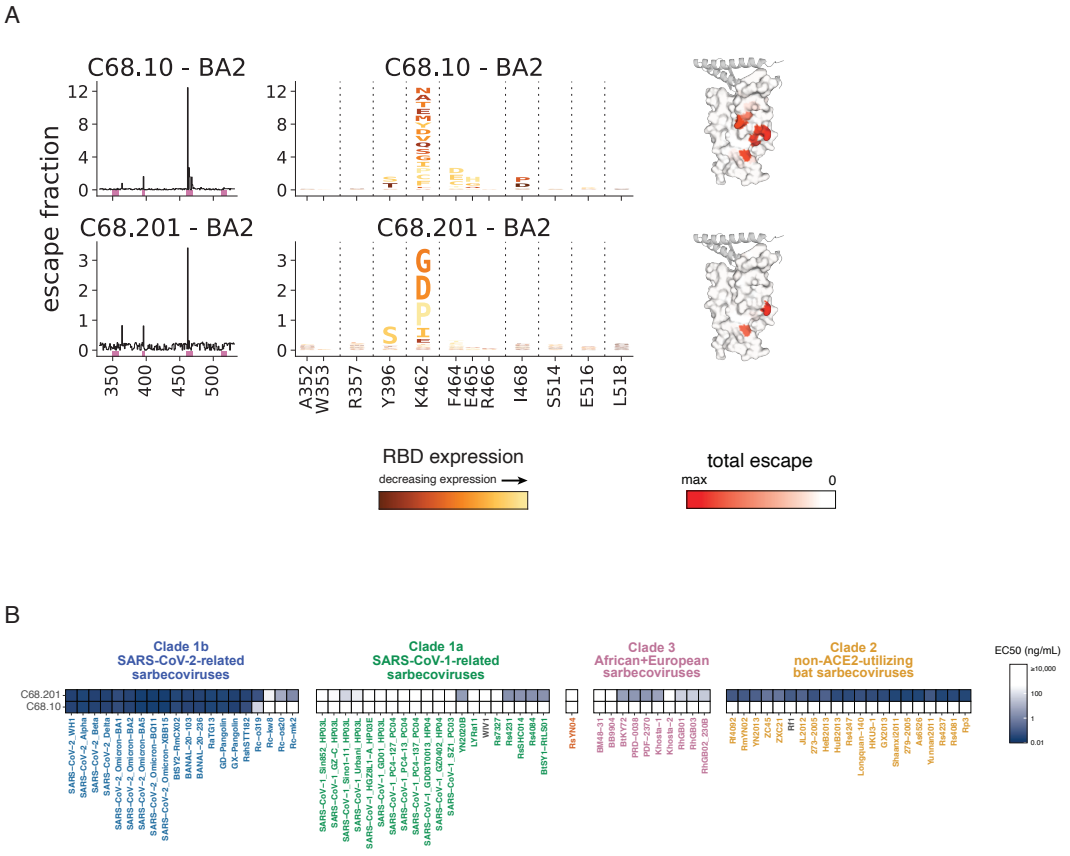

Supplementary Figure 2.7. Epitope profiling and pan-sarbecovirus RBD binding activity for C68 mAbs.

(A) Complete escape maps of antibody-binding escape mutations for C68 mAbs using a yeast-displayed SARS-CoV-2 RBD deep mutational scanning system (Omicron BA.2 RBD). Line plots (left panel) show escape at each site in RBD. Residue colors are assigned based on effect these mutations have on RBD expression (with yellow indicating mutations deleterious for RBD expression). The height of letters in the logo plots indicate level of escape by that amino acid at that site. Logo plot residue numbering is based on SARS-CoV-2 Omicron BA.2 (B) Pan-sarbecovirus RBD yeast display to assess C68 mAbs sarbecovirus RBD binding breadth. EC50 value represents the geometric mean across the independent barcodes for corresponding sarbecovirus RBD.

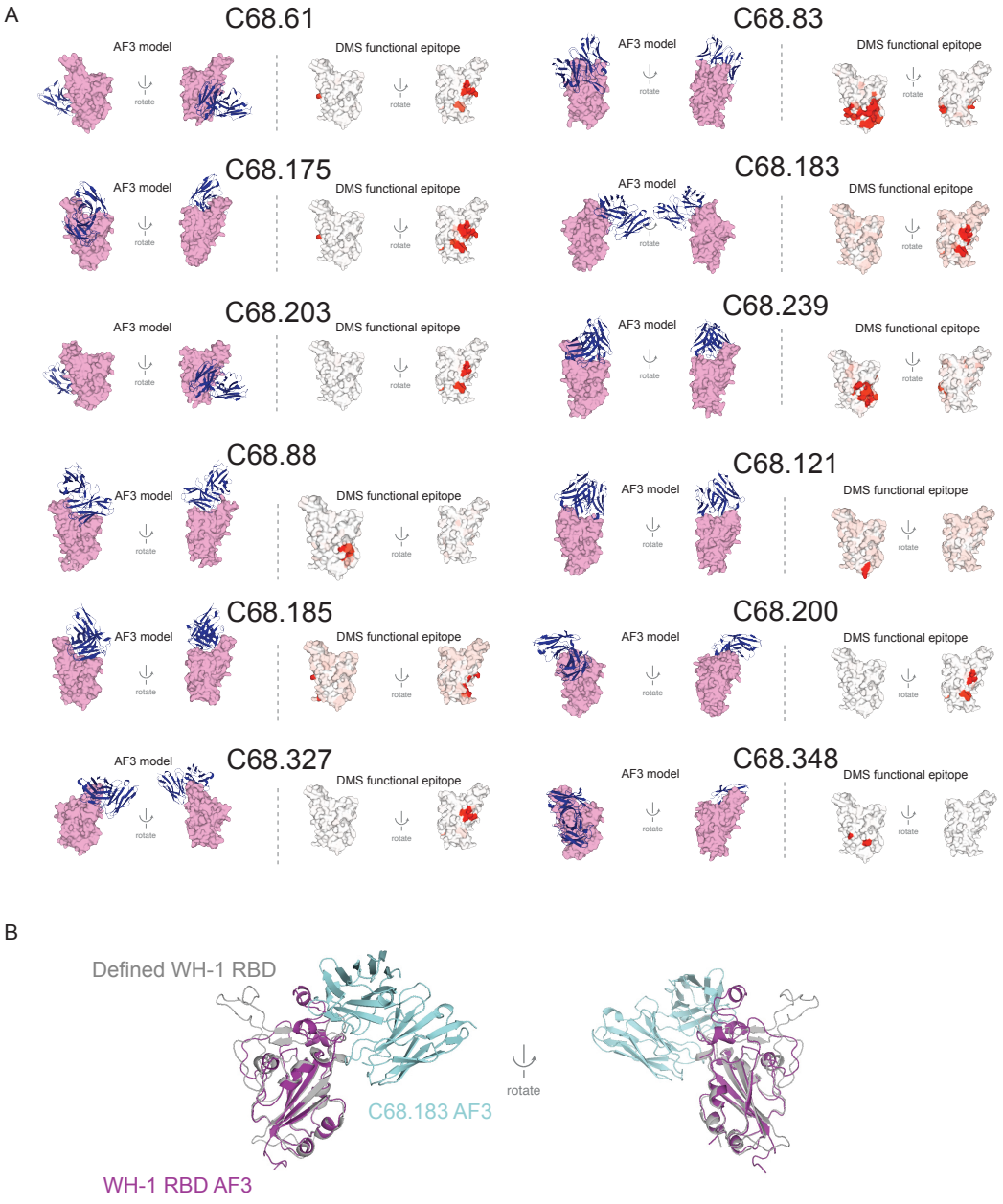

Supplementary Figure 2.8. Predictive Alphafold 3 modeling of mAb:RBD structures. (A) Concordance between predicted AF3 and experimental DMS epitopes. For each antibody, views from two equivalent angles are shown for the predicted AF3 model on the left and the DMS epitope on the right (details as in **Figs. 2.3A** and **2.4A**). (B) Example of an improperly predicted RBD structure from the C68.183:RBD AF3 model. A structural alignment is shown between the

experimentally determined RBD structure from PDB 6M0J (gray) and the predicted C68.183-bound RBD (purple), with predicted C68.183 chains shown in light blue, demonstrating accurate modeling of the RBD core but inaccurate modeling of the ACE2-contact loops.

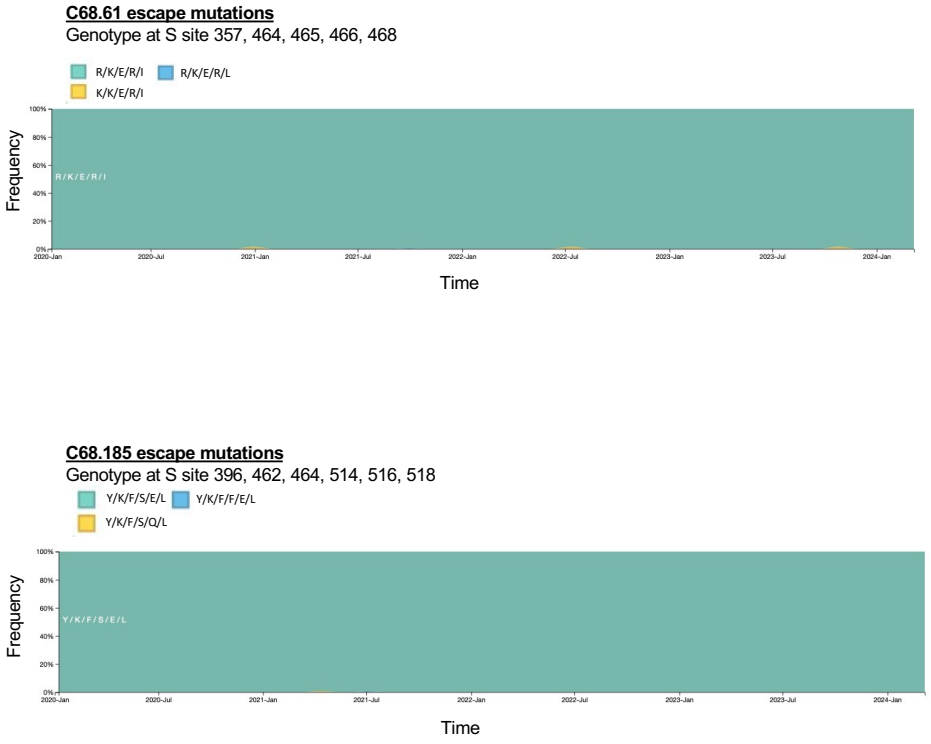

Supplementary Figure 2.9. Frequency of viral genomes containing C68 RBD binding escape mutants.

Area plot indicating the frequency of RBD binding escape mutants (from **Figure 2.4A**) found in SARS-CoV-2 sequences (Nextstrain) for C68.61 (top panel) and C68.185 (bottom panel) over time. Circles in teal are the residues found in the SARS-CoV-2 reference sequence (Wuhan-Hu-1) whereas mutations or deletions are indicated by yellow/blue circles. Depicts 3900 SARS-CoV-2 viral genomes sampled between Dec 2019 and Mar 2024 (**S2.2 Table**). (Nextstrain: https://nextstrain.org, CC-BY-4.0 license)

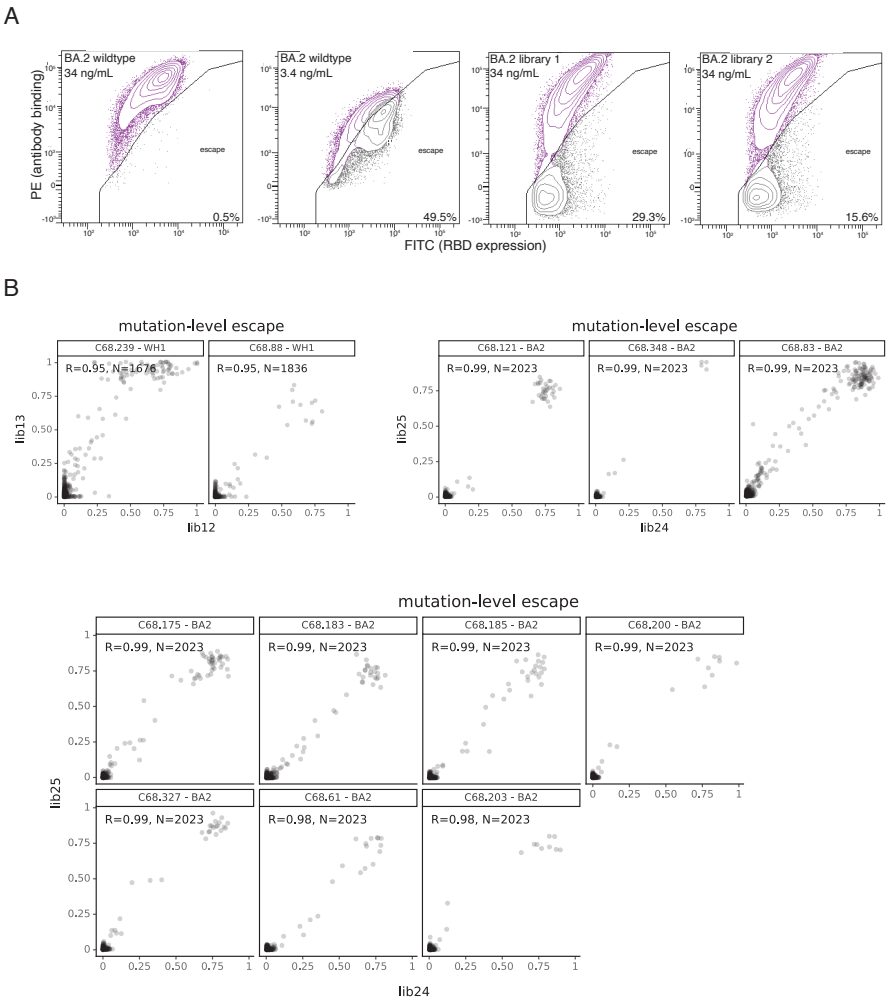

Supplementary Figure 2.10. Yeast displaying SARS-CoV-2 RBD deep mutational scanning library gating strategy and correlation between screens using independently generated libraries.

(A) Gating strategy to identify antibody escape mutants by gating on yeast mutants with reduced antibody binding. A yeast strain expressing the unmutated RBD of Wuhan-Hu-1 or Omicron BA.2 and flow cytometry were used to identify an EC90 and then yeast libraries were incubated with that EC90 concentration of mAb. Cells are incubated with PE-conjugated 1:200 goat anti-human-IgG and 1:100 FITC-conjugated chicken anti-Myc-tag. Cells are then gated on unmutated WH-1 or Omicron BA.2 control cells to identify escape mutants with >10x loss in antibody binding. (B) Correlation of mutation-level escape from independently generated mutant RBD libraries.

Supplementary Table 2.1. Amino acid sequences for C68 cross-reactive antibodies characterized in this study.

From (135), accessed here: https://ndownloader.figstatic.com/files/50045907

Supplementary Table 2.2. SARS-CoV-2 sequence accession IDs and acknowledgements table.

From (135), accessed here: https://ndownloader.figstatic.com/files/50045910